NTNU – Trondheim
Norwegian University of
Science and Technology

Critical Assessment of Non-linear Wave Loads in the Design of Offshore Wind Turbines

Øivind Paulshus

Marine Technology
Submission date: June 2014
Supervisor: Sverre Steen, IMT

Norwegian University of Science and Technology
Department of Marine Technology

Scope of work

MASTER THESIS IN MARINE TECHNOLOGY SPRING 2014

for
Stud. techn. Øivind Paulshus

A Critical Assessment of Non-linear Wave Loads in the Design of Offshore Wind Turbines

The background for this project is the ongoing planning and feasibility studies of the creation of large wind farms at Dogger Bank. Good wind conditions makes this a well suited site for offshore wind industry. The harsh environment combined with shallow water, might create significant non-linear wave loads which is a challenge in the design calculations against ULS. Different models can be used to include non-linear wave load effects in the time domain analysis, but the choice of model might largely affect the resulting design loads. The scope of this work is to assess the different models in the view of design load calculations, conservatism and water depth limitations.

The Student shall:

- Present different models to create non-linear effects in time domain analysis, including the background theories and assumptions
- Present models and methods used at deep water and assess in what degree these can be used in more shallow water
- Present and discuss methods and requirements to design loads from industrial standards.
- Perform time domain analysis with different models with the use of commercial software and self developed routines. Load conditions must be according to industrial practice and site parameters must be defended
- Perform statistical calculation from the realizations and assess the methods in the view of design loads and conservatism

- Discuss the results in the view of time duration and the number of realizations.

The work scope may prove to be larger than initially anticipated. Subject to approval from the supervisors, topics may be deleted from the list above or reduced in extent. In the thesis the candidate shall present his personal contribution to the resolution of problems within the scope of the thesis work. Theories and conclusions should be based on mathematical derivations and/or logic reasoning identifying the various steps in the deduction.

The candidate should utilise the existing possibilities for obtaining relevant literature. The thesis should be organised in a rational manner to give a clear exposition of results, assessments, and conclusions. The text should be brief and to the point, with a clear language. Telegraphic language should be avoided. The thesis shall contain the following elements: A text defining the scope, preface, list of contents, summary, main body of thesis, conclusions with recommendations for further work, list of symbols and acronyms, references and (optional) appendices. All figures, tables and equations shall be numerated.

The supervisors may require that the candidate, in an early stage of the work, presents a written plan for the completion of the work. The original contribution of the candidate and material taken from other sources shall be clearly defined. Work from other sources shall be properly referenced using an acknowledged referencing system.

The report shall be submitted in two copies: - Signed by the candidate - The text defining the scope included - In bound volume(s) - Drawings and/or computer prints which cannot be bound should be organised in a separate folder. - The bound volume shall be accompanied by a CD or DVD containing the written thesis in Word or PDF format. In case computer programs have been made as part of the thesis work, the source code shall be included.

Ownership NTNU has according to the present rules the ownership of the thesis. Any use of the thesis has to be approved by NTNU (or external partner when this applies). The department has the right to use the thesis as if the work was carried out by a NTNU employee, if nothing else has been agreed in advance.

Supervisors:
Jørgen R. Krokstad (principal research engineer professor II)

Deadline:
June 10, 2014

Øivind Paulshus
Trondheim, January, 2014

Preface

This Master Thesis has been written during the spring semester at the Norwegian University of Science and Technology 2014. The thesis has been written to fulfill the requirement for completing the degree of Master of Science at the Department of Marine Technology in Trondheim, Norway. The work process has been challenging and time consuming in the development of numerous Matlab scripts, where some implementations have been highly academically rewarding. Also the choice of parameters to the analysis did show to be time consuming. Many ideas have developed through the process, and I might have experienced that work limitations should be set at an earlier stage. It was a hard work to finish this thesis, but I am grateful for my choice of topic.

Acknowledgments

I would like to thank my supervisor, Prof. II Jørgen Krokstad, a principal research engineer in Statkraft. He has introduced me to the wind mill industry, for which I am truly grateful. One year of valuable conversations, including a trip to Smøla is highly appreciated.

The subject was also set to give me valuable knowledge for my beginning employment in DNV. I am truly grateful that a trip to the office of DNV in Copenhagen was made possible, thanks to my supervisor and Dr. Techn. Erik Asp Hansen, Head of Project Certification at DNV Wind Energy. I received a warm welcome and was given valuable input to my work.

I wish to thank Jørn Birknes and Thomas B. Johannessen for providing me highly valuable references for knowledge and implementation of kinematic models.

I will also thank PhD candidate Daniel Zwick and Postdoc Lene Eliassen for their valuable experiences in Fedem. I will also thank my office mates for creating a warm and positive working atmosphere.

Øivind Paulshus

Trondheim, 10. 6. 2014

Abstract

Good wind conditions make Dogger Bank a well suited site for offshore wind industry. The harsh environment combined with shallow water, create significant non-linear wave loads which must be accounted for in the ultimate limit state design calculations (ULS). The application of different non-linear wave models have been given a wide critical assessment throughout the thesis. A monopile substructure is considered at depths of 25 and 45 meter.

The DNV standard OS-J101 give the industrial practice for design of offshore wind turbines, and is followed by large contractors in the industry. The standard defines load cases involving the 50 year sea state parameters and the 50 year wave height.

The irregular 2nd order wave model is presented, including stretching and extrapolation which are methods to account for the surface elevation. Linear and 2nd order kinematics, stretching of linear kinematics to the 1st and 2nd order surface, and 1st and 2nd order extrapolation models, have all been assessed, using the 50 year sea state values.

A cut-off value has been needed to truncate the wave spectrum, to avoid unphysical high frequencies in the inertia load. The proposed cut off to the 2nd order theory has been applied to all models to make a comparison more meaningful. The 2nd order theory is not valid at 25m due to an unphysical enlargement of low frequency components. The problem has been avoided by adjusting the depth parameter. The method has been applied carefully, and the implications have been discussed.

The kinematic models are all applied to the structure with Morison equation, which is a load model consistent to the 1st order. This is the load model according to the standard, but FNV, a load model consistent to 3rd order has been included for comparison. The methods are studied in both static and dynamic load calculation. The conservatism between models have been addressed. The influence of non-linearity at 25m contra 45m is studied by spectral and extreme value analysis.

The structural model in Fedem showed unexpected high excitation at the natural frequency. This required a parameter modification to make the comparison of load models meaningful. The load models have all been compared in the view of dynamic excitation.

The standard requirements for the Wind Industry define 50 year sea state parameters inconsistent with the rules well known to oil and gas installations. The conservatism between the methods have been assessed by performing an extreme value analysis in the time domain using Fedem.

Wave models to apply the 50 year wave height have also been addressed. The design wave will be highly depth limited at 25m and stream function wave theory is required to give a realistic representation of the vertical asymmetric wave profile. The wave can be applied as regular but a wave train of design waves are not realistic to occur.

Embedding is a much used method in the verification process. A stream function wave is embed into a stochastic realization to make the loads and dynamics more realistic. The method is widely applied, but to structures that are dominated by drag loads. At Dogger Bank, the dimensions are larger, and inertia loads are found to dominate completely. How this affects the method will be discussed.

Statistic consequences when violating the stochastic nature of the time series have been analyzed. The effect to the dynamic response of the structure is also studied. The use of stream function waves and embedding is compared to linear regular waves in the view of conservatism. The implications when describing a wave close to breaking by the use of stream function, will also be addressed.

Improvements to the embedding method is created and compared to the method applied in the industry.

Sammendrag

Gode vindforhold gjør Doggerbank til et egnet sted for vindmøller til havs. Det harde miljøet kombinert med grunnt vann, gir betydelige ulineære bølgelaster som det må tas hensyn til ved design mot ekstremlaster (ULS). Bruken av ulike ikke-lineære bølgemodeller gis en bred og kritisk vurdering gjennom oppgaven. Et stolpefundament (monopile) vil bli betraktet ved 25 og 45 meters vanndyp.

DNV standarden OS-J101 gir den industrielle praksis for vindmøller til havs, og følges i stor grad av leverandører og utbyggere i industrien. Standarden definerer lastkondisjoner som involvberer 50 års sjøtilstandparametere og 50 års bølgehøyde.

Irregulær andreordens bølgemodell er presentert, inkludert metoder for å ta høyde for bølgehevning som Wheeler strekking og ekstrapolering av kinematikk. Lineær og andreordens kinematikk, strekking til første og andreordens bølgeoverflate, samt første og andreordens ekstrapolasjonsmodeller, har alle blitt vurdert.

Bølgespekteret må kortes av ved en gitt frekvens, for at ikke masskraften skal inkludere ufysisk høye frekvensverdier. Den foreslåtte verdien for bruk til andreordens kinematikkmodell, vil brukes i alle modeller slik at en sammenlikning blir mest mulig meningsfull. Andreordens teori er ikke gyldig ved 25 meters dyp, fordi lave frekvensverdier blir ufysisk forstærket. Problemet har blitt løst ved å justere dybdeparameteren i modellen. Metoden har blitt brukt forsiktig, og konsekvensene har blitt diskutert.

Kinematikkmodellene har blitt påført strukturen med bruk av Morisons likning, en modell konsistent til første orden. Dette er modellen som påkreves i standarden, men FNV, en modell konsistent til tredje orden har blitt inkludert for sammenlikning. Metodene er studert med både statisk og dynamisk lastanalyse. I hvilken grad de ulike metodene er konservative har blitt diskutert. Betydningen av ikke-lineariteter på 25m er sammenliknet med 45m på bakgrunn av frekvensplan- og ekstremverdianalyse.

Strukturmodellen i Fedem viste uforventet høy eksitasjon ved egenfrekvensen. Parametere brukt i analysen måtte modifiseres for at en sammenlikning av lastmodeller skulle være hensiktsfull. Lastmodellene har blitt sammenliknet med tanke på dynamisk forstærkning.

Standarden for vindindustrien angir bestemmelse av 50 års sjøtilstandparametere som ikke i samsvar med en mer underbygd metode påkrevd for olje og gass installasjoner. Graden av konservatisme mellom metodene har blitt vurdert ved å kjøre en ekstremverdianalyse i tidsplanet ved bruk av Fedem.

Bølgemodeller for å påføre 50 års bølgehøyde har også blitt vurdert. Designbølgen vil i stor grad være begrenset av vanndybden ved 25 meters dyp. En strømfunksjonsbølge er da påkrevd for å gi en realistisk representasjon av bølgehevningens vertikale usymmetri. Bølgen kan påsettes som regulær, men et tog av designbølger vil selvsagt være fullstendig statistisk urealistisk.

Embedding (innsetting) er en mye brukt metode i verifikasjonsprosessen. En strømfunksjonsbølge blir da innsatt in en stokastisk realisasjon for å lage laster og dynamikk mer realistisk. Metoden er mye brukt, men på strukturer som er dominert av drag-krefter. På Doggerbank er de påkrevde strukturdimensjonene større og massekrefter har blitt vist å være fullstendig dominerende. Konsekvensene dette har for metoden har blitt diskutert.

Statistiske konsekvenser når den stokastiske overflaten blir brutt, og en regulær bølge tvunget inn, har blitt analysert. Også effekten på den dynamiske responsen er studert. Bruken av strømfunksjonsbølge og embedding har blitt sammenlignet med lineære bølger med hensyn på hva som er konservativt. Konsekvensene når en bølge svært nære brytning blir beskrevet av strømfunksjon er også blitt tatt opp.

Forbedringer av metoden er laget og sammenlignet med metoden som faktisk brukes i industrien.

Contents

List of Tables

List of Figures

List of Symbols

Latin Letters

a	Wave amplitude
a	Substructure radius used in FNV model
C_A	Added mass coefficient
C_D	Drag coefficient in Morison equation
C_M	Mass coefficient in Morison equation
c_r	The phase velocity
C_V	The coefficient of variation
D	Substructure diameter
E_ij	Transfer function, 2nd order irregular surface elevation
f_p	Wave frequency according to T_P in the spectrum [Hz]
$f_{X_\tau}(x\|\vec{z})$	Conditional PDF of X given $\vec{z}$
$F_{X_\tau}(x_p\|\vec{z})$	Conditional CDF of X given $\vec{z}$
F	Applied force on a structure
F_d	Design load
F_k	Characteristic load
f_N	Natural period of a structure
$f_{\vec{z}}$	Joint probability distribution of parameters in $\vec{z}$
g	Gravity acceleration
g	Limit state function
h	Water depth
H	Transfer function between load and structural response
H	Wave height
H_{50yr}	Wave height of 50 year return period
H_S	Significant wave height
k	Wave number
m_Top	Top mass, weight of the nacelle, hub and airfoils
p	Percentile of a CDF
p_F	The probability of failure

P_ij	Transfer function, 2nd order irregular velocity potential
Q	The total volumetric flow rate
t	Time
T	Wave period
T_P	The peak period in the wave spectrum
r	Dynamic structural response parameter
r_0	Static structural response parameter
S	Spectral value
S_d	Design load effect
S_k	Characteristic load effect
v_k	Stiffness proportional damping ratio
v_m	Mass proportional damping ratio
u	Horizontal wave velocity
u_0	Horizontal wave velocity evaluated at MWL
U	Wind speed
w	Vertival wave velocity
x	Coordinate in horizontal direction
x_r	Coordinate in horizontal direction fixed to the wave crest
X	Fourier coefficent to the stream function
X	Stochastic variable
X_τ	Stochastic variable in a sea state of duration τ
x_{crit}	Critical value of X
x_p	$X-$value at a percentile given by the CDF
$z =$	Coordinate in vertical direction, defined as 0 at the MWL
$\vec{z}$	Environmental parameters
z^{mod}	Modified z coordinate used for Wheeler Stretching

Greek Letters

β	Ratio between the load frequency and natural frequency
Δt	Times step
ϵ	Wave steepness parameter
γ	Peakedness parameter to JONSWAP spectrum
γ_f	Load factor
λ	Wave length
μ	Expected value
ω	Wave frequency in radians per second
ω_P	Wave frequency according to T_P in the spectrum
ω_N	Natural period of a structure
ϕ	Velocity potential, potential theory
ψ	Stream function, potential theory
σ	Standard deviation
τ	Sea state duration in hours
ζ	Structural damping ratio
ζ	Surface elevation
$\zeta^{(1)}$	Linear Surface elevation
$\zeta^{(2)}$	2nd order Surface elevation
ζ_{max}	Crest height

List of Abbrevations

ALS	Accidental Limit State
BSF	Base shear force
CDF	Cumulative distribution function
DAF	Dynamic amplification factor
DFT	Discrete Fourier Transformation
DNV	Det Norske Veritas
DOF	Degree of freedom
FFT	Fast Fourier Transformation
FLS	Fatigue Limit State
FNV	Faltinsen − Newman − Vinje
IDFT	Inverse Discrete Fourier Transformation
JONSWAP	Join North Sea Wave Project
MSL	Mean surface level
MWL	Mean water line
NREL	National Renewable Energy Laboratory
OM	Overturning moment
PDF	Probability density function
TMD	Top mass displacement
ULS	Ultimate Limit State

Chapter 1

Introduction

Good wind conditions make Dogger Bank a well suited site for offshore wind industry. The harsh environment combined with shallow water, create significant non-linear wave loads which must be accounted for in the ultimate limit state design calculations (ULS). Sophisticated wave models are used to give a realistic representation of the environmental conditions, but there are large differences between the models in the view of conservatism.

The offshore wind industry is highly cost oriented and must challenge to drive down cost without compromising on safety. The need for complex environmental models are needed, but over-conservative design methods are of great importance to avoid due to economic considerations. Hundreds of similar foundations might be planned for, and the conservatism of design parameters might determine the feasibility of the entire project.

The application of different non-linear wave models have been given a wide critical assessment throughout the thesis. A monopile substructure is considered at depths of 25 and 45 meter.

Chapter 2 will give an introduction of higher order wave theory, which provide explanations and equations required to understand the discussions throughout the thesis. Chapter 3 proceeds the explanations to irregular wave models, and present how the models are implemented for later analysis. Depth related problems will be discussed.

The design and building of offshore windmills are able to take great advantages from decades with experience from the offshore oil and gas industry in the North Sea. The wind mill structure is highly dynamical and a non-linear load model applied for oil and gas installations will be compared to the load model specified in the offshore wind standard. Load cases involving extreme wave conditions are defined in the standard. The requirements will be explained and discussed in the view of rules applied to oil and gas.

Dynamic analysis will be done in Fedem Windpower, and the structural model will be presented. Load models will be compared both static and dynamic. Extreme value analysis will be performed and the influence of non-linearity at the 25 and 45 meter structure will be assessed.

Non-linear wave models are applied in the industry to create a more realistic representation of the loads from the 50 year largest wave. The method will be discussed in the view of statistic, dynamic and static load consequences. Also the conservatism compared to regular models will be assessed.

All figures and material presented in this thesis which has not been referenced to other sources, has been produced by the author. The following software versions have been utilized through the work process:

- MATLAB version R2013a
- Fedem Windpower version 7.1

Chapter 2

Regular Wave Theory

2.1 Governing equations and boundary conditions

To develop a kinematic description of waves, we have to make three fundamental assumptions about the fluid:

- Inviscid
- Irrotational
- Incompressible

Irrotational flow means that:

$$\vec{\omega} = \vec{\nabla} \times \vec{V} = \vec{0} \tag{2.1}$$

Then the velocity field is conservative and we can express the vectorfield with a scalar ϕ. This can be found in Calculus [9].

$$\vec{V} = \vec{\nabla}\phi \tag{2.2}$$

In fluid mechanics, ϕ is the velocity potential. Incompressible flow means that the following expression must be fulfilled.

$$\vec{\nabla}\vec{V} = 0 \tag{2.3}$$

When we combine these two results, we get the governing equation:

$$\vec{\nabla}^2\phi = 0 \tag{2.4}$$

This is also known as the Laplace equation. The pressure in the fluid is then expressed by Bernoulli's equation:

$$p + \rho g z + \rho\frac{\partial\phi}{\partial t} + \frac{\rho}{2}(\nabla\phi)^2 = C \tag{2.5}$$

Which means that the left hand side of the equation must be constant when following a stream line.

Boundary conditions is given by:

- Kinematic condition: No flow through the sea bottom
- Kinematic condition: The velocity to a fluid particle on the surface must equal the velocity of the surface
- Dynamic condition: The pressure given by Bernoulli's equation must be constant at the surface

These are mathematically expressed in Faltinsen [10]. The result for 2 dimensions are given below.

Kinematic conditions.

$$\frac{d\phi}{dz} = 0, \text{ on } z = -h \tag{2.6}$$

$$\frac{\partial\phi}{\partial z} = \frac{\partial\zeta}{\partial t} + \frac{\partial\phi}{\partial x}\frac{\partial\zeta}{\partial x}, \text{ on } z = \zeta(x,t) \tag{2.7}$$

Dynamic condition.

$$g\zeta + \frac{\partial\phi}{\partial t} + \frac{1}{2}(\nabla\phi)^2 = 0, \text{ on } z = \zeta(x,t) \tag{2.8}$$

I have here used h as depth and ζ as the surface elevation.

2.2 Airy Wave Theory

Linear wave theory is derived by neglecting all non-linear terms in the boundary conditions, like $\phi\phi$ and $\phi\zeta$. The equation above will then reduce to:

$$\frac{\partial\phi}{\partial z} = \frac{\partial\zeta}{\partial t}, \text{ on } z = \zeta(x,t) \tag{2.9}$$

Dynamic condition.

$$g\zeta + \frac{\partial\phi}{\partial t} = 0, \text{ on } z = \zeta(x,t) \tag{2.10}$$

We are allowed to do this because we assume waves with a small wave height to wave length ratio, and that ϕ is proportional to this. Terms containing powers of ζ and ϕ in the non-linear condition will be small because this ratio then is in power. We can use the dynamic condition to make an expression for ζ and substitute it in to the kinematic condition. The combined boundary condition solved for ϕ is then given by Faltinsen [10].

$$\frac{\partial^2\phi}{\partial t^2} + g\frac{\partial\phi}{\partial z} = 0, \text{ on } z = \zeta(x,t) \tag{2.11}$$

We cannot find a simple solution to this, because it shall be valid at the free surface elevation. We can avoid the problem with a Taylor series expansion. Given by Pettersen [11]:

$$\phi(x, z = \zeta, t) = \phi(x, 0, t) + \zeta(x, t) * \left.\frac{d\phi}{dz}\right|_{z=0} + O(\zeta^2) \tag{2.12}$$

Linear wave theory only use the first term in the expansion. Equation 2.11 will then be satisfied at $z = 0$, and we finally get the partial differential equation for ϕ:

$$\frac{\partial^2\phi}{\partial t^2} + g\frac{\partial\phi}{\partial z} = 0, \text{ on } z = 0 \tag{2.13}$$

The solution is found in DNV [12]:

$$\phi = \frac{ga}{\omega}\frac{\cosh k(z+h)}{\cosh kh}\cos(-\omega t + kx) \tag{2.14}$$

This must be substituted into eq. 2.10, which give the linear surface elevation

$$\zeta = a\sin(-\omega t + kx) \tag{2.15}$$

The velocity profile (equation 2.14) inserted into the free surface boundary condition (equation 2.13) for $z = 0$, gives the dispersion relation. This is an important relation that connects the wave number to the frequency:

$$\omega^2 = kg\tanh kh \tag{2.16}$$

The theory is valid when $H/\lambda < 1/20$.

All the symbols used in the equations are found in the list of symbols.

2.3 Stokes Wave theory

The non-linear boundary conditions given by equation 2.7 and 2.8 can be combined and solved for ϕ. This gives a highly non-linear equation, that ϕ must satisfy at the free surface elevation.

$$g\frac{\partial\phi}{\partial z} + \frac{\partial^2\phi}{\partial t^2} + \frac{1}{2}\frac{\partial}{\partial t}\vec{V}^2 = -\frac{1}{2}\frac{\partial\phi}{\partial x}\frac{\partial}{\partial x}\vec{V}^2 - \frac{\partial\phi}{\partial x}\frac{\partial^2\phi}{\partial x\partial t}, \text{ on } z = \zeta(x, t) \tag{2.17}$$

This is valid in the xz-plane with $\vec{V} = \vec{\nabla}\phi$. The equation cannot be solved at $z = \zeta(x, t)$, which means that Taylor expansion again must be utilized. This can be done to whatever order we want, which means that the equation that ϕ must

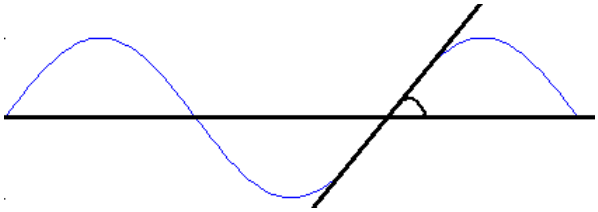

Figure 2.1: Wave steepness

satisfy can be of any order. Stokes used a perturbation approach to solve the problem.

$$\phi = \bar{\phi}_1\epsilon^1 + \bar{\phi}_2\epsilon^2 + \bar{\phi}_3\epsilon^3 + ... \ \mathrm{O}(\epsilon^n) \tag{2.18}$$

The perturbation parameter ϵ must be small, so that higher order terms get smaller and smaller. The wave steepness $\zeta_a k$ is commonly used for ϵ. Wave steepness is easy to derive from the wave profile:

$$\frac{d\zeta}{dx} = \frac{d}{dx}\zeta_A \sin kx = \zeta_A k \cos kx \tag{2.19}$$

The parameter is easy to understand from figure 2.1.

The parameter appears in the first order solution of ϕ. It also appear in the Taylor expansion in equation 2.12, because $\zeta\phi_z = \zeta k\phi = \epsilon\phi$.

The equation is solved for higher order by substituting the perturbed expression for ϕ into the non-linear equation 2.17, that ϕ has to satisfy. Taylor expansion of the equation must be done corresponding to the order of accuracy. The trick is then to gather terms with equal order of ϵ:

$$\epsilon^1(expression_1) + \epsilon^2(expression_2) + \epsilon^3(expression_3) + ... = 0 \tag{2.20}$$

This is an n'th order equation of epsilon, where each coefficient is given by $expression_i$. Each coefficient is a function of variables t, x, y and z. The only way to ensure this to be zero, is if each coefficient separately equals zero. Solving for the first expression will give us the Airy wave theory. By this approach, we can always add more and more accurate solution terms to our existing solution.

First order problem
This gives the Airy wave theory. Equation 2.13 is actually the requirement that the first term in eq. 2.20 is zero!

Second order problem
The strategy to find the second order Stokes wave is to solve the second term in eq. 2.20. The expression is found in Birknes [13]:

$$\frac{\partial^2\phi^{(2)}}{\partial t^2} + g\frac{\partial\phi^{(2)}}{\partial z} = -\eta^{(1)}\frac{\partial}{\partial z}\Big(\frac{\partial\phi^{(1)}}{\partial t^2} + g\frac{\partial\phi^{(1)}}{\partial z}\Big) - \frac{\partial}{\partial t}(\nabla\phi^{(1)}\nabla\phi^{(1)}), \text{ at z} = 0 \tag{2.21}$$

The solution of the equation is:

$$\phi^{(2)} = \frac{3}{8}\zeta_A^2\omega\frac{\cosh 2k(z+h)}{\sinh^4 kh}\sin 2(kx-\omega t) \tag{2.22}$$

Then $\phi = \phi^{(1)} + \phi^{(2)}$ must be substituted in to equation 2.8. By keeping 2nd order terms of ϵ, the equation to solve becomes:

$$\zeta^{(2)} = -\frac{1}{g}\Big(\frac{\partial\phi^{(2)}}{\partial t} + \zeta^{(1)}\frac{\partial^2\phi^{(1)}}{\partial z\partial t} + \frac{1}{2}\nabla\phi^{(1)}\nabla\phi^{(1)}\Big), \text{ at z} = 0 \tag{2.23}$$

This is also found in Birknes [13]. The solution is:

$$\zeta^{(2)} = \frac{1}{4}k\zeta_A^2\frac{\cosh kh}{\sinh^3 kh}(2+\cosh 2kh)\cos 2(kx-\omega t) \tag{2.24}$$

Equation 2.22 and 2.24 are found in Myrhaug [14]. We see that the second order Stokes wave profile depends on depth. Figure 2.2 shows the 1st and 2nd order components. We see that the crest becomes higher and the trough wider.

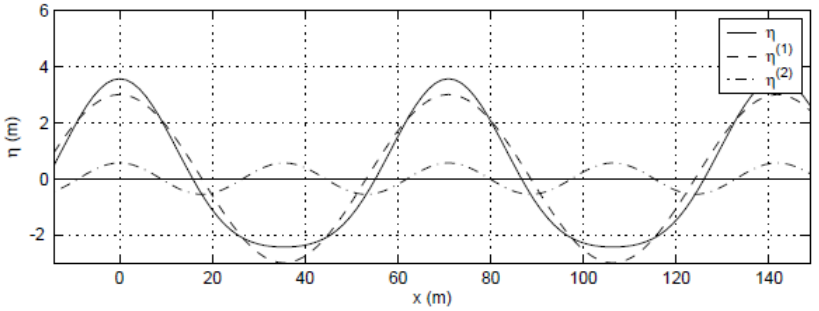

Figure 2.2: First and second order wave components, from Brorson [2]

Ursell number

Myrhaug (2006) derives the Ursell number from the ratio between the first and second order wave potential.

$$R = \frac{3}{8}\frac{kacosh2kh}{\sinh^3 kh\cosh kh} \tag{2.25}$$

For deep water, $kh \gg 1$. Then we have that $\sinh kh \sim \cosh kh \sim \exp(kh)/2$, which gives the ratio:

$$R = \frac{3}{8}\frac{ka\exp(2kh)/2}{\exp(kh)/2\exp(3kh)/2} = 3e^{-2kh}ka \tag{2.26}$$

At shallow water, $kh \ll 1$. Then we have that $\sinh kh \approx kh$ and that $\cosh kh \approx 1$. The ratio will then be:

$$R = \frac{3}{8}\frac{a/h}{(kh)^2} = \frac{3}{8}U_r \tag{2.27}$$

This is known as the Ursell number, and is used as a measurement for the degree of non-linearity. DNV (2010) defines the Ursell number as: $U_R = \frac{H\lambda^2}{d^3}$. With this definition Stokes waves are not valid when $U_r > 30$, then Stream function wave theory or cnoidal waves must be used. The linear theory was valid for $20H < \lambda$.

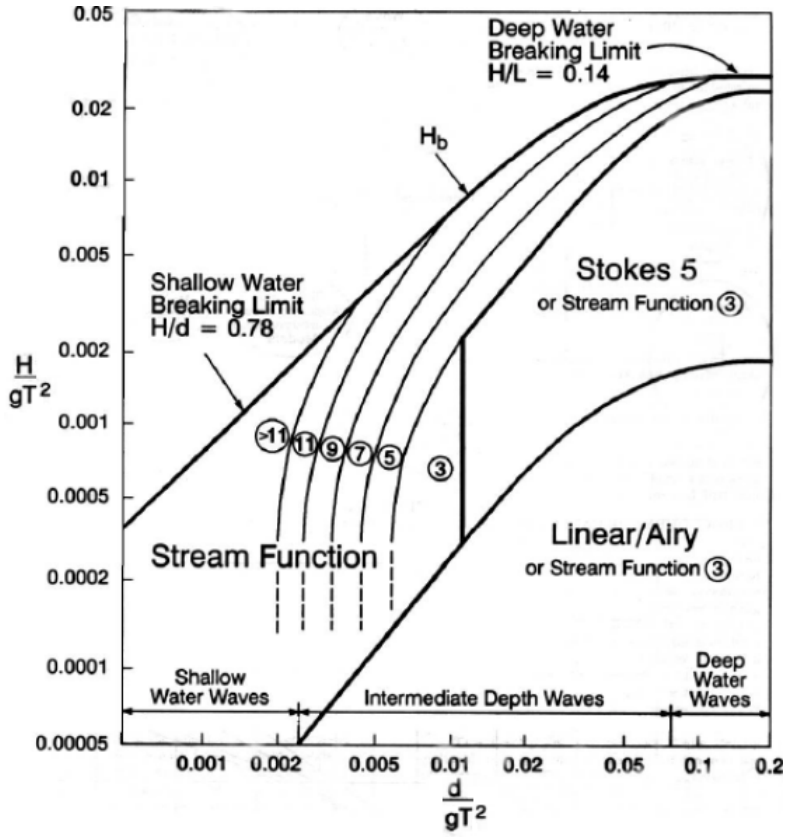

Figure 2.3: Applicability of Wave theories from Usfos Hydrodynamics Manual [3]

The perturbation method will converge with a speed dependent on the size of the perturbation parameter. A Stokes 5th order wave give accuracy to the wave breaking limit when $7H = \lambda$.

Third order theory
Higher order Stokes theory will also need a correction to the given dispersion relation in eq. 2.16, which will be a perturbed function equal to ϕ and ζ:

$$\omega^2 = \epsilon^1\bar{\omega}_1^2 + \epsilon^2\bar{\omega}_2^2 + ...O(\epsilon^n) \tag{2.28}$$

There is no correction in 2nd order theory (because $\bar{\omega}_2^2 = 0$) but there is a correction

for 3rd order, which is given for deep water in Brorson [2]:

$$\omega_1^2 + \omega_3^2 = kg(1 + (\frac{kh}{2})^2) = kg(1 + \epsilon^2) \tag{2.29}$$

The next theory

2.4 Dean's Stream function wave

The Stokes Wave theory gives an analytic understanding and solution to the wave problem. The Stream function theory is a solution to the non-linear boundary conditions for waves, given by eq. 2.6, 2.7 and 2.8. These equations are fulfilled by an iteration procedure, which is done by a completely numeric approach, made possible by the introduction of computers.

Coordinate system
We use a coordinate system (x_r, z) that is fixed to the crest, moving with the phase velocity c_r. The sea bottom is fixed in the global (x, z)-system and will move with the speed $-c_r$ relative to the crest. This is shown in figure 2.4 taken from Brorson [2]. The wave is symmetrical about the crest as in Stokes theory.

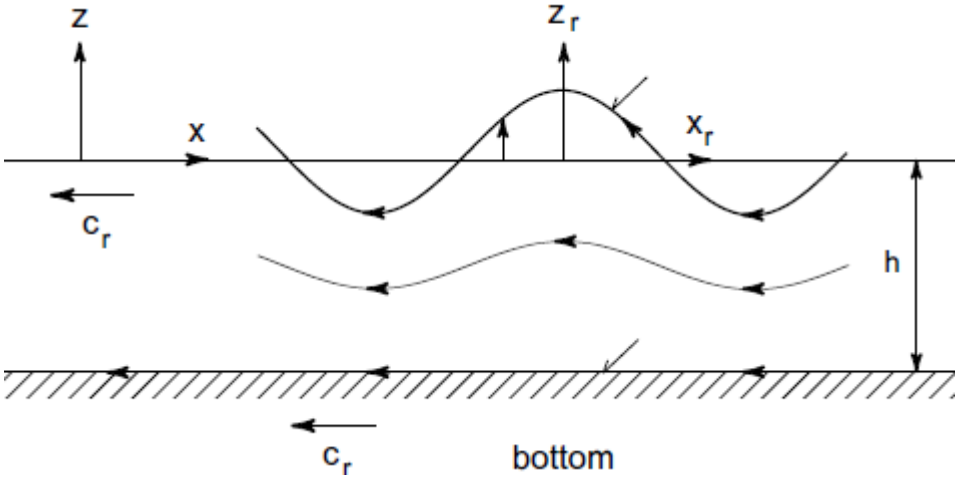

Figure 2.4: Stream function coordinate system from Brorson [2]

Potential theory - Stream function
We will again use potential theory and solve everything in the (x_r, z)-system. The flow will in this system be stationary, the surface elevation is constant! We are then allowed to use the stream function, which besides the velocity potential is a mathematical tool to represent flow in potential theory. Stream function is defined

in Kundu [15]:

$$u = -\frac{\partial \psi}{\partial z} \text{ , and } w = \frac{\partial \psi}{\partial x} \tag{2.30}$$

The governing equation, the Laplacian, is now due to the irrotational property:

$$\frac{\partial^2 \psi}{\partial z^2} + \frac{\partial^2 \psi}{\partial x^2} = 0 \tag{2.31}$$

Boundary conditions

A stream function has some important physical properties. A stream line, given by $\psi(x_r, z) =$ constant, will be tangent to the flow, which means no flow across a stream line! Another is that $\Delta\psi$ between two streamlines gives the volumetric flow rate in between. *The kinematic boundary* conditions will no simplify. No flow across the sea bottom becomes:

$$\psi = Q, \text{ on } z = -h \tag{2.32}$$

No flow across the sea surface becomes:

$$\psi = 0, \text{ on } z = \zeta(x, t) \tag{2.33}$$

This is indicated in figure 2.4. The constant Q is the total volumetric flow rate given by:

$$Q = \int_{-h}^{\zeta} u dz \tag{2.34}$$

The constant will be negative. The *Dynamic condition* given by equation 2.8 will also simplify due to stationary flow. The term $\frac{\partial \phi}{\partial t}$ will disappear, but includes the unknown constant R:

$$\rho g \zeta + \frac{1}{2}(u^2 + w^2) = R \tag{2.35}$$

Proposed solution

The main idea is to write ψ with a proposed solution, with the general form found in Brorson [2]:

$$\psi(x_r, z) = c_r(z + h) + \sum_{n=1}^{N} X(n) \sinh nk(z + h) \cos n(-\omega t + k x_r) + Q \tag{2.36}$$

The governing equation and the kinematic condition is now automatically satisfied. The stream function is even about the crest, same as the elevation. The solution is written as a Fourier series to an even function with N terms. N is the order of wave theory. The order needed depends on wave height and depth. This is shown in figure 2.3. The function gives periodicity since $\psi(x_r, z) = \psi(x_r + \lambda, z)$.

System of equations

The proposed solution must be inserted into the boundary conditions and evaluated at points in the (x_r, z)-system. For a wave of order N, we will have to evaluate at $N+1$ points (x_i) to get the required number of equations. Two boundary conditions at each point gives $2N + 2$ equations. The number of unknowns is:

- N unknown coefficents $X(n)$
- N+1 unknown surface elevations ζ_i at points x_i
- Q (in eq. 2.36)
- R (in eq. 2.35)
- k (the wave number in eq. 2.36)
- c_r (the phase velocity eq. 2.36)

We then need 3 more equations. We know that *mean elevation* must equal zero:

$$\bar{\zeta} = \int_0^L \zeta dx_r = 0 \tag{2.37}$$

In addition, the *phase velocity* is defined as

$$c_r = \omega/k$$

and finally the *wave height* is defined as:

$$H = \zeta_{max} - \zeta_{min}$$

The $2N + 5$ unknowns can be solved from the $2N + 5$ equations. These are non-linear, and require a Newton Raphson iteration which can be read about in Brorson [2].

Chapter 3

Irregular sea

The sea surface is irregular. It consists of many waves propagating upon each other. The wave components will often be assumed to propagate freely, but will in reality be able to interact with each other. The degree of interaction will depend on parameters as depth, significant wave height and peak period, which all will be discussed in this chapter. The sea is random in nature, and will never create the exact same elevation history twice. A tool to describe a surface is the energy spectrum, which will be presented in the first section. The creation of spectra, and the link between frequency- and time domain will be presented in the following. The Second order irregular model and methods to account for the free surface elevation will be described. This is important because of the shallow water at Doggerbank.

3.1 Wave spectra and linear time realizations

An irregular sea can be represented by summing linear regular waves. All interaction between wave components is then neglected, but the result is rather good in most cases because the error will be of 2^{nd} and higher order. The regular waves will have different phase, which is given randomly from a uniform distribution. We write the phase belonging to wave number i with ϵ_i. The wave profile can now be written as a sum of cosine functions:

$$\zeta(x,t) = \sum_{i=1}^{N} a_i \cos(-\omega_i t + k_i x + \epsilon_i) \tag{3.1}$$

By using linear waves, the resulting velocities and accelerations will be a sum of all the individual wave components in the same way (this is shown in the section about 2nd order theory).

Waves contains energy and the contribution per horizontal area of wave component number n, E_n depends on its wave amplitude:

$$\frac{E_i}{\rho g} = \frac{1}{2}a_i^2(\omega_i) \tag{3.2}$$

The wave amplitude can be written as a function of the wave frequency, Myrhaug [14].

$$\frac{1}{2}a_i^2 = S(\omega_i)\Delta\omega \tag{3.3}$$

If we let $\Delta\omega$ go to zero, $S(\omega_i)$ will be a continuous spectrum that distributes the wave energy related to frequency.

The wave spectrum is characterized by two important parameters:

- T_P = the period which contains most energy
- H_S = the mean value of height for the one third largest waves

These parameters are constant in the sea state, which often is defined to last for 3 hours. They will be explained in the following subsection. Different functions are used to describe the spectrum, and they all use H_S and T_P as input parameters. A much used spectrum is JONSWAP (Join North Sea Wave Project), which is given in DNV [6]:

$$S(f) = \frac{\alpha g^2}{(2\pi)^4} f^{-5} \exp\left(-\frac{5}{4}\left(\frac{f_p}{f}\right)^4\right)\gamma^{\exp\left(-\frac{1}{2}\left(\frac{f-f_p}{\sigma f_p}\right)^2\right)} \tag{3.4}$$

Where:

- $\alpha = 5(H_S^2 f_p^4/g^2)(1 - 0.287\ln\gamma)\pi^4$
- $\sigma = 0.07$, when $\omega < \omega_p$, and $\sigma = 0.09$, when $\omega > \omega_p$
- γ = peak enhancement factor

The γ-factor is found in Myrhaug as a function of Hs and Tp:

$$\gamma = \exp[3.484(1 - 0.1975\alpha\frac{T_P^4}{H_S^2})] \tag{3.5}$$

Where $\alpha = 0.036 - 0.0056Tp/\sqrt{Hs}$. These parameters are based on deep water studies. JONSWAP works fine for wind generated sea.

3.1.1 Introduction to the wave spectrum

The wave elevation process can be sampled in time, and a histogram can be created to show the occurrence of elevation heights. The result will create a probability

distribution of the surface. The mean surface value is set to zero, which equals the still water level. The variance is found from the sample.

$$\sigma^2 = \frac{1}{N}\sum_{i=1}^{N}\zeta(t_i)^2 \tag{3.6}$$

N is the number of sampling points. The variance depends on the sampling time length. When the measuring starts, it might be calm water and the variance is more or less constant. Then, when the wind starts to blow, the waves will grow larger which imply a change to the variance. We usually restrict a sea state duration to 3 hours. This is the time where we are allowed to assume constant sea state parameters T_P and H_S.

But how is the variance portion connected to a wave component? We find this by studying the variance from a linear irregular sea, found in Tucker [16]:

$$\begin{aligned}\zeta(t)^2 &= \sum_{i=1}^{N}\zeta_{Ai}\sin(\omega_i t+\epsilon_i)\sum_{j=1}^{N}\zeta_{Aj}\sin(\omega_j t+\epsilon_j) \\ &= \sum_{i=1}^{N}\sum_{j=1}^{N}\frac{1}{2}\zeta_{Ai}\zeta_{Aj}(\cos[(\omega_i-\omega_j)t+\epsilon_i-\epsilon_j]-\cos[(\omega_i+\omega_j)t+\epsilon_i-\epsilon_j])\end{aligned} \tag{3.7}$$

The variance is then found by averaging this expression in time. We will find that only the difference frequency-terms for $i = j$ gives contributions to the variance:

$$\sigma^2 = \frac{1}{T}\int_T \zeta(t)^2 = \sum_i \frac{1}{2}\zeta_{Ai}^2 \tag{3.8}$$

If we connect this with eq. 3.3, we see how the variance contribution from each spectral component is expressed by its wave amplitude. We see that the variance portion is the same as the energy portion.

The Spectrum is found by taking the discrete time history of wave elevation into the frequency domain by Dircrete Fourier Transformation (DFT). Each wave amplitude found in the elevation process will then be linked to a frequency. The DFT-procedure to find such spectral components is given below, and it is just a discrete form of the familiar Fourier Transformation (see Newman [17]).

$$\begin{aligned}Z(k) =& \frac{2}{N}\sum_{j=1}^{N}\zeta(j)\exp\big(-i\frac{2\pi k}{T}j\Delta t\big), \text{ for k = 1, N/2-1} \\ X(0) =& \frac{1}{N}\sum_{j=1}^{N}\zeta(j) \\ X(\frac{N}{2}) =& \frac{1}{N}\sum_{j=1}^{N}\zeta(j)\cos(\frac{\pi N}{T}j\Delta t) \\ Z(k) =& X(k) - iY(k)\end{aligned} \tag{3.9}$$

Z is the complex wave components, N is the number of time sampling points, T is the time signal length, and Δt the time spacing between sampling points. It is now a total of N numbers (of X and Y) in the frequency domain representing the signal, equal to the N sampling points of the original time signal. All the information is taken care of, and is valid for a general signal of any shape.

The complex wave components, Z, is actually the amplitude of the wave component, but with the random phase built in to it. Then we can create each spectral component given by:

$$S(k)\Delta\omega = \frac{X(k)^2 + Y(k)^2}{2}$$

This procedure must be repeated many times, for different time signals of the sea state, to create a spectrum that is a reliable representation of the sea state. A smooth spectra is calculated by averaging spectral values over short intervals of $\Delta\omega$. The MATLAB package WAFO [18] has a built in function "dat2spec.m" which calculate a spectral estimation from a given time signal. This will be used as a tool throughout the thesis.

The specter is also found analytically by studying the auto-correlation of the time signal. This is the covariance of the signal starting at time t, and the signal starting at some time $t + \tau$. This can be read about in Newman [17].

Seed
The ratio between real and imaginary parts of Z, taken from the samples, give the phase of each spectral component and will justify the assumption of random phases that is uniform distributed. This assumption will give us a linear wave elevation process, where all the wave components travel independently. Such a process is easy to construct by equation 3.1. A given set of random phases in the equation will always give us the same time signal. Random numbers are created by computer algorithms. We can control the computer to generate the same set of random numbers, by giving the "seed" to the random number generator. This is used in this thesis to be able to study different load models given by the exact same wave elevation history. The MATLAB function "rng.m" is used to specify the seed.

3.1.2 Link between Time domain and Frequency domain, DFT

The discrete analysis by DFT gives important relationships between time and frequency domain. The spectral components are found automatically at equal distant frequencies creating k waves over the time signal:

$$\omega_k = \frac{2\pi k}{T} \tag{3.10}$$

The highest frequency is the **Nyquist Frequency** and becomes:

$$\omega_{N/2} = \frac{2\pi k}{T} = \frac{\pi N}{T} = \frac{2\pi T/\Delta t}{T} = \frac{\pi}{\Delta t} \tag{3.11}$$

This is 1 half-wave over 1 time step. The longest frequency becomes 1 half wave over the whole period.

When given Fourier coefficients from DFT, the inverse procedure IDFT will reconstruct the original time signal:

$$\zeta(j) = X(0) + \sum_{k=1}^{N/2} \Big(X(k)\cos(\frac{2\pi k}{T} j\Delta t) + Y(k)\sin(\frac{2\pi k}{T} j\Delta t) \Big) \tag{3.12}$$

If we want a random sea, we can use Fourier coefficients found from the spectrum in combination with the random phases. The random phases ϵ_k distribute between real and imaginary values:

$$Z(k) = X(k) - iY(k) = \zeta_{Ak}\exp(-i\epsilon_k) = \zeta_{Ak}(\cos\epsilon_k - i\sin\epsilon_k) \tag{3.13}$$

The spectral components are chosen by the relationships provided by DFT, according to T and Δt of the chosen time signal. It has been important to have knowledge about this topic through my thesis, and will be shown in the subsection about MATLAB implementation.

3.1.3 Linear Kinematics

The kinematic spectra, $S_x(\omega)$, are easy to find because the kinematic amplitudes for each spectral component is a linear function of the wave amplitude given from the wave spectrum. Eq. 3.14 relates the kinematic amplitude to the kinematic spectrum.

$$x(\omega) = \sqrt{2S_x(\omega)d\omega} \tag{3.14}$$

The kinematic amplitudes are found from the linear velocity potential (eq. 3.19) evaluated at $z = 0$:

$$\begin{aligned} u(\omega) &= \omega a \frac{\cosh kh}{\sinh kh} \\ u_t(\omega) &= \omega^2 a \frac{\cosh kh}{\sinh kh} \end{aligned} \tag{3.15}$$

We then get the following expressions for the spectra by combining eq. 3.14 and 3.16, for then substituting $a = \sqrt{2S(\omega)d\omega}$.

$$\begin{aligned} S_{vel}(\omega) &= S(\omega)\omega^2 \frac{\cosh^2 kh}{\sinh^2 kh} \\ S_{acc}(\omega) &= S(\omega)\omega^4 \frac{\cosh^2 kh}{\sinh^2 kh} \end{aligned} \tag{3.16}$$

The result are shown in figure 3.1, plotted all the way up to the Nyquist frequency. The upper tail of the wave spectra has been a topic of much discussion. The derived acceleration spectra has a slow decay, and it is questionable in what degree it is

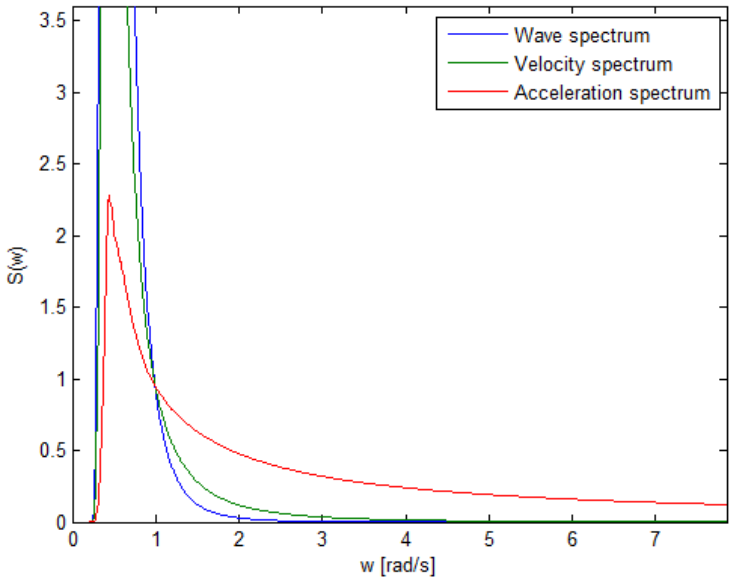

Figure 3.1: Velocity and acceleration spectra from a JONSWAP wave spectrum

physical or not. There will be to much energy in the higher frequencies. How to apply linear kinematics will be discussed later in the chapter. The wave spectrum is restricted to represent 1st order derivatives of the velocity potential, such as the velocity.

Figure 3.2 show surface elevation, velocity and acceleration at three different Δt. The highest frequency according to each time step, follows the Nyquist frequency $\omega_{Ny} = \pi/\Delta t$. The surface profile show no change between the time steps, the profile has converged. This might be confusing, because the plot of $\Delta t = 0.4$s is quite different from the others. However, the plots are the same at $t = 0$, but due to the inclusion of higher frequency components at smaller steps (through DFT), another realization is in fact created which will be more and more visible for increasing time. Also the velocity is seen to converge. There is on the other hand no sign of convergence in the acceleration profile. The plot has been done for a ten times finer time step, and still no sign of convergence. We must at some point truncate the spectrum to avoid high frequencies. We must be aware of that such a cut of frequency will affect our result, and might give significant changes in the outcome of dynamical response problems.

3.1.4 MATLAB implementation

It is important to have full knowledge about DFT because it gives full control between time and frequency domain. In the MATLAB implementation, the user

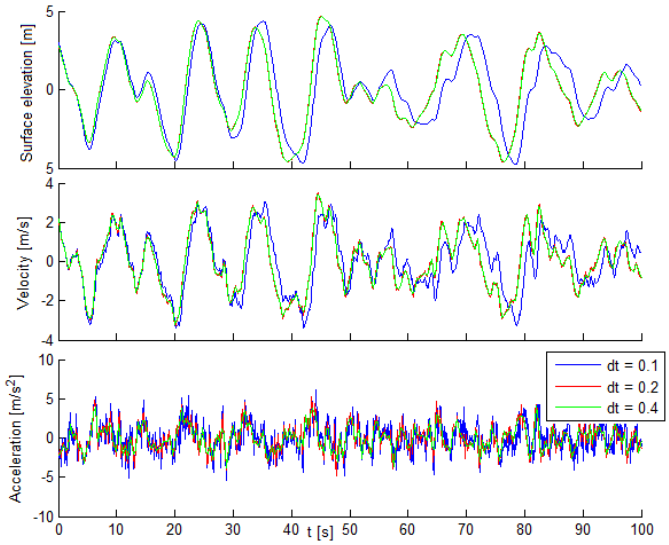

Figure 3.2: Convergence of surface elevation, velocity and acceleration by use of ω_{Ny}

specify the wanted length (T) and time step (Δt) for the wanted time signal. The program find the number of sampling points $N = T/\Delta t$, which it assure to be an even number. It will then need $(N/2 + 1)$ evenly spaced frequencies according to eq. 3.10, from $k = 0$ to $k = N/2$. The largest frequency (Nyquist frequency, ω_{Ny}) is only dependent on Δt (eq. 3.11), and a longer duration (T) gives a smaller step ($\Delta\omega$) between the spectral components. Figure 3.3 show these relations. The evenly spaced frequencies causes the signal to repeat at time T, because period T_k is the k-th multiple of time duration T. T is the least multiple for all T_k which means that all sine and cosine functions have turned back to the starting values, all functions at the same time.

A sea state should often be simulated for 3 hours. This is no point if the signal starts to repeat after 1 hour due to frequency components less than $N/2$. On the other hand, twice as many frequencies would contain enough information to create a signal of 6 hours. We see that DFT gives the optimal number, and must be used!

Cut specter from below

The program will automatically cut the specter from the left. It will start from left and find the component which has a ratio 10^{-9} of the mean specter value. These small frequencies contains very low energy, and the corresponding waves give approximately no contribution to the total wave elevation. Figure 3.4 show a specter with $H_S = 9.56m$ and $T_P = 12.76s$ with a logarithmic y-axis. It is unproblematic to cut these low frequencies in relation to the velocity and acceleration spectra, since they have even less magnitude for $\omega < 1$ due to the transfer functions

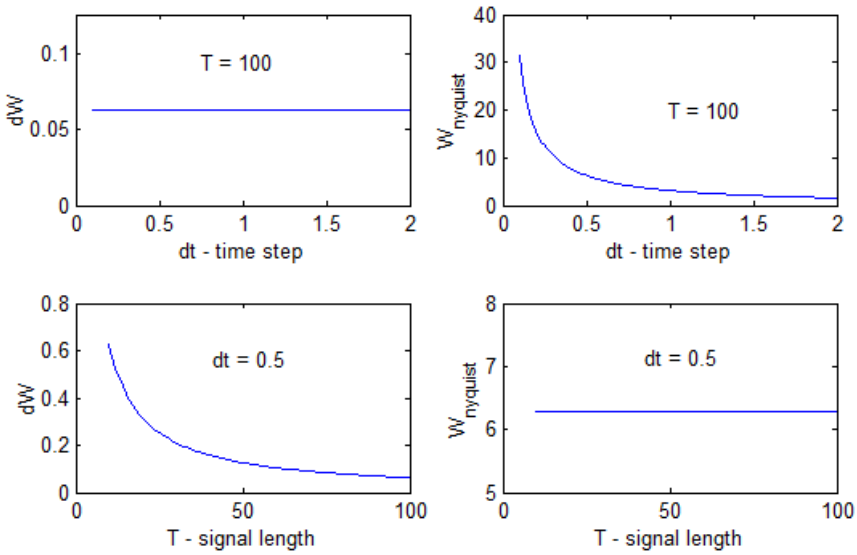

Figure 3.3: The relations between Δt and T to ω_{Ny} and $\Delta\omega$

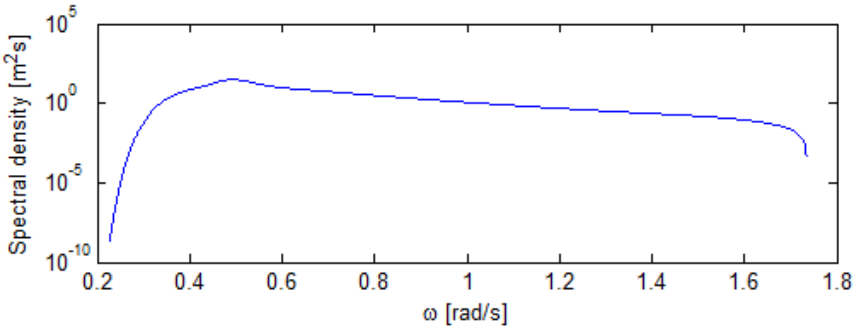

Figure 3.4: Cut of spectra, shown with logarithmic y-axis

given in eq. 3.16. In this specter $\omega_P = 0.493$, and the first included frequency is $\omega = 0.2287$. This will reduce the number of frequencies significantly!

Cut off frequency

The DFT is general and can take care of any signal. But for our sea elevation signal, the number of frequencies can be reduced a lot due to the shape of the wave spectrum. Figure 3.1 show how the wave spectrum (blue line) becomes almost zero long berfore ω_{Ny}. There is very little energy for high frequencies, and there is for some value ω no effect of including higher frequencies on the resulting signal in time domain. The program gives the opportunity to set a cut off frequency, and the need for this will be seen later in the chapter.

Fading at the Cut off frequency
The cut off frequency,ω_{max}, might be at a significant spectral value, which will introduce noise to the process. A simple linear fading is implemented in the code, stretching from ω_{max} to $1.2\omega_{max}$

3.2 Second order theory

In the chapter about wave theory, the waves are represented by a velocity potential. This is solved by satisfying the governing equation and the boundary conditions. All theory about second order waves at finite water depth is taken from the Master Thesis by Birknes [13]. The first order boundary condition is given in eq. 2.13. The irregular problem at first order is solved by assuming the following solution:

$$\phi^{(1)} = \sum_{j=-N}^{N} F(z) \exp i\theta_j \tag{3.17}$$

The second order boundary condition is given in eq. 3.18. The solution to the irregular problem is assumed to be:

$$\phi^{(2)} = \sum_{i,j=-N}^{N} F(z) \exp i(\theta_j - \theta_i) + At \tag{3.18}$$

The 2nd order problem is complicated to solve. The solution is given here, but a derivation is not included. This can be found in Birknes [13].

Velocity Potential

$$\phi^{(1)} = \sum_{j=1}^{N} \frac{ga_j}{\omega_j} \frac{\cosh k_j(z+h)}{\cosh k_j h} \sin\theta_j \tag{3.19}$$

$$\begin{aligned}\phi^{(2)} = &- \sum_{i,j=1}^{N} a_i a_j P_{ij}^{+} \frac{\cosh|k_i + k_j|(z+h)}{\cosh|k_i + k_j|h} \sin(\theta_i + \theta_j) \\ &- \sum_{i,j=1}^{N} a_i a_j P_{ij}^{-} \frac{\cosh|k_i - k_j|(z+h)}{\cosh|k_i - k_j|h} \sin(\theta_i - \theta_j) + At\end{aligned} \tag{3.20}$$

$$P_{ij} = -(1-\delta_{-i,j}) \frac{\frac{g^2 k_i k_j}{2\omega_i\omega_j} - \frac{1}{4}(\omega_i^2 + \omega_j^2 + \omega_i\omega_j) + \frac{g^2}{4}\frac{\omega_i k_j^2 + \omega_i k_i^2}{\omega_i\omega_j(\omega_i+\omega_j)}}{\omega_i + \omega_j - g\frac{|k_i+k_j|}{\omega_i+\omega_j}\tanh|k_i+k_j|h} \tag{3.21}$$

I will only use spatial derivatives of ϕ. The value A will not be of interest.

Surface elevation

$$\zeta^{(1)} = \sum_{1=1}^{N} a_i \cos\theta_i \tag{3.22}$$

$$\zeta^{(2)} = \sum_{i,j=1}^{N} a_i a_j E_{ij}^{+} \cos(\theta_i + \theta_j) + \sum_{i,j=1}^{N} a_i a_j E_{ij}^{-} \cos(\theta_i - \theta_j) \tag{3.23}$$

$$E_{ij} = -\frac{1}{g}(\omega_i + \omega_j)P_{ij} - (1 - \delta_{-i,j})\left(\frac{gk_ik_j}{4\omega_i\omega_j} - \frac{1}{4g}(\omega_i^2 + \omega_j^2 + \omega_i\omega_j)\right) \tag{3.24}$$

The Kronecker Delta ($\delta_{-i,j}$) is defined as 1 if $i = -j$, and 0 else. This is used so that both E_ij and P_ij is 0 when $\omega_i = -\omega_j$. The meaning of the indicy "$-i$" is as follows:

$$\begin{aligned} \omega_{-i} &= -\omega_i \\ k_{-i} &= -k_i \\ \epsilon_{-i} &= -\epsilon_i \\ P_{i,j}^{-} &= P_{i,-j}^{+} \\ E_{i,j}^{-} &= E_{i,-j}^{+} \end{aligned} \tag{3.25}$$

The equations has been implemented in MATLAB to represent a 2nd order time realization. How this is done is explained in the next subsection.

This theory will diverge and be unphysical when reducing water depth to shallow water. It is not known when the theory becomes too inaccurate for practical purposes.

Deep water.
2nd order theory is much used in deep water, where the equations get much simpler. The following equations are taken from Johannessen [19]:

$$\zeta^{(2)} = \sum_{i=1}^{N}\sum_{j=1}^{N} \frac{1}{4} a_i a_j \Big((k_i + k_j)\cos(\phi_i + \phi_j) - (k_i - k_j)\cos(\phi_i - \phi_j) \Big) \tag{3.26}$$

$$\phi^{(1)} = \sum_{i=1}^{N} a_i \frac{\omega_i}{k_i} e^{k_i z} \sin\phi_i \tag{3.27}$$

$$\phi^{(2)} = -\sum_{i=1}^{N-1}\sum_{j=i+1}^{N} a_i a_j \omega_j (k_i - k_j)\sin(\phi_i - \phi_j) e^{(k_i - k_j)z} \tag{3.28}$$

These equations base on the deep water dispersion relation, $\omega_i^2 = k_i g$.

Frequency to time domain for the surface elevation
The wave spectra represent all the wave components that creates the total elevation process. Waves in the elevation process can be of two different kind:

- Free waves propagating unaffected of other components. This is $\eta^{(1)}$, linear waves.
- Waves created by interaction of two or more wave components. This is $\eta^{(2)}$, non-linear waves

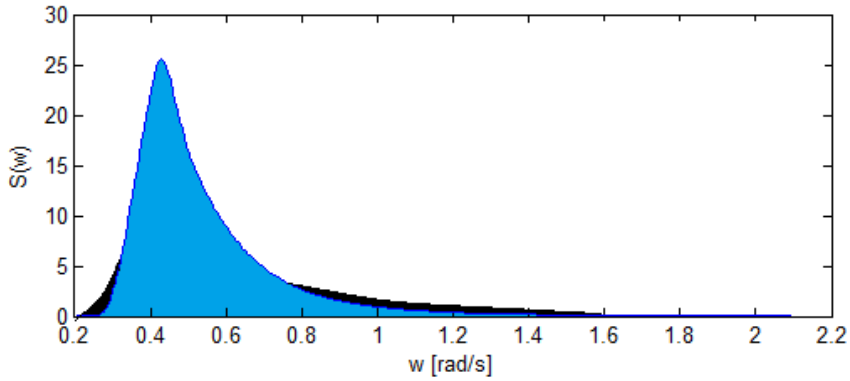

Figure 3.5: Spectra from non-linear process

Figure 3.5 show a wave spectra of a sea state (blue color). We must be careful when using 2nd order irregular theory, because the energy of the spectra is already contained in using $\zeta^{(1)}$ only. When adding $\zeta^{(2)}$ we will create to much energy in the process, colored black in the figure.

When going from time to frequency domain, all the waves will get the same type of representation independent of the wave is linear or non-linear. DFT procedure will represent the signal as amplitudes of free waves in the frequency domain. The procedure will only see the frequency, and do not know if this is a single, sum or difference frequency. When constructing the spectrum, the information about real and imaginary values are lost. The variance of the elevation process will be maintained in the spectrum, but the assumption of random phases following a uniform distribution is now violated.

An **iteration procedure** is required to create the correct balance between linear and 2nd order components, so they totally make up H_S.

Instead of using this approach which is comprehensive, there is good results in second order theory by introducing a **cut-off frequency**, given by DNV [12] and Stansberg [20]:

$$\omega_{max} = \sqrt{2g/H_S} \tag{3.29}$$

The frequency is proposed by Stansberg and valid at deep water. This will truncate the spectrum at the given value and let the higher order frequencies be due to the sum-spectral components at intermediate water. There is no sum-frequencies in the deep water model, and this will then be the highest frequency. We must be careful when applying a cut-off value because the velocity spectra and especially the acceleration spectra contains much more energy for high frequencies (see figure 3.1).

Instead of truncating the spectrum for the second order contribution, another method is to introduce a bandwidth parameter that restrict the maximum differ-

ence between frequencies allowed to interact. This will not be studied any further, but can be read about in Johannessen [4]. Figure 3.6 is taken from this paper and visualize the use of interacting frequencies in the bandwidth method and the cut-off frequency method.

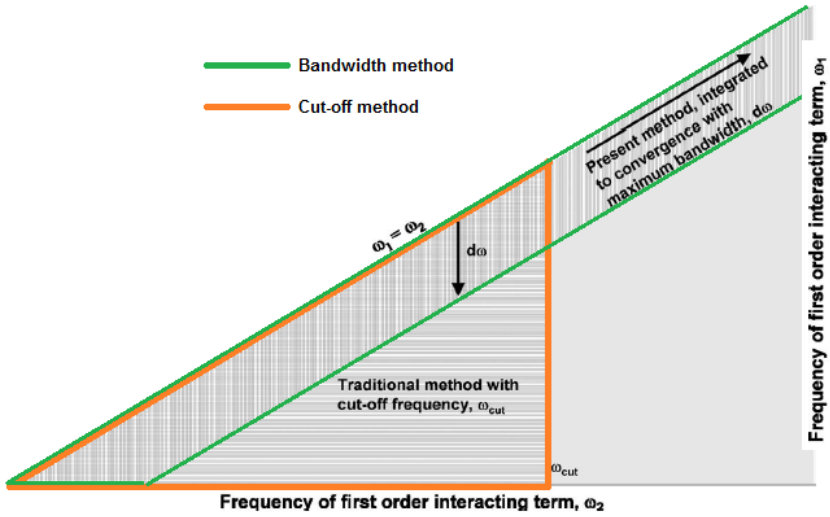

Figure 3.6: Bandwidth method for second order contribution, Johannessen [4]

3.2.1 MATLAB implementation, running time and verification

MATLAB implementation

Equation 3.12 show the IDFT procedure. Most commercial program use FFT algorithms of this equation to create a time signal from a spectrum with given random phases. This require all frequencies up to the Nyquist frequency, but is still the best approach regarding computation time. However, this require full knowledge about the applied FFT algorithm. It will also be comprehensive to implement in a 2nd order wave model.

IDFT has been used in the two MATLAB implemented codes "wave_profile.m" and "kinematics.m". The frequencies to involve can then be chosen freely. Equations 3.19 to 3.24 use summations over all frequency components. This will require 2 for loops i MATLAB. This will then be placed in one time loop, and also one vertical coordinate loop when calculating kinematics. This approach means 4 nested for loops, which will require very long computation time. This is NOT implemented.

MATLAB has built in functions for matrix multiplication which is extremely fast.

The equations are implemented by using a matrix **M** of size N^2. Each element contain a combination of the indices i and j. Matrix **M** will be evaluated in two nested loops, for time and z-coordinate. It is for each evaluation summed by using matrix multiplication with vectors containing wave amplitudes. This is shown below:

$$\phi(t,z) = \begin{bmatrix} a_1 & a_i & a_N \end{bmatrix} \times \begin{bmatrix} M_{11} & M_{1j} & M_{1N} \\ M_{i1} & M_{ij} & M_{iN} \\ M_{N1} & M_{Nj} & M_{NN} \end{bmatrix} \times \begin{bmatrix} a_1 \\ a_j \\ a_N \end{bmatrix}$$

Matrix M is in all cases symmetric as $M = M^T$ or $M = -M^T$. This is not utilized in the MATLAB code because the matrix multiplication is superior. This could be used to speed up the calculation if the code was implemented in FORTRAN.

The spectrum will automatically be cut at $\sqrt{2g/H_S}$ as presented above, when running second order calculations.

Running time

The running time is found for different time durations and time steps, and is the time for the calculation of linear, 2nd order deep and finite wave elevation and wave kinematics at the points needed in the Fedem model presented in chapter 5. It is the time length that increases the CPU time, because the cut-off value of

Duration [s]	100	250	400	550	700	850	1000
Delta t = 1s	0.74	0.9	1.99	4.19	7.94	14.1	22.14
Delta t = 0.5s	0.95	1.51	3.61	8.00	15.12	26.81	43.71

$\sqrt{2g/H_S}$ is applied. Half the time step will not increase spectral components, but only evaluate the matrices twice.

Verification of second order implementation

We have different tools to validate the implementation:

- Compare the elevations visually
- Compare the values obtained from finite and deep theory, due to the different implementations
- Finding the variance of the time signal
- Finding the specter

The small time steps applied in figure 3.2 are unnecessary to represent the surface elevation. A time step of $\Delta t = 1$s, should be short enough to study the process. Figure 3.7 show the different implementations for a time period of 300s. It shows how the 2nd order theory increase the crest heights, and that this is most distinct in the finite depth model. The water depth is 200m which makes the two theories

almost similar and easier to compare. Sea state parameters are given by sea state 1 in table 5.3 in chapter 5. The different implementations show good agreement. The standard deviation from 5 such calculations of different seeds are presented in

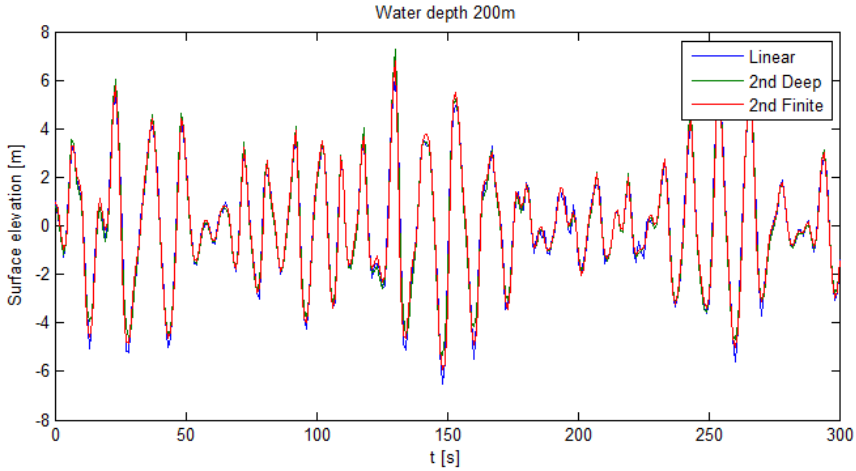

Figure 3.7: Wave elevation results for different theories

table 3.1. The wave spectra for each process has been calculated with the function

Seed number	Linear	2nd Deep	2nd Finite
1	2.3985	2.3951	2.4130
2	2.3870	2.4076	2.3924
3	2.3878	2.3986	2.3958
4	2.3925	2.3554	2.4268
5	2.3950	2.4016	2.4007

Table 3.1: Standard deviations calculated for different seeds

"dat2spec.m" from the MATLAB package WAFO. To increase the reliability of the spectral estimate, the time duration is increased to 3000s. The results are shown in figure 3.8, which show very good agreement between the implementations.

The wave kinematics has been verified the same way.

3.2.2 Finite Water depth and sensitivity to input parameters

The 2nd order irregular wave model at deep water will reduce the crest velocity due to the difference-frequency components. This might be unexpected because the wave elevation is given higher crests. Also eq. 2.22, the regular expression for $\phi^{(2)}$, give a sum-component which increases the crest kinematic. However, this

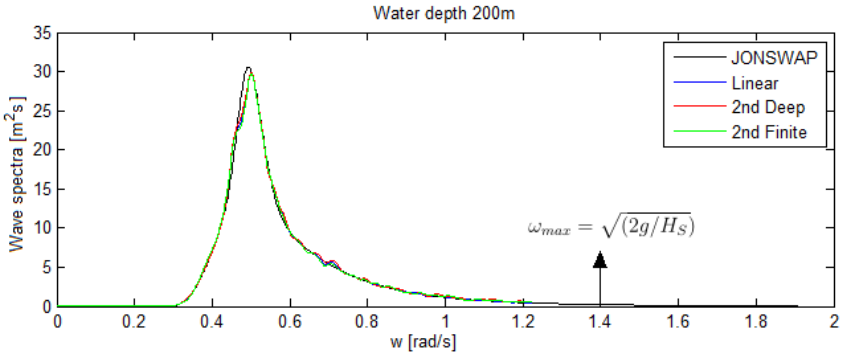

Figure 3.8: Wave spectra calculated from time series of $\Delta t = 1$ and duration 3000s

component will soon vanish moving onto deeper water. At intermediate water depths, the sum-frequency components will increase, and the higher crest velocity will also be observed in the irregular model.

Second order theory is not valid at lower water depths, because low frequency components become unphysical large. Exactly when the theory gives bad predictions is not known, but we can easily see how the difference frequencies blow up the results. Figure 3.9 gives the 2nd order finite surface elevation at 31.5m water depth together with the linear elevation. The result is not physical!

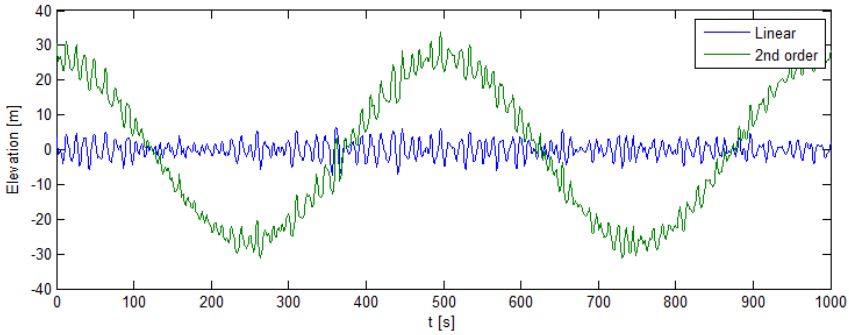

Figure 3.9: Unphysical enlargement of low frequency components in second order process

We will now study the effect of different parameters to the processes of surface elevation, velocity and acceleration.

Depth
Figure 3.10 show the impact of water depth to the standard deviation. The figure is found by calculating the surface elevation, velocity and acceleration at different water depths. Calculation has been performed for water depth 25m up to 30m, by

increasing the depth level by 0.2m. Then from 30m and up, with a step of 0.5m.

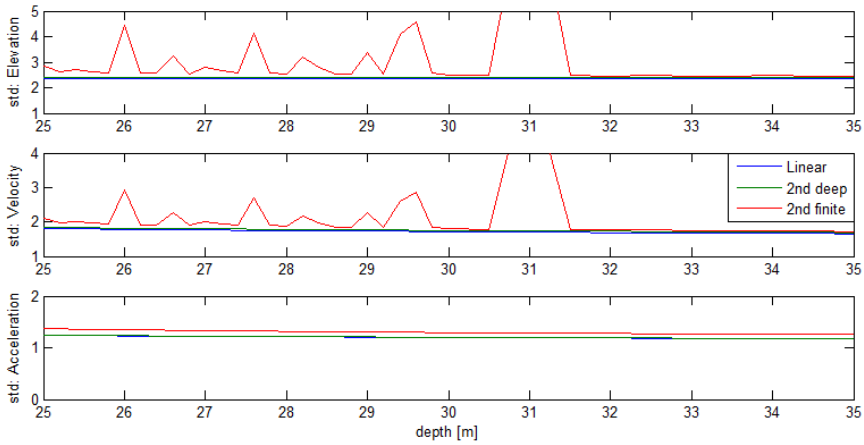

Figure 3.10: Standard deviation of surface elevation, velocity and acceleration (at MWL) for changing water depth

Seed
Changing the seed is not found to have any impact of the result given above, only small numerical differences.

Site parameters
Surprisingly, changing the site parameters H_S and T_P do not give much change to the result in figure 3.10. The problem must then be numerical.

Choice of Frequencies
The choice of frequencies to create the 2nd order contribution is found to create the blow-up of difference frequencies in my implementation. This is a numerical problem, and there is no physics in to it. This was found when investigating the result in figure 3.10 for different values of Δt and time duration. A such calculation is shown in figure 3.11. Figure 3.9 is the elevation process at depth 31.5m, the most

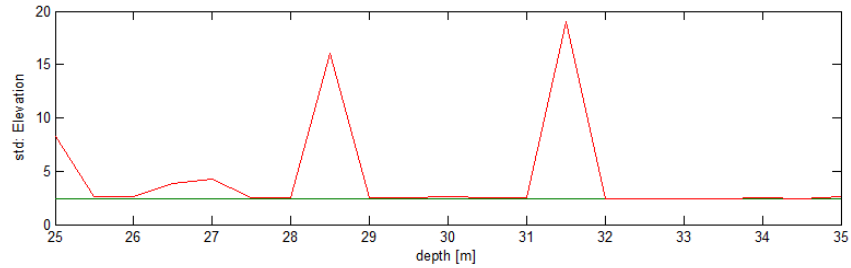

Figure 3.11: Standard deviation of surface elevation for changing water depth

extreme blow up according to the picture. This figure does not tell if the physics of 2nd order theory is valid or not at a given water depth, but in what degree we have numeric difficulties.

3.3 Kinematic models and MATLAB implementation

3.3.1 Extrapolations with Stokes theory

In **Stokes theory**, the velocity potential is only valid to the mean surface level at $z = 0$. For increasing order, the satisfaction of the true boundary condition at $z = \zeta$ will be better and better, but always imposed at $z = 0$. This is shown in figure 3.12 below. However, the velocity potential at the free surface is approximated by

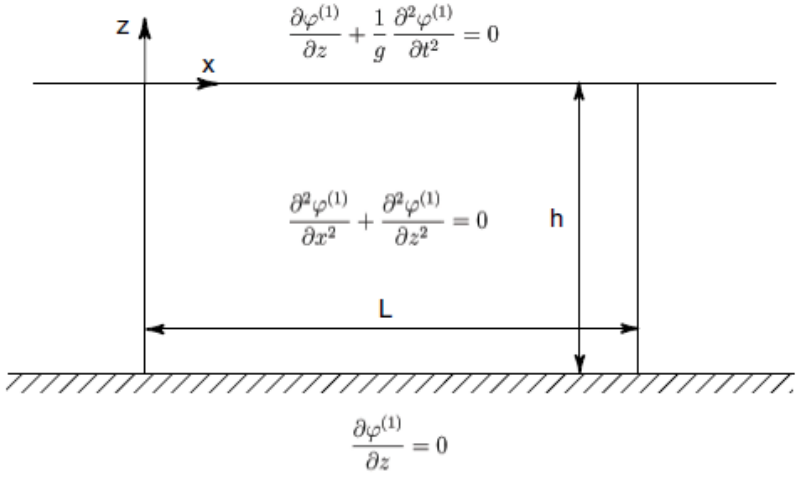

Figure 3.12: Stokes Boundary value problem, from Brorson [2]

Taylor expansion (see equation 2.12) which then actually gives the kinematics in both crest and trough. The wave velocity under a **crest** consistent to first order theory becomes:

$$u(x,z,t) = \begin{cases} \phi_x(x,t)\big|_{z=0} & \text{at } 0 < z < \zeta \\ \phi_x(x,z,t) & \text{at } z < 0 \end{cases} \tag{3.30}$$

The velocity at $z = 0$ will actually also be valid in the through, but this is difficult to visualize.

Extrapolation of the wave kinematics according to DNV [12] is done according to Stokes theory as shown above, but only in the crest. The kinematic at the trough surface is given by evaluating the velocity potential using $z = \zeta(t)$. This

method is then consistent to first order theory in the crest as given in equaton 3.30. Extrapolation to the second order use the same principle. It extrapolates the kinematic in the crest consistent to 2nd order according to Taylor expansion.

$$u(x,z,t) = \begin{cases} \phi_x^{(1)}(x,t)\big|_{z=0} + \phi_x^{(2)}(x,t)\big|_{z=0} + z \times \phi_{xz}^{(1)}(x,t)\big|_{z=0} & \text{at } 0 < z < \zeta(t) \\ \phi_x^{(1)}(x,z,t) + \phi_x^{(2)}(x,z,t) & \text{at } z < -\zeta(t) \end{cases} \tag{3.31}$$

Figure 3.13 show the resulting velocity distribution: The linear and 2nd order

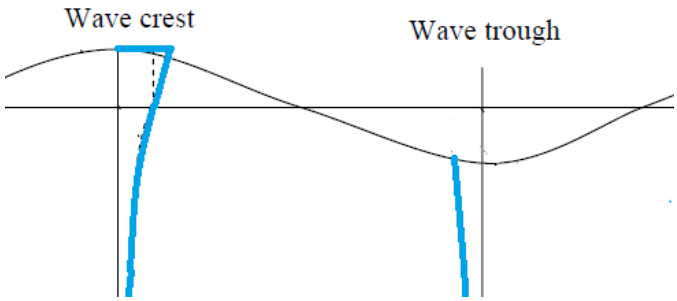

Figure 3.13: 2nd order extrapolation of wave kinematics

extrapolation is implemented in MATLAB, both using the finite and deep water theories.

3.3.2 Stretching

Stretched Airy theory, or the Wheeler modification, distributes the wave kinematic to the instantaneous wave elevation. Figure 3.14 shows how. We replace the z−coordinate in the expression for the velocity and acceleration with a modified coordinate according to formula 3.32 given by DNV [12].

$$z^{mod} = \frac{z - \zeta(t)}{1 + \zeta(t)/h} \tag{3.32}$$

The kinematic in the water column, from depth h to $z = 0$, is then at a given time instant stretched up or down to the instantaneous surface elevation. This is easy to implement in MATLAB, by making new stretched z-coordinates to the already calculated kinematics in z^{mod} according to eq. 3.32. The implementation allow us to choose kinematic order and which order of the surface elevation to use.

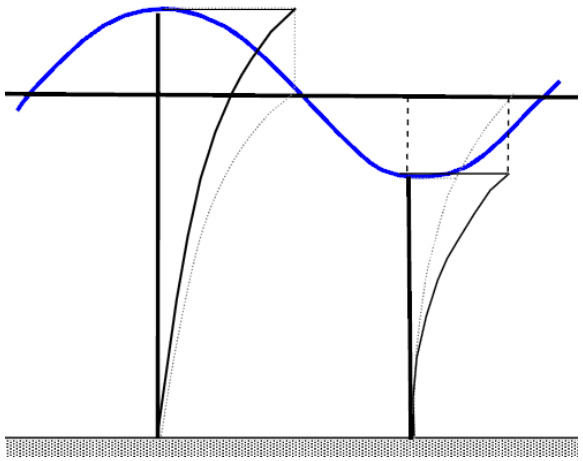

Figure 3.14: Stretching of wave kinematics from Usfos Hydrodynamics Manual [3]

3.3.3 Discussion of methods and where to truncate the spectrum

The extrapolation and stretching method is compared in Stansberg [20] for the resulting velocity at a regular crest. Stretching is shown to give a significant reduction of kinematics which is approximated by assuming the exponential profile (given as $\exp(kz)$ at deep water) to continue above the mean surface. We can then calculate the vertical shift in velocity from $z = 0$ to $z = \zeta_{max}$, where ζ_{max} is the crest height.

$$\frac{\Delta u}{u_0} = \exp(ka) - 1 \approx ka \tag{3.33}$$

The second order extrapolation give the crest velocity as

$$u = u_0 + \omega k a^2 \tag{3.34}$$

when inserting the deep water regular $\phi^{(1)}$ into equation 3.31, and denote the velocity at $z = 0$ as u_0.

The reduced crest kinematic due to a Stretching model will be reduced by using a second order elevation input. The crest velocity will then equal the second order interpolation. This will happen because all the wave components in the second order surface profile will be added as if they were free and linear near the surface. The velocity from the 2nd order amplitude, A, will be found as if it was linear. The relation between linear wave amplitude, a, and the deep water velocity is given by: $u_0 = \omega a$. The same relation will be for A, but then the wave frequency is 2ω. We also have the relation between 1st and 2nd order wave amplitude: $A = ka^2/2$.

$$u = u_0 + 2\omega A = u_0 + 2\omega(0.5ka^2) = u_0 + \omega k a^2 \tag{3.35}$$

The effect of this will be strongly reduced around $z = 0$, in which the result with second order elevation will be equal to that of first order elevation. This leads to prediction of kinematics with a reduction of approximately 10-20% around $z = 0$ and in the trough.

Stretching is also less robust because it violates the fundamental governing equation that all wave theories builds on. Another aspect is that the effect of the free 2nd order components which arise close to the crest must be restricted. Both Stansberg [20] and DNV [12] recommend to use a cut of frequency of 4 times the peak spectral frequency: $\omega_P = 2\pi/T_P$

$$\omega_{max} = 4\omega_P \tag{3.36}$$

This frequency is not based on any clear physical criteria, opposed to the cut off frequency $\sqrt{2g/H_S}$ applied in 2nd order theory.

Truncation of spectrum

We must truncate the spectrum, to avoid unphysical high frequencies. There are ongoing discussions about how this should be done, because the truncation in large degree decides the resulting kinematic, especially for acceleration as we could see in figure 3.2. However, the cut-off frequency proposed by Stansberg is well reasoned and must be used with *2nd order theory*. The highest possible frequencies will then become twice the cut of value, $2\omega_{max}$, due to the sum frequencies. The different kinematic models will later be compared, and they should be consistent with each other. Therefore the same cut-off value is chosen for all models.

Then, the time step needed to represent the processes must be according to the use of $2\omega_{max}$ as the Nyquist frequency (to include the sum-frequencies in the second order model). A table of cut-off frequencies and resulting time steps are shown in table 3.2. Sea state values will be presented in chapter 5, and the calculated cut-off values are according to H_S taken from table 5.3. I make it easy for myself

Sea state:	1	2	3	4	5
ω_{max}	1.4323	1.3808	1.3374	1.3050	1.2787
Δt_{ny}	1.097	1.1376	1.175	1.204	1.228

Table 3.2: Cut-off frequencies and time step according to Nyquist

and choose to use $\Delta t = 1$ in all the sea states. I will now show that this time step will be enough to represent all the effects created in a second order finite wave elevation. Figure 3.15 show a spline of $\Delta t = 0.01$s between data points calculated with $\Delta t = 1$ and $\Delta t = 0.1$. We must zoom in largely to distinguish between them.

3.3.4 Safe input parameter, depth, to second order model

All dynamic simulations with 2nd order kinematics will be done for a time step of 0.5 seconds, and a duration of 20 minutes. The static load calculations in chapter

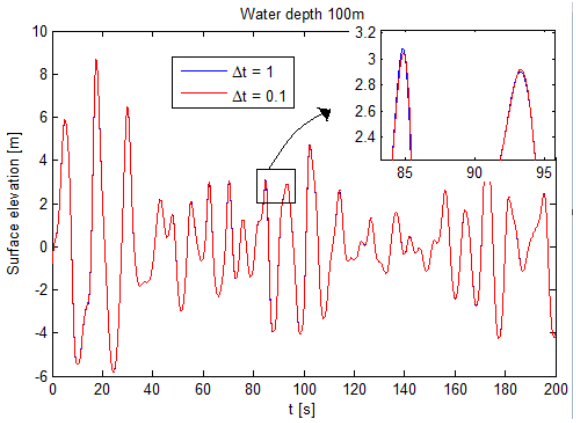

Figure 3.15: Spline between time realizations of different time steps

9 will be done for many seeds. To speed up the calculation, longer time durations will be split into simulations of 1000s. The time step will be 1s.

Sensitivity to input parameters were discussed in section 3.2.2. The result in figure 3.10 were done with the parameters needed in the dynamic simulation, and the analysis in figure 3.11 for the static at 25m. This analysis has been extended to include 45m. A safe depth as input parameter has been found for all calculations:

- Static calculation at h = 25m, $\Delta t = 1$, $T = 1000s$: 29m
- Static calculation at h = 45m, $\Delta t = 1$, $T = 1000s$: 45m
- Dynamic calculation at h = 25m, $\Delta t = 0.5$, $T = 1200s$: 30m

Figure 3.16 and 3.17 shows a cut from a time duration with parameters for the dynamic calculation at depth 25m. Site parameters are given from sea state 1, table 5.3. The cut will be further explored in the view of different load models in chapter 6. The kinematics in the first figure is given at MWL, both linear and finite 2nd order. The 2nd order correction increases the result due to the sum frequency components. This is opposite of the deep water correction which reduces the crest kinematics by the difference-terms.

The second figure show the extrapolated kinematics of both order calculated at the surface. We see how the linear model decreases below the surface level, and that the second order get a significantly increase in the crest due to the 2nd order term from the Taylor expansion.

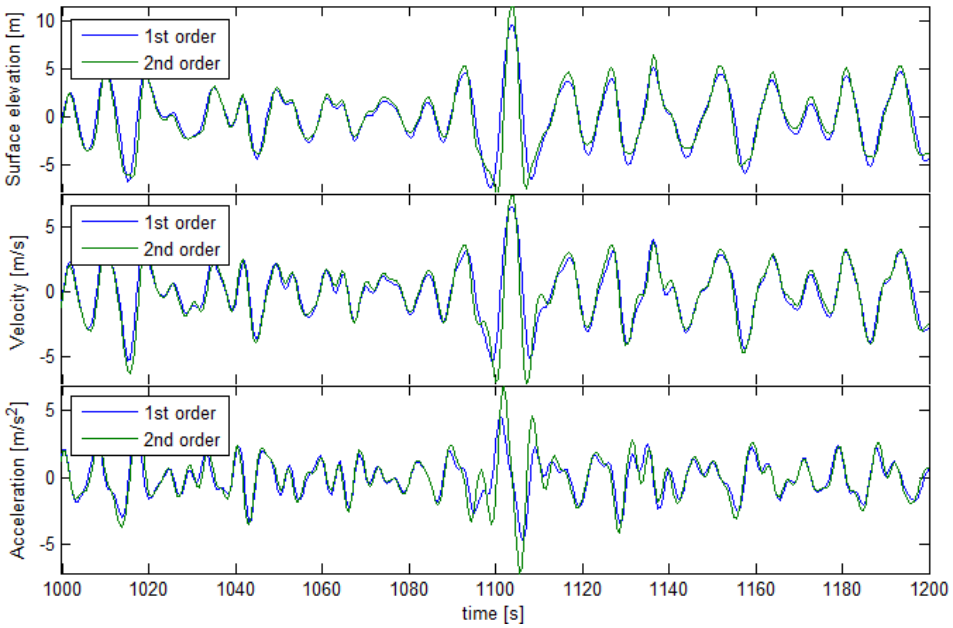

Figure 3.16: Processes at 30m water depth

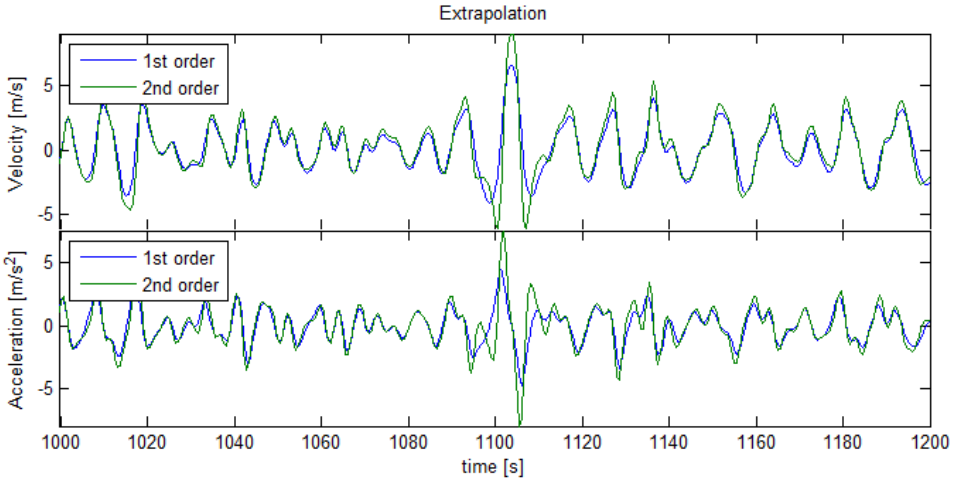

Figure 3.17: Processes at 30m water depth, extrapolation

Chapter 4

Industrial practice and standards

This chapter is written to highlight the ULS requirements in the design of offshore wind turbines. Three industrial standards are used:

- "Environmental conditions and environmental loads" by DNV [12]
- "Design of offshore wind turbines" by DNV [6]
- "Action and Action effect", NORSOK Standard [21]

The first standard gives a general recommended practice in the calculation of loads from wind, waves and current. It is meant to be a supplement to other more specialized standards, as the 2nd listed which gives the complete requirements to offshore wind mill design. The 3rd is a national standard which is created to ensure the offshore petroleum safety. The concepts and principles in these standards which are relevant for the design against ULS will be explained. Standard requirements are not always written precisely, and different methods might be recommended in offshore wind and petroleum respectively. In addition, more practical approaches might be useful. These aspects will be discussed in the last section.

4.1 Design loads and Principles

Safety classes
A safety class is determined in DNV [6] from the purpose of the structure. Three safety classes are involved:

- *Low safety class:* Failure imply low risk for personal injuries, pollution, economical consequences and neglible risk to human life.

- *Normal safety class:* Failure imply some risk for personal injuries, pollution and the possibility for large economic consequences.

- *High safety class:* Failure imply high possibility for personal injuries or fatalities, significant pollution and large economic consequences.

The wind turbine support structure and foundation will be unmanned and should be designed for the normal safety class. The *target safety* is an annual probability of failure of 10^{-4}. The high safety class, used for manned structure requires a probability of failure of 10^{-5}.

Limit States
When dealing with uncertain environmental loads at structures, dimensions must be made to tolerate forces up to an annual probability of excess. The annual probability of excess must be low to ensure the structure is safe and economic answerable. The standards give guidance for which level of probability a structure must be dimensioned for. DNV [6] and NORSOK [21] refer to the same design controls:

- Ultimate Limit State (ULS) - correspond to the maximum load-carrying resistance

- Accidental Limit State (ALS) - correspond to the maximum load-carrying restistance of (rare) accidental loads

- Fatigue Limit State (FLS) - correspond to failure cumulative damage of repeated loads

The annual probability of excess that the structure must be dimensioned for, depends on the life period of the structure. Oil and gas installations are usually dimensioned for a 100 year life period, and the *ULS* load will then be due to the worst load combination through these 100 years. That corresponds to an annual probability of excess of 10^{-2}. ALS control has become more important the last decade. This is to ensure that the structure tolerate loads given by more rare incidents with an annual probability less than 10^{-4}. This might be if an object is dropped from a crane by accident, or an extreme sea state causes breaking waves. FLS is to ensure the structure to tolerate fatigue through its life period.

ULS control at offshore wind mill structures is the concern through this work. These structures are dimensioned for a 50 year life span, and must then be prepared for loads of an annual probability of excess equal to 0.02.

4.1.1 Design by the partial safety factor method

A structure or a structural component will be designed so that the design load effect (S_d) is less than the design resistance (R_d).

$$S_d \leq R_d \tag{4.1}$$

When the structure is subject to a combination of simultaneous loads, the design load effect should be given by the most unfavorable combination, and there are two approaches to do this given by DNV [6].

Approach 1:

$$\begin{aligned} S_d &= \sum_{i=1}^{N} \gamma_{fi} S_{ki} \\ S_{ki} &= f(F_{ki}) \end{aligned} \tag{4.2}$$

The characteristic load effect S_{ki} (strain or stress) is determined in a structural analysis from the characteristic load F_{ki} which can be a bending moment, torsion or shear force. Partial safety factors are included as a conservative safety margin to increase the design load. The approach assume independent loads which makes the total load effect a linear function of the involved processes. This approach should be used when a best possible dynamic response representation is the primary concern.

Approach 2:

$$\begin{aligned} S_d &= f(F_{d1}, ..., F_{di}, ..., F_{dN}) \\ F_{di} &= \gamma_{fi} F_{ki} \end{aligned} \tag{4.3}$$

The design load effect is determined in a structural analysis using the design loads directly, and allows a non-linear combination of loads. This approach should be used when the concern is a proper representation of material and geometric non-linearities.

4.2 Searching for the most unfavorable load effect

We let all slowly varying environmental parameters like H_S, T_P and wind speed, U, be gathered in the vector $\vec{z}$. The joint probability density function of these parameters is denoted $f_{\vec{z}}(\vec{z})$. The conditional probability density function of the largest value of a specified load or load effect, X, in a sea state of duration τ, given the parameters $\vec{z}$, is given by

$$f_{X_\tau}(x \big| \vec{z}) \tag{4.4}$$

Structural failure is described by a limit state function, which is defined as negative in the domain of failure. We define a critical value x_{crit} which will create failure, and let the value $x_p(\vec{z})$ be a percentile from the conditional distribution of X_τ.

$$F_{X_\tau}(x_p|\vec{z}) = p \tag{4.5}$$

Then we get failure as a function of the environmental parameters $\vec{z}$:

$$g(\vec{z}; x_{crit}) = x_{crit} - x_p(\vec{z}) \tag{4.6}$$

This defines a region of integration of all the parameters in $\vec{z}$. The integration limits of variable x is defined as $x_{crit} < x_P(\vec{z})$.

The probability of failure p_F is determined by the following expression, Haver [22]:

$$p_F = \int \int_{g<0} f_{X_\tau}(x|\vec{z}) f_{\vec{z}}(\vec{z}) dx d\vec{z} \tag{4.7}$$

where $d\vec{z} = dz_1 dz_2 ... dz_N$.

We want to determine the value x_{crit} which the structure must tolerate. The value p_F is the annual probability of excess equal to 0.02, according to the 50 year life span.

$$p_F = \frac{\tau}{50 \times 365 \times 24} \tag{4.8}$$

when τ is measured in hours. Remember that eq. 4.4 distributes the largest value in each sea state.

Choosing a dimensioning property X
The value X in the distribution must be an important dimensioning property at the structure. At a monopile wind mill foundation, *the overturning moment* and *the base shear force* at the sea bottom are such important design parameters. These will be investigated throughout this work.

Partial safety factor approach
Our structure is subject to wind and wave loads simultaneously, and the approaches given by equation 4.2 and 4.3 will not be feasable. DNV [6] tells us to instead establish the characteristic load effect S_k as a function of the simultaneous loads, and then apply a common load factor to get the design load effect:

$$\begin{aligned} S_d &= \gamma_f S_k \\ S_k &= f(F_{k1}, ..., F_{ki}, ..., F_{kN}) \end{aligned} \tag{4.9}$$

S_k will be the stochastic variable X in equation 4.7. The ULS load factor, γ_f, is given by the standard:

- $\gamma_f = 1.35$
- $\gamma_f = 1.1$ - In abnormal wind load cases

4.2.1 Long term statistic analysis - All sea state approach

The challenge in establishing ULS loads is to provide reliable statistical data to base the calculations. Environmental conditions with long return periods must be extrapolated from the available data. Larger amount of reliable data decreases the uncertainties in these estimated extreme load and load effects. This is discussed in chapter 5 about site conditions. **Metocean** data is required, which is scatter diagrams with frequencies for the combinations of different environmental parameters. We will in the following assume that fair enough data is provided.

Lets us look at the overturning moment, X, determined (arbitrary) of H_S alone given by eq. 4.5. The wind speed might be determined by $U = \mathrm{E}(U|H_S)$ and $T_P = \mathrm{E}(T_P|H_S, U)$. The relation between X and H_S is illustrated as the blue line in figure 4.1a. This is the easiest way to represent eq. 4.7, since there is only one environmental parameter. The red line gives the critical value, and the two separate black colored areas show where the limit state function is negative. The green line is the PDF of Hs (scaled to be visible on the figure).

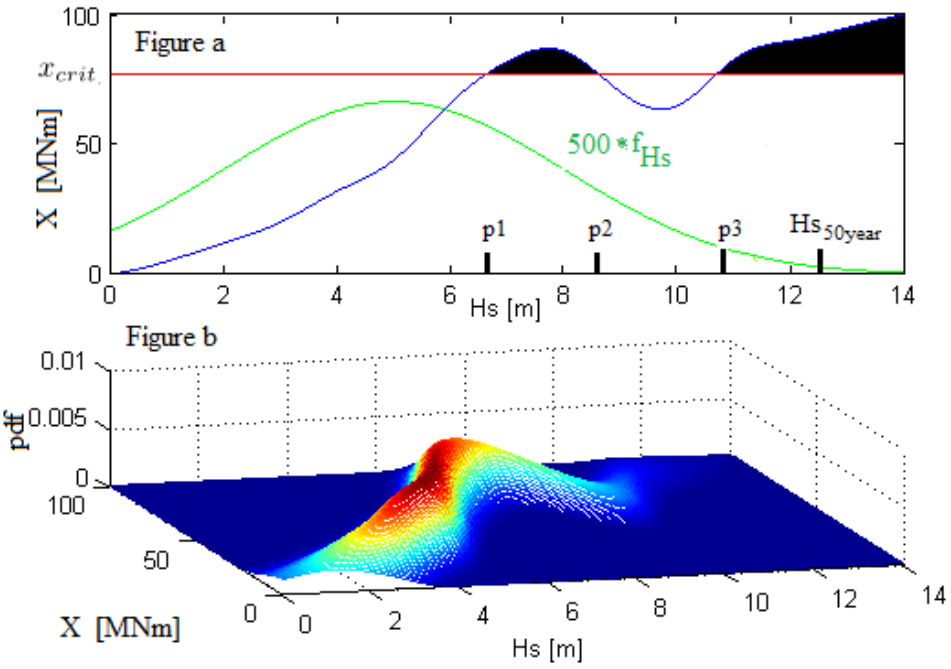

Figure 4.1: Contour line

Figure b shows an arbitrary joint probability density function of X and H_S that lies upon figure a (this PDF is what we integrate in eq. 4.7, over the black areas in figure a). The density in the example show to concentrate around the green line in figure a, the value x_p from eq. 4.5 with $p = 50\%$. We see how the probability density function in dimension H_S (the x-axis) diminishes to almost nothing up to the 50 year value. The probability of structural failure from eq. 4.7 get a contribution from both areas. **The x_{crit}-level is the unknown parameter**, and is found by solving the equation with the probability of failure, p_F, given by eq. 4.8.

Difficulties with N environmental parameters
When X is a non-linear function of the environmental process, the value x_p in eq. 4.5 must be found by repeated analysis in the time domain for each combination of environmental parameters in $\vec{z}$. It will be very time consuming to establish this relation even with only 2 or 3 parameters (as Hs, Tp and U). Unless the limit state function is established, and all involved probability distributions are known, the value x_{crit} of a 50 year return period can not be solved. The *contour method* is an approach to avoid the problem and find the dimensioning values!

4.2.2 Contour method

We will now assume that the PDF in figure 4.1b is even more concentrated around the median value, so it actually can be treated as a Dirac-Delta function:

$$f_{X\big|\vec{z}} = \delta\big(x - x_p(\vec{z})\big) \tag{4.10}$$

The integration over x in eq. 4.7 is then avoided due to the integration property of the Delta function. Equation 4.7 is then simplified to:

$$p_F = \int\int_{g<0} f_{\vec{z}}(\vec{z}) d\vec{z} \tag{4.11}$$

The problem is the limit state function, g, which is still unknown.

The integration limits in figure 4.1a would be: $p1 < Hs < p2$ and $Hs > p3$, with the points pi market on the x-axis. However, this process can NOT be solved with the contour method. Contour lines of equal probability, which for this one dimensional case becomes points, are given directly by the PDF (green function in figure a). The requirement for using the contour method is that lower and lower exceeding probability, must respond to a higher and higher response value. This is not the case in the example, where the x_p-value creates two black areas.

However, in the given example, the parameter Tp is a function of Hs. If we treat them as two independent variables, we have to look at a two dimensional domain. Figure 4.2 show statistics from a site in the North Sea, Haver [23]. A scatter diagram is plotted with the following contour lines created by extrapolation of the

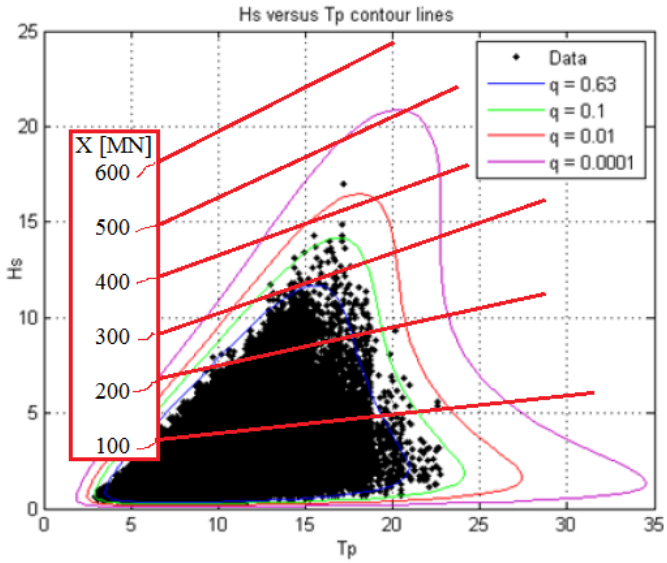

Figure 4.2: Arbitrary contour lines with arbitrary Overturning Moment Response

data. The probability of being outside the outer contour is 10^{-4}. Arbitrary contour lines for overturning Moment Response, is put onto the figure with red lines.

The figure show how **the maximum response value on a contour increases for decreasing contour exceeding probability**. If this is assumed to be true for the characteristic load or load effect that is studied, the contour line method will give reliable results! Finding x_c from equation 4.7 is then reduced to finding the maximum value X_τ along the environmental contour of probability p_F.

4.3 Proposed load cases by DNV

DNV propose different load cases for the ULS control. It combines environmental conditions in different windmill operative situations. All ULS cases are for the return period of 50 years. Here are some examples of operative situations that must be tested for ULS:

- Power production: Conditions combining wind and waves
- Power production plus occurrence of fault
- Start up
- Normal shut down
- Emergency shut down

- Parked, standing still: Extreme wave and wind conditions

Some of the load cases involve the wave conditions of 50 year return period. These are given in table 4.1.

Design situation	Load case	Wind condition	Wave condition	Other conditions	Other
Power production	1.6a	NTM $v_{in} < U_{10,hub} < v_{out}$	SSS $H_S = H_{S,50yr}$	Wind generated current, 1-year water level	
	1.6b		SWH $H = H_{50yr}$		
Parked, standing still, or idling	6.1a	EWM Turbulent wind $U_{10,hub} = U_{10,50yr}$	ESS $H_S = H_{S,50yr}$	50-year current 50-year water level	
	6.2a		EWH $H = H_{50yr}$		Loss of electrical network connection (abnormal)
	6.1c	RWM Steady wind $U_{10,hub} = 1.1 \times U_{10,50yr}$	ESS $H_S = H_{S,50yr}$		

Table 4.1: Proposed load cases by DNV

Abbreviations:

ESS	The extreme sea state
EWH	The extreme wave height
EWM	The Extreme Wind Speed Mode
NTM	The Normal Turbulence Model
RWM	The Reduced Wind Speed Model
SSS	The Severe Sea State
SWH	The severe wave height

4.3.1 Load case 6.1a and 6.2a

Load case 6.1a and 6.2a will be investigated throughout this work.

Load case 6.1a
Load case 6.1a use the extreme sea state. The significant wave height shall be taken as the 50 year return period from the *unconditional* distribution of Hs. F_{Hs} is the fitted distribution to available data, and the distribution of one year maximum value is given by the following relation:

$$F_{Hs,1yr}(Hs_{1yr}) = F_{Hs}^{N} \tag{4.12}$$

Where N is the number of sea states per year. The design sea state, Hs_{50yr}, is then found by the 98% value from this distribution:

$$Hs_{50yr} = F^{-1}_{Hs,1yr}(0.98) \tag{4.13}$$

T_P variation shall be done at Hs_{50yr}, by choosing reasonable values. This method of variation is not given precisely.

Load case 6.2a
Load case 6.2a use the extreme wave height. This wave height is the one single wave with a return period of 50 years. This shall be based on long term analysis from scatter diagram, to establish the unconditional probability distribution of the single wave height $F_H(h)$:

$$F_H(h) = \int_{Hs}\int_{T_P} f_{H|H_S,T_P}(H|H_S,T_P) f_{H_S,T_P}(H_S,T_P) dH_S dT_P \tag{4.14}$$

This distribution will be powered with the expected number of waves through one year, N, to create the distribution of the annual largest wave:

$$F_{H,1yr}(h) = F_H(h)^N \tag{4.15}$$

The largest wave through the 50 year design period is then found by the 98% value:

$$H_{50yr} = F^{-1}_{H,1yr}(0.98) \tag{4.16}$$

The wave period of this wave shall be varied, which in deep water is given by

$$11.1\sqrt{H_{S,50yr}/g} \leq T \leq 14.3\sqrt{H_{S,50yr}/g} \tag{4.17}$$

where $H_{S,50yr}$ is the significant wave height from load case 6.1a. At shallow water, the period will have a lower limit due to the consideration of wave breaking:

$$T > \sqrt{34.5\frac{h}{g}\tanh^{-1}(\frac{H}{0.78h})} \tag{4.18}$$

Wind condition
The load cases shall be combined with the extreme wind speed model, EWM, with turbulence. The 10 minute mean wind speed of 50 year return period at the hub height, $U_{10,50yr}$, shall be used and is found from a conditional distribution of U_{10} given H_S. Turbulence shall be modeled with the standard deviation taken as: $\sigma_{U,c} = 0.11 \times U_{10,50yr}$.

Misalignment
The misalignment between wind and waves is specified to be misaligned in multiple directions. Misalignment shall be based on statistical data. Multiple load directions shall be considered, and the worst case shall be taken. Multiple directions is specified as not required on the axisymmetric monopile.

4.4 Discussion and comments

4.4.1 Kinematic reduction factor

A wave kinematic reduction factor can be used to account for the actual wave directionality on an irregular sea surface. DNV [12] recommend to use such a factor in the design calculations using extreme waves and sea states (load case 6.1a and 6.2a). Another view is stated in Haver [23]: The directionality in extreme wave events differ from normality, in such a way that the waves can be assumed to be more or less long crested when hitting the structure. A kinematic reduction factor is recommended to not be included.

The value is not included in the calculations. This might be conservative. The reduction factor is defined as the ratio between the r.m.s. (root middle square) value of the in-line velocity and the r.m.s. value of the velocity in an unidirectional sea. The factor is found to reduce the loads by 10-15%.

4.4.2 Searching for design loads

Load case 6.1a require us to search for extreme loads with sea state parameters given by a reasonable Tp variation at the 50 year significant wave height, $H_{S,50yr}$. This is different to the practice given in NORSOK [21], which require the analysis to follow the 50 year contour line. The use of 50 year contour line for design purposes is well reasoned on a statistical basis, but the Tp variation at $H_{S,50yr}$ is not.

Guidelines for the range of Tp variation is not given, as it is for the wave period to be used with the design wave in load case 6.2a. However, the variation must be reasonable, and it seems reasonable to base the variation on the conditional distribution of Tp given Hs, $f_{T_P|H_S}(t)$. This distribution will anyway be available because it is needed to establish the contour line. The mean value of the distribution will be the actual Tp-value connected to $H_{S,50yr}$. The probability level of a lower limit for the variation will in the next chapter be chosen. The Tp level might be unphysical due to wave breaking consideration, and this will be accounted for.

Accounting for the short term response variability
The contour line method will underestimate the extreme response levels by neglecting the response variability due to different short term sea state realizations, DNV [12]. This results from replacing the conditional distribution of X with a Delta-function using the median value, $x_{50\%}$, see eq. 4.10. The method works well in the example, where the joint distribution (figure 4.1*b*) actually is concentrated around this value. To account for the short term variability in non-linear problems, the standard tells us to instead use the $x_{90\%}$-value, or multiply $x_{50\%}$ with a factor of 1.1 to 1.3.

The method of Tp-variation at $H_{S,50yr}$ might be another solution to the problem, but the high $x_{90\%}$-value is at the time specified to be used.

Extreme value distribution
In a narrow banded process, where the surface elevation is assumed to be Gaussian distributed, a Rayleigh distribution is used to distribute the peaks. Narrow banded means that the process only includes a short range of frequency components, which results in only one peak between each zero up crossing. The distribution is taken from Myrhaug [14]:

$$F_H(H) = 1 - \exp\left(-2\left(\frac{H}{H_S}\right)^2\right) \tag{4.19}$$

A parameter X that has a linear relation to H, will get the same distribution by substitution of the H-value. Also the extreme value distribution used for H will then be valid for parameter X. This is the Gumbel distribution, DNV [12]:

$$F_G(x) = \exp\left(-\exp\left(\frac{x-u}{a}\right)^2\right) \tag{4.20}$$

The following relations give the mean and variance:

$$\begin{aligned} \sigma =& 1.283a \\ \mu =& u + 0.557a \end{aligned} \tag{4.21}$$

Parameters which are not given by the Rayleigh distribution, can also be assumed to follow the Gumbel distribution. This is useful to create the extreme value statistics of non-linear loads and load effects.

The short term response variability must be given an estimate for each combination of Hs and Tp. Time realizations must be carried out for a number of seeds, and the Gumbel distribution must be fitted to the largest value found through each. Each realization should be given a duration of 30min to 3 hours, depending on the environmental parameters to consider.

The standards do not specify clearly how the design values shall be found. The approach in this work is to run 20 seeds of 50 minute time duration for each sea state. The value $X_{90\%}$ is found from a Gumbel estimate, and the mean across considered sea states is found as the final design parameter.

4.4.3 Design wave parameters: H_{50yr}

The way of finding the PDF of wave heights by equation 4.14 is extensive. A short cut can be done to get approximate values for the design wave. This is done by using the conditional distribution of wave heights, $F_{H|Hs,Tp}$, and using values of Hs and Tp along the 50-year contour line. The sea state lasts for 3 hour, and

the expected number of waves through this duration is found directly by the wave spectra, by calculating the mean wave period:

$$T_1 = 2\pi \frac{\int_0^\infty S(\omega) d\omega}{\int_0^\infty \omega S(\omega) d\omega} \tag{4.22}$$

This gives $N = 3600 \times 3/T_1$. The distribution of the largest wave in the sea state is then found:

$$F_{H_{max,3hr}} = F^N_{H\big|H_S,T_P}(h) \tag{4.23}$$

The preliminary value of the design wave of 50 year return period can now be found as a percentile of this equation. Statkraft [24] use this method, and the percentile is set to 0.85:

$$H_{50yr} = F^{-1}_{H_{max,3hr}}(0.85) \tag{4.24}$$

This method will be used in chapter 5 to calculate the design wave.

Chapter 5

Site conditions and the Fedem Windmill model

5.1 Site Conditions

Dogger Bank is located east of England covering an area of 8549.43 square kilometers. There is ongoing planning and feasibility studies of the creation of several large wind farms at different locations. The water depth, shown in figure 5.1, ranges from 20 to 50 meters, which makes it suitable for bottom fixed windmill structures. The harsh environment in the North Sea combined with shallow water, creates challenges when determining design loads to the foundation structure. Non-linear wave models as presented in the previous chapters is important to get the best possible and realistic description of the wave loads.

The irregular sea models need the sea state parameters H_S and T_P, and all the wave induced loads will at the end be determined by this. It is important to know these values with a low uncertainty, to best determine the design loads. However, it is difficult to get certain values, especially when determining the values for ULS. We need parameters for sea states with a return period of 50 years. This is done by analyzing scatter diagrams of H_S and T_P and using the contour method as described in chapter 4.2.2. Data material to establish reliable values would need to be very extensive and gathered for a very long time. The extensive amount of data is usually not available, and fitting of probability distributions to the available information must be done to extrapolate the information to regions of low probability.

The scatter diagram of H_S and T_P values are usually created by a hindcast model, which in the field of oceanography is a numerical model used to extend available data to periods and areas where no observations have been done. Such data is provided by the Norwegian Meteorological Institute. Sea state data for each 3 hours

over the last 50 years is available at several locations in the North Sea, including Dogger Bank. In an internal report by Statkraft [24], this data material is analyzed. Eight different locations with different water depths have been considered. The sea state parameters with a return period of 50 years are determined, and they are found to be quite similar for the different locations. Three such sea states found in the report are given in table 5.1. In the master thesis by Engebretsen [1], a

Sea state	Hs	Tp
1	10	14.7
2	11	15.2
3	12	15.8

Table 5.1: Extreme sea states at Dogger Bank.

complete 50-year contour line is calculated at a location just north of Dogger Bank (shown in figure 5.1). The water depth is 80.6m. The contour line is given in figure

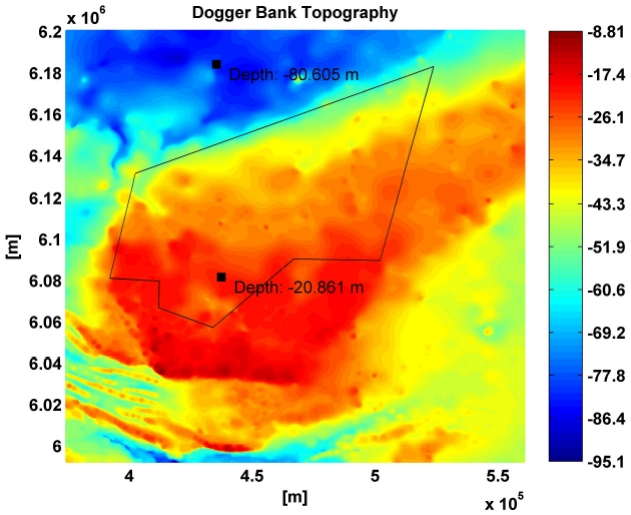

Figure 5.1: Dogger Bank Topography taken from Engebretsen [1]

5.2, and we see that it agrees with the selected sea states from the Statkraft report which are pointed in. The given sea states could actually been found from the same data material, with the values of T_P taken as the expected value given each H_S. This is assumed to be true throughout this work, and the given contour in figure 5.2 will serve as the basis in all load calculations. We see in figure 5.2 that the contour is only valid when $H_S > 4.79$m. This is because only these values were used when the probability distribution was fitted to the data.

In the thesis of Svangstu [25], a wave tank experiment of waves changing on a sloping bed was performed. Engrebretsen [1] builds on this study and concentrates

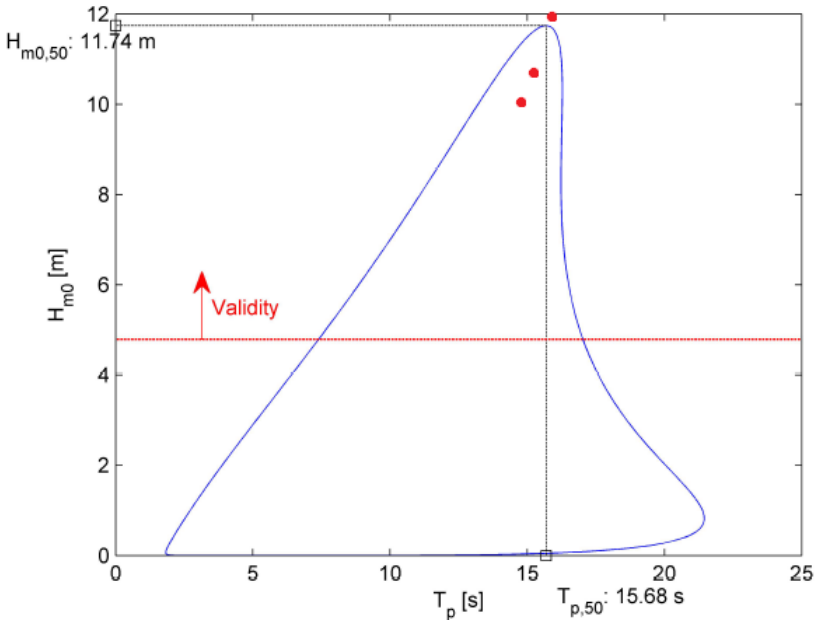

Figure 5.2: Contour line taken from Engebretsen [1]

much about the suspicion that the hindcast model from the Norwegian Meteorological Institute over-predicts the H_S values at Doggerbank, due to shallow water effects which are not included in the calculation. A numerical program that calculates the change in a wave spectra due to propagation on a sloping bed, is used to simulate how the sea state values of 50 year return period changes between the northern and southern point (figure 5.1). The sea state values at the northern point is assumed to be well predicted by the hindcast model and serve as input to the analysis. The result is compared to the experiments by Svangstu and concluded to be within agreement.

The H_S values found by Engebretsen are significant smaller than the corresponding values from the hindcast model.

	Initial		Engebretsen		Hindcast model	
Sea state	Hs [m]	Tp [s]	Hs [m]	Tp [s]	Hs [m]	Tp [s]
1	12.00	16.80	7.42	16.89	10.20	15.98
2	10.10	15.32	7.31	15.38	8.60	15.03
3	10.10	14.64	7.08	14.64	8.30	14.45

Table 5.2: Change in H_S values for 3 large storms propagating to shallow water at Doggerbank: Results by Engebretsen [1] compared to the hindcast model by the Norwegian Meteorological Institute.

It is also stated in the Statkraft report [24] that the values in the report is only really reliable to about Hs= 6m, and that the values in extreme sea states might be as much as 10% over-predicted. The conflicting information, makes it difficult to choose sea state values.

5.1.1 Extreme Sea state parameters for load case 6.1a

It seems to be very conservative to base the design loads on sea state parameters according to table 5.1. However, the values from Engebretsen are not verified, and in absence of other values, there is no other choice than basing the calculations on the conservative values as required by the standards. More research about how waves transform from deep to shallow water might be a large cost benefit for the offshore wind industry.

Contour line
Selected sea states in the search for design loads are presented in table 5.3. Number 1 to 4 is taken from the contour line by Engebretsen, and number 5 is the sea state of the maximum Hs-value in table 5.1. The sea states is only picked out from the contour to the left of this point, where the T_P value is lower. The effect of dynamic amplification is then increased, and critical design loads might be found even though the H_S values are lower. The contour line is obtained without considering

Sea state	Hs	Tp
1	9.56	12.76
2	10.29	13.52
3	10.97	14.28
4	11.52	15.04
5	12.00	15.80

Table 5.3: Extreme sea states at Dogger Bank.

wind speed or directionality, according to the recommended practice described in subsection 4.3.1.

Tp variation according to the load case
As described in chapter 4, the standard require us to vary the T_P value at the largest Hs (given by eq. 4.12). This will be Hs = 12, from sea state 5 in table 5.3. The Tp values shall be reasonable varied, but further guidelines are not given. The variation seems reasonable to do in the basis of the conditional distribution of Tp given the largest Hs. The distribution, $f_{Tp|Hs}(t)$ used by Engebretsen [1] to construct the contour line is applied. The distribution is evaluated at Hs = 12, and a distribution of Tp is found. The result is given in figure 5.3. The variation will be done with lower Tp values, again to trigger the dynamics. The colored area is given to Tp = 14 which correspond to the probability of a little less then 2.5%. The value might be unphysical in terms of creating breaking waves, taking

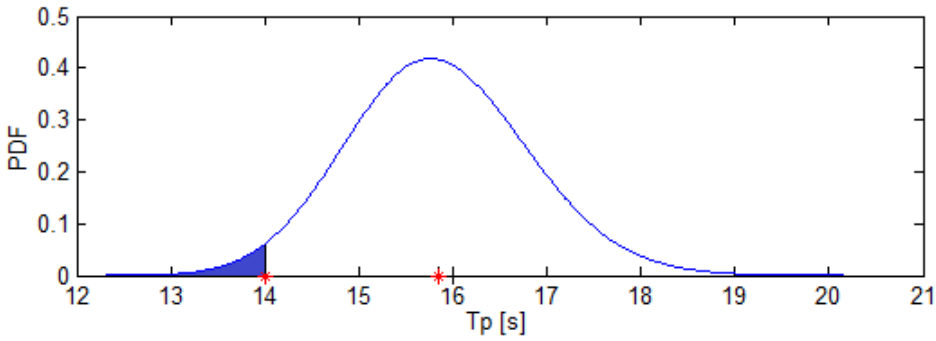

Figure 5.3: Contour line

the water depth in to consideration. This has been assessed with the embedded stream function method that will be outlined in chapter 8.4. 40 stream function waves were embedded in to stochastic realizations at a large crest. Wave breaking were shown at 25 locations, but the Tp value will still be chosen to increase the variation of the results. The many wave breakings in the sea state might be seen as a critique to the method of Tp variation. Three Tp values will be considered:

| 14.0 | 14.9 | 15.8 |

Table 5.4: Tp variation at Hs = 12m

Chapter 6, 7 and 9.1.1 use sea state 1 in table 5.3 in the irregular sea calculations. Chapter 8 and 9.3 assess load case 6.2a using sea state 5.

5.1.2 Extreme wave parameters in load case 6.2a

The extreme wave height according to load case 6.2a is found from long term analysis. It is reasonable to assume that the largest wave will occur in one of the sea states of 50 year return period, given in table 5.1. The approach described around equations 4.23 and 4.24 will be used to find H_{50yr}. The method require the conditional probability distribution of H, such as the Rayleigh distribution in eq. 4.19. More sophisticated distributions are presented below.

Næss proposed a modified input parameter to the Rayleigh distribution to account for the band width in the wave spectrum, DNV [12]:

$$F_H(H) = 1 - \exp\left(-\left(\frac{H}{\alpha_H H_S}\right)^2\right) \tag{5.1}$$

		Height [m]	Crest [m]
Depth	Sea state	Naess	Forristall
25m	1	18.94	13.57
	2	20.81	15.35
	3	22.66	17.19
45m	1	18.94	11.80
	2	20.81	13.11
	3	22.66	14.50

Table 5.5: Extreme waves as parameters to load case 6.2a

The value α_H is given by:

$$\alpha_H = \frac{1}{2}\sqrt{1-\rho} \tag{5.2}$$

The paramater ρ describe the bandwidth and is by the standard proposed to be a function of the peak enhancement factor γ in the JONSWAP specter given in eq. 3.4.

$$\rho = -0.000191\gamma^3 + 0.00488\gamma^2 - 0.0525\gamma - 0.605 \tag{5.3}$$

Forristall distribution is used to distribute the crest heights and is based on a second order wave model. The distribution is found in DNV [12]:

$$F_C(C) = 1 - \exp\left(-2\left(\frac{C}{\alpha_C H_S}\right)^{\beta_C}\right) \tag{5.4}$$

The parameters are given in the standard as a function of the wave steepness and the Ursell number (see eq. 2.27), both based on the mean wave period from the specter and the corresponding deep water wave number.

50 year wave heights
Calculation of the design wave height at water depth 25m and 45m according to equation 4.23 and 4.24 is done in MATLAB and presented in table 5.5. The sea state numbers refer to table 5.1. The modified Rayleigh distribution by Næss is used to calculate the wave heights (the Rayleigh distribution gives to large values by not including the spectral band width effects).

Wave breaking
It is not given that the values in table 5.5 are physical. Due to depth limitations, it must be checked if some of the values should be limited by wave breaking. This is done by using Stream function theory of order 10. A wave period is needed in the assessment. The deep water T-variation to be applied with H_{50yr} (T_{low}-T_{high}) are given by equation 4.17. The lower limit must in addition be adjusted to T_{lim} by depth limitations, see eq. 4.18. Values obtained from these equations are given in table 5.6, using the wave heights at 25m. The resulting complex numbers of T_{lim} in sea state 2 and 3 indicate that the wave heights are unphysical. Table 5.7 show the breaking limits calculated using the obtained values T_{low} & T_{high}. We see from

State	T_{low}	T_{high}	T_{lim}
1	11.2	13.63	14.3
2	11.75	15.14	complex
3	12.28	15.82	complex

Table 5.6: Wave period variation at deep water and the depth limited value at 25m water depth

	25m depth		45m depth	
Hs	Hb at T_{low}	Hb at T_{high}	Hb at T_{low}	Hb at T_{high}
10	17.55	18.74	26.13	31.06
11	17.86	18.86	27.28	31.68
12	18.10	18.96	28.23	32.17

Table 5.7: Wave breaking limits in meters at $T_{low}(H_S)$ and $T_{high}(H_S)$ determined by 10th order Stream Function Theory

this analysis that the wave breaking limit is exceeded for all the waves at depth 25m, even when applying T_{high}. To be able to perform a reasonable wave period variation at 25m, the design wave is chosen as the breaking height at T_{low}. Then the deep water T-variation can be used. It is the highest wave that is interesting for the load case, and then the parameters for the analysis are determined:

- H = 18.10m
- $T_{low} = 12.28$s
- $T_{high} = 15.82$s

5.2 The Fedem Windmill model

This work will assess the effects of non-linear wave loads on the monopile substructure at two different water depths. The Dogger Bank topography can be studied in figure 5.1, and the chosen depths are in the lower and upper limits of feasible wind farm areas:

- $h = 25m$
- $h = 45m$

Such different water depths are chosen to give a better illustration of the effect of depth from the wave loads. Structural models are created in the program Fedem at each depth. The models have been used to determine dimensions by modal analysis. Only the 25m model will be used for dynamic simulations in the time domain.

A very short introduction to Wind turbines are given, then the design basis and a detailed description of the Fedem model is presented.

5.2.1 Offshore Wind turbines, monopile substructure

Wind turbines used for commercial production of electric power are with few exceptions created as horizontal axis wind mills. The blades are mounted to a hub which again is connected to a nacelle containing the gearbox and the generator. The nacelle is placed on top of a tower, which again for the offshore installations, is placed on top of a substructure. Different substructures have been proposed as suitable foundation for offshore wind turbines. Different design concepts is shown in figure 5.4. The monopile is a popular alternative, due to the relatively cheap fabrication,

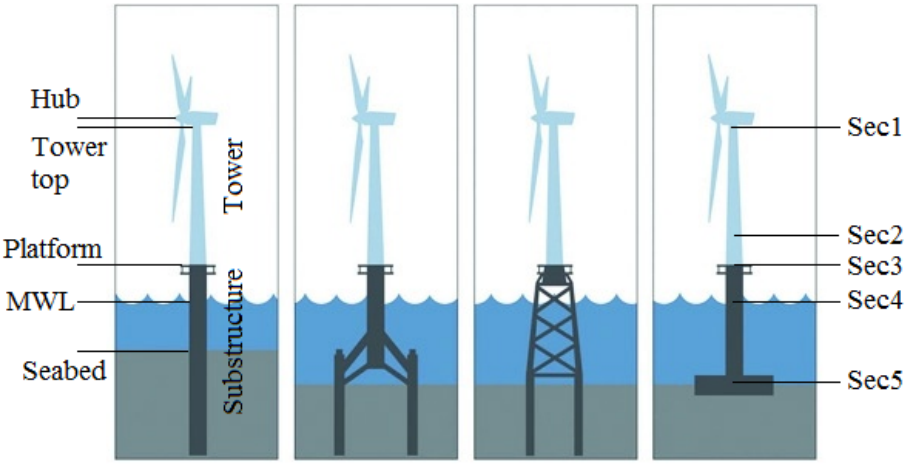

Figure 5.4: Different windmill substructure concepts [5]

which is important in the creation of many similar structures. A monopile structure is according to DNV [6] well suited for areas with movable seabed and scour, and where the water depth is less than 25 meters. At deeper water, the monopile shall be supported by additional beams piled into the soil at the foundation. The possible disadvantage is the high flexibility giving a lower natural frequency compared to windmills using other substructure foundations. The natural frequency is then closer to the frequencies from environmental loads, which imply that dynamic amplification is more likely to occur. Deflection and vibration of the tower might be a problem.

Platform level
The platform is shown on figure 5.4. This is created for installation, maintenance and inspections. The level must be placed in a safe distance above the highest crests that are expected to occur through the 50 year design period.

1P and 3P
1P and 3P is a fundamental consideration of all wind turbines. The wind mill get cyclic excitation created by the turning airfoils, mainly at the rotation frequency ($1P$) but also significantly at the blade passing frequency ($3P$). This gives strict limitations on the natural frequencies to avoid resonance in the structure. The frequency of the first bending mode in the structure happen to be of the same magnitude as 1P and 3P, and is therefore placed between these two frequencies. The lower and upper frequency range of 1P creates an allowed range to place the natural frequency. This will be shown in figure 5.5 for the actual design.

5.2.2 Upwind design Basis

The wind mill model in Fedem is based on the turbine in part B of the Upwind Design Basis [26]. This is designed for a water depth of 25m. The design is again based on the NREL (National Renewable Energy Laboratory) generic 5.0 MW turbine. The properties of the NREL generic turbine are given in table 5.8.

Property	**Value**	**Unit**
Rated power	5	MW
Rotor diameter	126	m
Mass of rotor and nacelle	350	ton
Cut-in wind speed	3	m/s
Rated wind speed	11.4	m/s
Cut-out wind speed	25	m/s
Nominal rotor speed	0.202	Hz
Lower bound rotor speed	0.115	Hz
Upper bound rotor speed	0.202	Hz

Table 5.8: NREL generic 5MW design

The lower and upper bound of rotor speed creates the allowed range for the first natural frequency between: $0.202 - 3 \times 0.115$. A safety margin of 10% is in addition applied as shown in figure 5.5.

Some dimensions of the tower are given in table 5.9. Sec1 and Sec2 refer to the cross sections pointed out in figure 5.4. The heights refer to the mean water level, MWL. The tower is shaped as a cone.

	Height [m]	Diameter [m]	Thickness [mm]
Hub	85.16		
Sec1	82.76	4	30
Sec2	14.76	5.6	32

Table 5.9: Upwind design

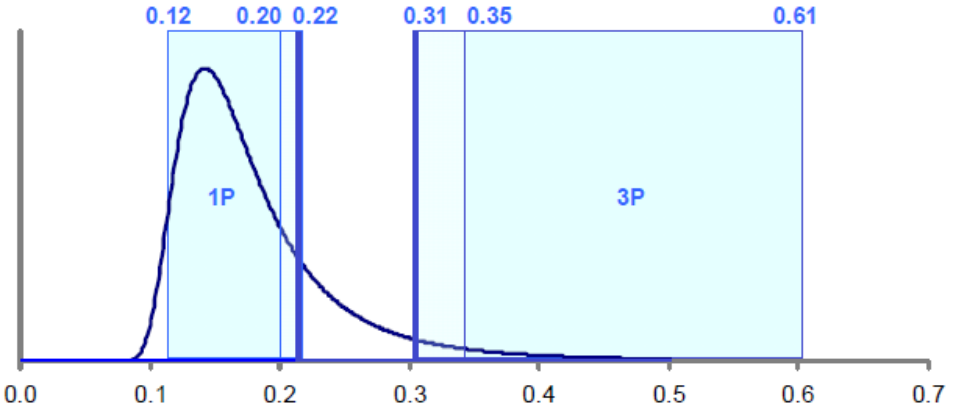

Figure 5.5: Allowed frequency range between 1P and 3P

5.2.3 Fedem model

The Fedem model follows the Upwind design basis. The natural frequencies in the Upwind model is unknown, but we know the allowed frequency range of 0.22-0.31Hz. The same dimensions are mainly kept in the tower, but the substructure is modified to adapt the models in to the allowed frequency range. The total mass of rotor and nacelle in the built 5MW model in Fedem is different from the mass given in the Upwind Design Basis. This might be the reason for the needed modifications also at the 25m model. The final dimensions for both water depths are given in table 5.10.

	Height [m]	Diameter [m]	Thickness [mm]
Hub	85		
Sec1	83	4	35
Sec2	25	5.6	35
Sec3	15	6.00 / 8.00	35
Sec4	0	6.00 / 8.00	50 /35
Sec5	-25 / -45	6.00 / 8.00	50 /35

Table 5.10: Dimensions of the Fedem models

Table 5.11 gives the natural frequencies of the structures. YZ refer to bending in

Description	h = 25m	h = 45m
First bending, YZ	1.555	1.277
First bending, XZ	1.556	1.278

Table 5.11: Natural frequencies of the Feedem models given in rad/s

the YZ-plane, which is the plane of the rotating blades. The first mode in each direction is easy to find using Fedem. The values of the second bending mode is not given: These are more difficult to determine because Fedem find all modes, including more local modes in the blades and nacelle components. The 2nd bending mode is of little interest in terms of dynamic excitation, but it gives a significant contribution in the quasi-static response picture. This is due to large deflections along the substructure and tower in its modeshape, which then is significantly excited by wave loads.

Comment
The 45m substructure violate the requirements that 1P and 3P sets to the natural frequency (see figure 5.5). The frequency could not be further increased, without creating a monopile of completely unrealistic dimensions. The chosen diameter is set to 8m, which is above the fabrication capabilities at the present day. This indicate that another substructure concept should be applied at depth 45m.

Structural coefficients

- Top mass, $226 tons$
- Steel density, $\rho = 7850$ kg/m^3
- Poissons's ratio, $\nu = 0.3$
- Young's modulus, E = 210 000 MPa
- Shear modulus, G = 81 000 MPa

The complete model, with a closer view at the monopile substructure and the soil pile model is shown in figure 5.6. The substructure is created by beams that are linked by nodal points. The wave loads will be applied in these nodal points, and a closer distribution around the MWL is chosen to improve the effect of free surface load integration. The soilpile model is built in to Fedem and is also created by beams. The model gives a more realistic boundary condition at the sea bottom, including the effects of soil stiffness and soil damping. The structural damping of the beams in the substructure and in the soil model will be discussed in chapter 7.

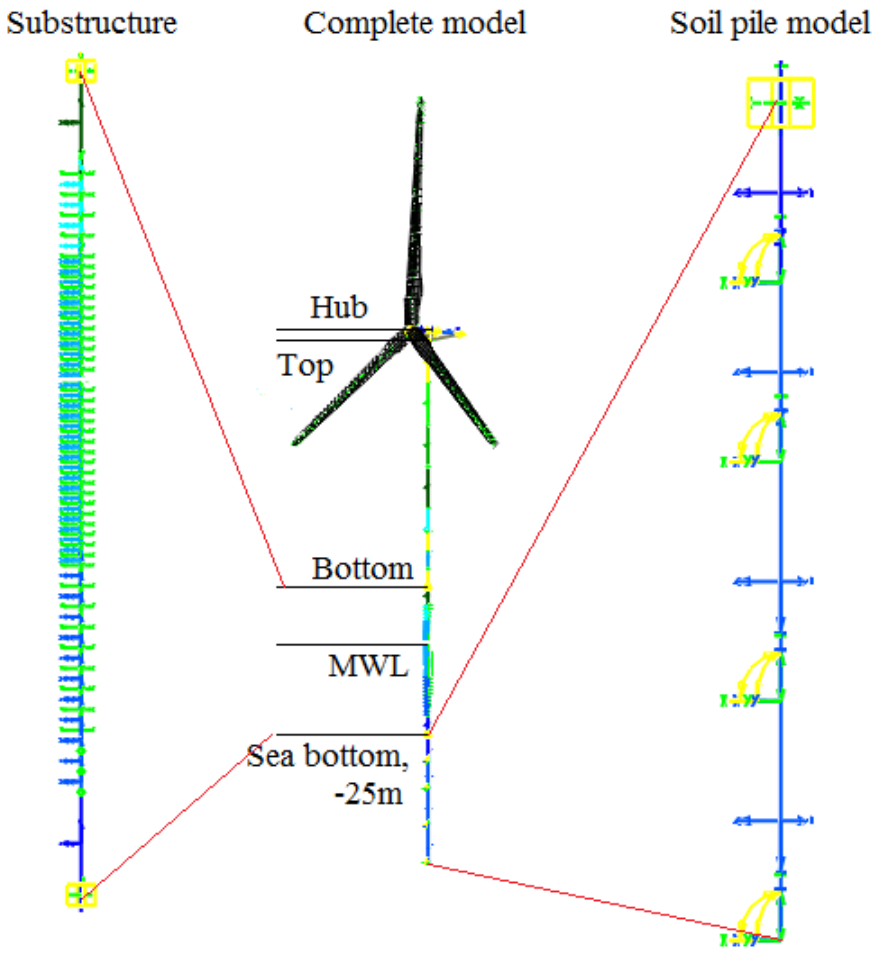

Figure 5.6: The Fedem Windmill Model

Chapter 6

Hydrodynamics

According to the DNV standard for the Wind mill industry [6], hydrodynamic load calculation shall be done by the use of Morison equation. This require representation of the wave velocities and acceleration, which has been presented with different models in chapter 3. The different hydrodynamic load contributions will be presented, and the relative importance between them will be discussed based on the DNV standard. A 2nd order kinematic model is not necessary consistent to the 2nd order as a load model. This will be discussed and compared to the more consistent FNV model which has been much applied at deep water oil and gas installations.

The MATLAB implementation of different load models will in this chapter be compared and verified for the use in later chapters. The implementation will be compared with similar results obtained directly by the program Fedem.

All irregular time series of loads in this chapter, are calculated with parameters from sea state 1 in table 5.3.

6.1 Morison Equation

6.1.1 Hydrodynamic forces on a Monopile Substructure

Hydrodynamic forces are created from different effects:

- Froude-Krylov force: Load by the dynamic pressure from the undisturbed wave
- Diffraction force: Loads due to the presence of a body (scattering), giving a changed flow pattern

- Radiation force: Loads due to a moving object, creating waves and fluid motions
- Viscous drag: Drag force due to friction
- Viscous pressure drag: Drag force due to flow separation

The **Froude-Krylov force** is given by:

$$F_i^{FK} = -\int_S P n_i dS \tag{6.1}$$

Where the unit normal vector is pointing out in the fluid domain, and i denote the force direction. The pressure is calculated according to Bernoulli equation for unsteady potential flow (which is valid everywhere in the fluid). The pressure under the surface, P, becomes:

$$P = p - p_{atm} = -\rho g z - \rho \frac{\partial \phi}{\partial t} - \frac{\rho}{2}(\nabla \phi)^2 \tag{6.2}$$

The last term is of second order and will be neglected. The load from the dynamic pressure can then be simplified for a totally submerged body:

$$F_i^{FK} = -\int_S p_{dyn} n_i dS = \rho V a_i \tag{6.3}$$

If we set i = 1, it doesn't matter if the body pierce the surface, because n_1 is zero on the top and bottom anyway. Here V is the volume, which for a circular cross section equals $\pi D^2 dz/4$. The acceleration is to be evaluated at the midpoint of the volume.

The **radiation force** is due to waves created by the motion of the body:

$$dF_i^R = -\sum_{j=1}^{6} A_{ij} a_j + B_{ij} u_j \tag{6.4}$$

Radiation is important for a floating object, but at the monopile substructure only small motions will occur. These forces are not included in the calculations.

Diffraction force (or **scattering**) is force created by the changed flow pattern due to the presence of a body. The diameter, D, will be the characteristic size of the substructure. The ratio D/λ will decide the nature of scattering.

- $\lambda > 5D$ - Small volume structure - Uniform stream around the body cross section
- $\lambda < 5D$ - Large volume structure - Creation of waves propagating away from the body

Scattering around large volume structures is difficult to express mathematically. An own scattering potential must be calculated. McCamy and Fuchs theory has solved this for a regular linear wave. This theory will approach the simplified

theory for small volume structures at about $\lambda = 5D$. We have already seen in eq. 6.3 how pressure force can be expressed by acceleration. The long wave scattering used for small volume structures use the result from eq. 6.4. The body cross section standing still in a uniform stream, is equivalent with a body moving in still water.

$$dF_i^S = A_{ij}^{2D} a_j dz \tag{6.5}$$

The added mass coefficient for a circular cross-section has a simple analytical expression:

$$A_{circel}^{2D} = \rho \pi D^2/4 \tag{6.6}$$

The **drag force** term is due to the velocity square term in equation 6.2. This pressure gives zero load contribution in potential theory when the flow is uniform. Figure 6.1, to the left, shows the symmetrical pressure distribution. Reality does not coincide with this theory. There will be a net force in the flow direction, which is because the pressure is changed due to viscous effects. This is shown to the right in the same figure. The drag force must be found empirically and will on a circular

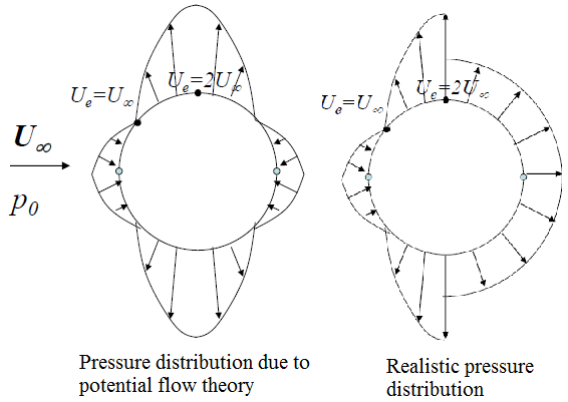

Figure 6.1: Pressure distribution around a circular cylinder, Greco (2012)

cylinder be both due to friction and flow separation.

6.1.2 Morison Equation

Morisons Equation is used to calculate forces on small volume structures, when $\lambda > 5D$. The wave acceleration in x−direction is given as a.

$$\begin{aligned} dF_M &= \rho \frac{\pi D^2}{4} C_M a dz \\ dF_D &= \frac{1}{2} \rho C_D D u|u| dz \end{aligned} \tag{6.7}$$

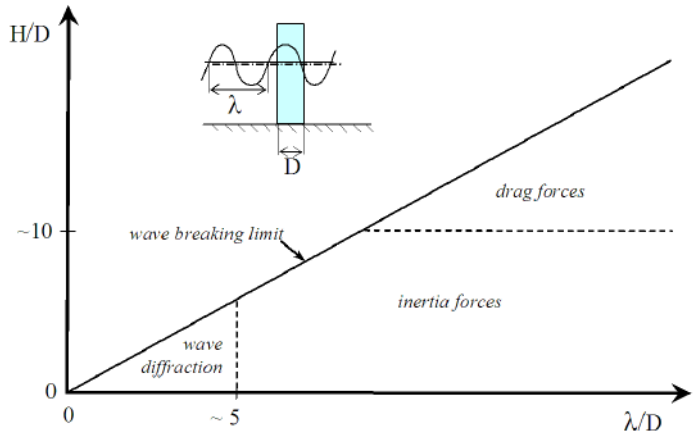

Figure 6.2: Different wave force regimes, DNV [6]

The first term is the **inertia force** which consists of the Froude-Krylov and diffraction force. It use the result from eq. 6.3 and 6.5. The **mass coefficient**, C_M, can be understood as:

$$C_M = \frac{\text{Displaced mass} + \text{Added mass}}{\text{Displaced mass}} = 1 + C_A \tag{6.8}$$

Number 1 gives the Froude-Krylov part. C_A vary with the cross section, which for a circular by eq. 6.6 equals 1.

The second term is the **drag force** which consists of viscous effects. This includes the empirical drag coefficient C_D.

Fedem calculates the body motions and will use the relative motion between body and fluid in morison equation. The radiation loads are then included. The kinematic at a strip of the structure is denoted with subscript b.

$$\begin{aligned} dF_M &= \rho \frac{\pi D^2}{4}(C_M a - C_A a_b)dz \\ dF_D &= \frac{1}{2}\rho C_D D(u - u_b)|u - u_b|dz \end{aligned} \tag{6.9}$$

The equations are according to Faltinsen [10] and the Fedem user manual [27].

6.1.3 Dominating forces

The load contribution from different effects depends on the structure size compared to wave length and wave height, and can be read directly from figure 6.2. The hydrodynamic coefficients C_M and C_D will be used in all load calculations. To

determine these, the size of an incoming regular wave is needed. Extreme loads are considered, and a wave is chosen as the most probable largest wave in a sea state of 30 minutes duration. This will give numbers to proceed in the calculations. The wave is found directly from the cumulative distribution

$$H = F_H^{-1}(1 - 1/N) \tag{6.10}$$

where F_H is the modified Rayleigh distribution by Næss. The corresponding wave period is chosen as $T = 0.9Tp$, and a 3^{rd} order Stokes wave is used to find the wave length.

Sea state 1 in table 5.3 is then used to find the ratios in figure 6.3, which for each water depth is marked on the figure. It show clearly that inertia loads will dominate on the structure.

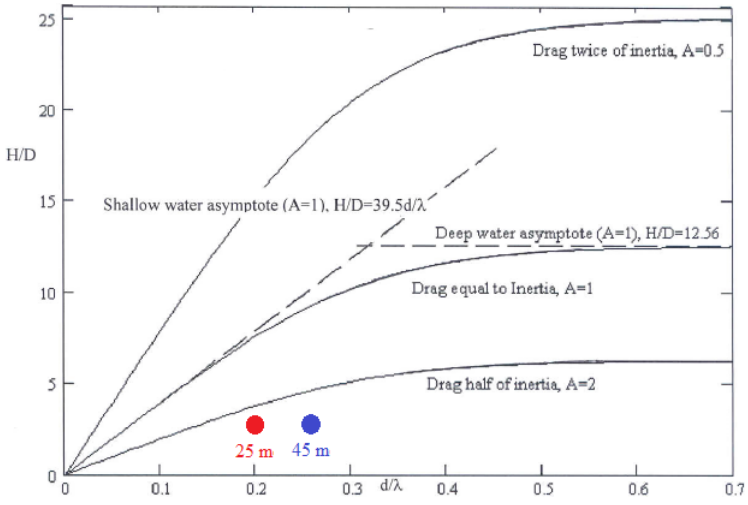

Figure 6.3: Relative magnitude of inertia and drag forces on a small volume strucure, DNV [6]

6.1.4 The search for C_M and C_D

DNV [6] propose how to find the hydrodynamic coefficient, which will determine the load magnitudes according to Morison equation. The method is followed, but the calculations is not exact science but base on empirical formulas.

Marine growth will give significant surface roughness to the structure. DNV [12] sets the surface roughness, k, given by marine growth to somewhere between 0.005 - 0.05 meter. The chosen value is the mean value set to $k = 0.0275m$. Growth will in addition change the structural diameter. Dogger Bank is located below 59 °N where the growth thickness is expected to be $t = 100mm$ after two

years. The new diameter becomes $D = 6 + 2t = 6.2$. The roughness ratio becomes $\Delta = k/D = 0.0047$.

The drag coefficient for steady state flow, C_{DS}, which capture the effects of flow separation must be found:

$$C_{DS}(k/D) = \begin{cases} 0.65 & \text{if } \Delta < 10^{-4} \text{ (smooth)} \\ (29 + 4log_{10}(\Delta))/20 & \text{if } 10^{-4} < \Delta < 10^{-2} \\ 1.05 & \text{if } \Delta > 10^{-2} \text{ (rough)} \end{cases}$$

The oscillating flow due to waves must be accounted for. This is described by the Keulegan-Carpenter number, $KC = U_{max}T/D$, U_{max} is the maximum orbital particle velocity. The drag coefficient is finally written as $C_D = C_{DS}(\Delta)\psi(\Delta, KC)$, where ψ is given as:

$$\psi(\Delta, KC) = \begin{cases} C_\pi + 0.1(KC - 12) & \text{if } 2 \leq KC < 12 \\ C_\pi - 1.0 & \text{if } 0.75 \leq KC < 2 \\ C_\pi - 1.0 - 2.0(KC - 0.75) & \text{if } KC \leq 0.75 \end{cases}$$

where
$C_\pi = 1.5 - 0.024(12/C_{DS} - 10)$

The inertia coefficient, C_A, is found from C_{DS} and KC. If $KC < 3$, then $C_A = 1$, which is the theoretical value. When $KC > 3$, we find C_A from

$$C_A = \max \left\{ \begin{array}{l} 1 - 0.044(KC - 3) \\ 0.6 - (C_{DS} - 0.65) \end{array} \right\}$$

The mass coefficient is then given by eq. 6.8: $C_M = 1 + C_A$.

All these equations, including the way of finding a large wave as described around equation 6.10, are implemented in the MATLAB function "CmCd.m". Final values are calculated from the sea states in table 5.3 and is presented in table 6.1. The

	Depth 25m		Depth 45m	
Sea state	Cm	Cd	Cm	Cd
1	1.80	0.98	1.89	0.75
2	1.79	1.02	1.88	0.78
3	1.77	1.06	1.86	0.81
4	1.75	1.09	1.85	0.84
5	1.74	1.12	1.84	0.86
Mean value	1.77	1.05	1.87	0.81

Table 6.1: Hydrodynamic coefficients at the Monopile substructure

result depends on the way a regular wave was selected, which might be taken up

for discussion. The coefficients is seen to be quite similar, the magnitude are more interesting than the actual digits, and the mean value will be used in all further load calculations.

Figure 6.4 show mass and drag load at the wind mill structure, given by state 1 table 5.3. It shows how the inertia loads dominate completely.

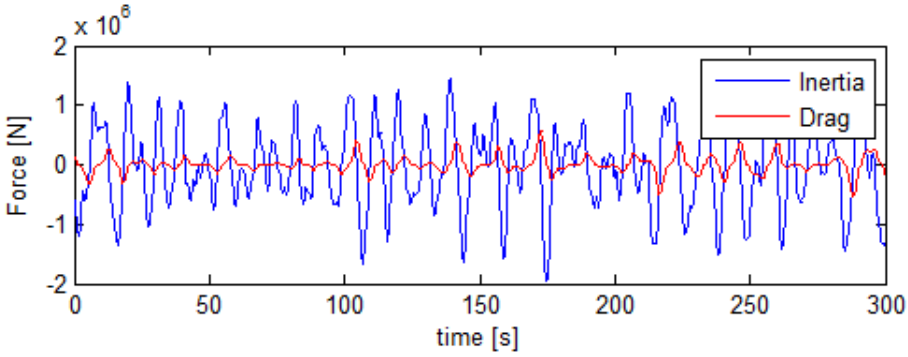

Figure 6.4: Linear sea calculation, drag vs inertia load

6.2 Load integration of kinematic models

The kinematic models presented in chapter 3 will be used in combination with Morison equation 6.7 to find the base shear force and overturning moment on the structure. The general analytical formulation is given by integrating the distributed loads to the free surface:

$$F = \rho\frac{\pi D^2}{4}C_M\int_{-h}^{\zeta(t)} a(z,t)dz + \frac{1}{2}\rho C_D D\int_{-h}^{\zeta(t)} u(z,t)|u(z,t)|dz \tag{6.11}$$

$$M = \rho\frac{\pi D^2}{4}C_M\int_{-h}^{\zeta(t)} (z+h)a(z,t)dz + \frac{1}{2}\rho C_D D\int_{-h}^{\zeta(t)} (z+h)u(z,t)|u(z,t)|dz \tag{6.12}$$

The wave steepness, ϵ (from eq. 2.19), is used in all Stokes theory to characterize the relative magnitudes of different order. In addition to the order of the wave kinematics, higher order load effects will be created due to the effect of free surface, moment arm and the 2nd order nature of drag. When referring to an order n, the order of magnitude is given by ϵ^n. In an irregular sea, the complication in interaction between frequency components increases for higher order. This is shown in my project thesis [28] to the 3rd order, but can be extended to any. The interaction of frequencies are given by any combination of plus/minus signs:

- 1st order: ω_i
- 2nd order: $\omega_i \pm \omega_j$

- 3rd order: $\omega_i \pm \omega_j \pm \omega_k$

The effect of free surface integration on the force can be studied in an analytical sense, by using Stokes theory fully consistent to first order, by using Taylor expansion both in the crest and trough:

$$\begin{aligned}\int_{-h}^{\zeta(t)} dF(z) &= \int_{-h}^{0} dF(z) + \int_{0}^{\zeta(t)} dF\big|_{z=0} \\ &= \int_{-h}^{0} dF(z) + \zeta(t) dF\big|_{z=0}\end{aligned} \tag{6.13}$$

If $\zeta(t)$ is of 1st order, the new load term is one order increased. This becomes even more complicated when integrating moment, due to the oscillating arm.

$$\begin{aligned}\int_{-h}^{\zeta(t)} (z+h) dF(z) &= \int_{-h}^{0} (z+h) dF(z) + \int_{0}^{\zeta(t)} (z+h) dF\big|_{z=0} \\ &= \int_{-h}^{0} (z+h) dF(z) + \frac{\zeta(t)^2}{2} dF\big|_{z=0} + \zeta(t) h dF\big|_{z=0}\end{aligned} \tag{6.14}$$

Now, also a 3rd order component is created.

Load models to consider from irregular kinematics

Only the 2nd and 3rd order terms are interesting, because higher order terms will be extremely small due to ϵ^n. The higher order effects will even though be mentioned, because they all will be carried through in the numerical calculation.

Model 1: Linear kinematics integrated to the MWL. The inertia load will be linear, and the drag load of second order. Force and moment will be at equal order.

Model 2: Second order kinematics at finite water. The kinematics is integrated to the MWL. The inertia load will now get a 2nd order load due to the 2nd order kinematic component. In case of drag load, the kinematic is squared, which creates a 4th order component. Force and moment are again at equal order.

Model 3: 1st order extrapolation, will integrate load and moment to the linear free surface level at $z = \zeta(t)$, according to the linear terms in eq. 3.31. The inertia load will now get a 2nd order load contribution around $z = 0$ due to the oscillating free surface. The drag load will then get a third order contribution. Inertia moment get a 2nd and 3rd order contribution, and drag moment a 3rd and 4th.

Model 4: Stretching to linear surface by replacing the z-coordinate in model 1 with z^{mod} according to eq. 3.32, will create load terms at the same orders as described in model 3.

Model 5: 2nd order extrapolation will use the second order kinematics model (Model 2) integrated to the linear free surface according to eq. 3.31. Inertia load get a 2nd and 3rd order contribution by integrating first and second order kinematic

components to the linear surface. Drag will then get a 3rd and 5th order (2^2+1). Inertia moment get 2nd, 3rd and 4th order contributions. Drag moment 3rd, 4th, 5th and 6th.

Model 6: Stretching to 2nd order surface. Linear kinematics will now be integrated to the 2nd order surface. Inertia load get 2nd and 3rd order terms, and drag 3rd and 4th. Inertia moment get terms up to the 5th order $(1+2^2)$ and drag up to the 6th $(2+2^2)$ due to the effect of 2nd order surface (see eq. 6.15).

6.2.1 MATLAB implementation

MATLAB calculate the kinematics along the structure in vertical coordinates specified by the user. The result is stored in a matrix with coordinates in the rows, and with time in the columns. The free surface is taken care of as illustrated in figure 6.5. Only submerged points will be given kinematics, the rest is set to 0.

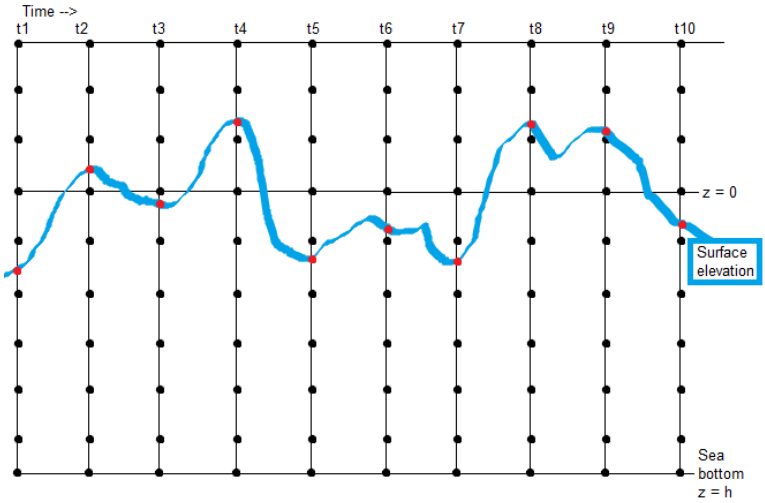

Figure 6.5: Matrix of kinematics

The load integration is done by using the trapezoidal rule on each column in figure 6.5. This is implemented in the function "morison1.m". This method is simple, but creates discontinuities which gets more visible for small Δt, because there will be a little jump when a nodal point go in or out of water. The effect is reduced with a small vertical spacing, Δz, but the calculation of kinematics use long CPU time, and a close spacing of vertical points can not be afford. The model, as shown in chapter 5, is created with nodal points of 0.5m spacing in the wave elevation zone. With this coarse spacing, the total load get discontinuous when applying the simple integration method.

A more sophisticated method, "morison2.m", is implemented which always integrates the kinematic to the free surface elevation. It splits the integration in two parts, by first using trapezoidal rule up to the highest submerged point, for then using trapezoidal rule again between this point and the free surface. It require that the kinematics is calculated at the free surface, and not just in the vertical coordinates specified on the structure. Both methods are shown in figure 6.6.

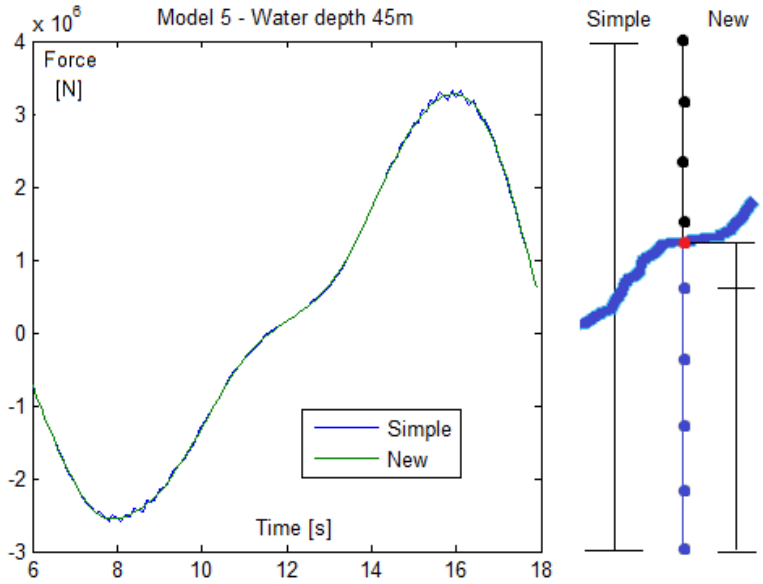

Figure 6.6: Load integration by "morison1.m" and "morison2.m" applied to model 5

A third method improves this further. This is called "morisonS2.m", which do the same as "morison2.m", but interpolates between the calculated kinematics. This creates a better representation of the exponential profile of the velocity potential. The method interpolates with 5 times the number of vertical coordinates specified by the user. A second order distribution is created, so that the points are closer spaced near the surface, as shown in figure 6.7. The method in "morisonS2.m" will not be used in further load calculations, because it was developed too late for the calculation process. It is regarded to be more accurate, and it reduces the needed number of points in vertical direction to calculate wave kinematics.

6.2.2 Load models in the time domain

All the load models have been compared in the time domain using the same seed. Figure 6.8 show the resulting force and moment from model 1, 3 and 4. The time

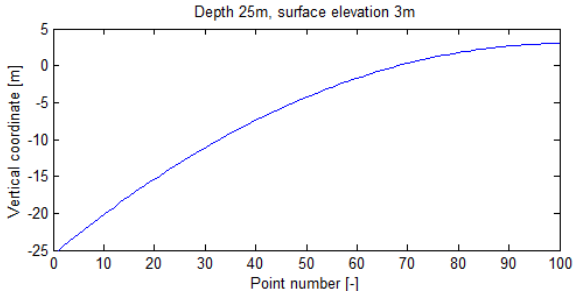

Figure 6.7: Distribution of vertical coordinates in "morisonS2.m"

step is set to 0.5s, the duration is 1200s, and the water depth applied to all models is 30m. This means that 30m kinematics has been applied to the structure at 25m water depth. All models are calculated from the JONSWAP spectra with $\gamma = 2.23$, Hs = 9.56 and Tp = 12.76, according to sea state 1 in table 5.3. The cut-off frequency applied is $\omega_{max} = \sqrt{2g/H_S}$ for all models. This is to be consistent with the second order models. A cut around the peak event (at $t = 1105s$) in this arbitrary

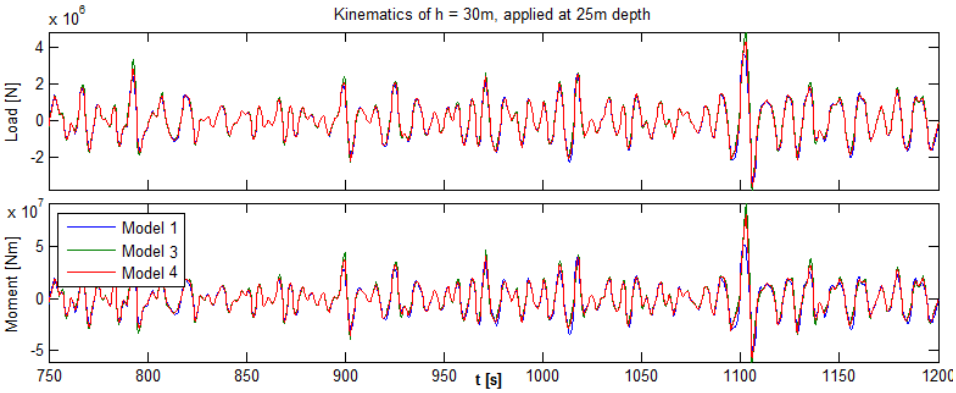

Figure 6.8: Load and moment from models 1, 3 and 4

time realization has been used to get and impression of the different models. The overturning moment (OM) is used as comparison, because the difference between the models get even more visible. The wave kinematics of this cut were actually given in figure 3.16 and 3.17 in chapter 3. These figures explains the differences between the models and is the reference when commenting the results below.

Figure 6.9 show the comparison between model 1 and 2, the only models integrating loads tho the MWL. The second order model give slightly larger maximal loads, which is easy to explain from the increased kinematics in figure 3.16 in chapter 3. The extrapolation models give much larger loads, especially model 5 which at this event create almost twice the load as in model 1 and 2. The reason is off course the large wave at this event creating a larger submerged area of the structure. Model

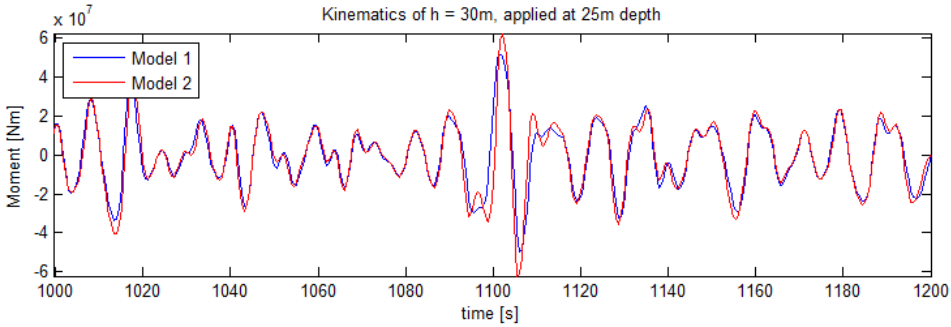

Figure 6.9: Overturning moment from model 1 and 2

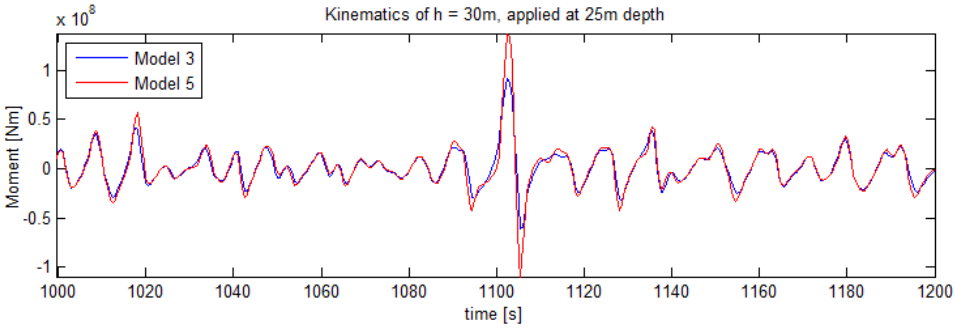

Figure 6.10: Overturning moment from model 3 and 5

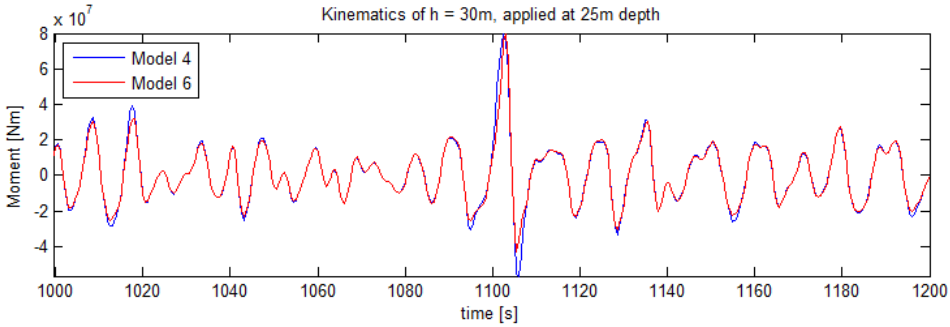

Figure 6.11: Overturning moment from model 4 and 6

6, using the 2nd order surface is found to give slightly lower loads compared to model 4 using the linear. The reason is more difficult to explain, but it might be because the wave crest in the 2nd order model is sharper. The dominating inertia load is out of phase with the crest, and might be at top where the 2nd order surface is lower then the linear.

6.2.3 Spectral analysis and discussion of Δt

To analyze the frequency components of the different load models, the spectra of the time series have been found. This is calculated with the function "dat2spec.m" in the WAFO packages [18]. Figure 6.12 shows the spectra of Load and moment from model 1, 3 and 4 with contribution of drag and inertia calculated separately. Remember that the wave spectra is given a linear fading stretching from $\omega_{cut} = \sqrt{2g/H_S} = 1.44$ to $\omega_{max} = 1.8212$ (described in chapter 3.1.4). Inertia from

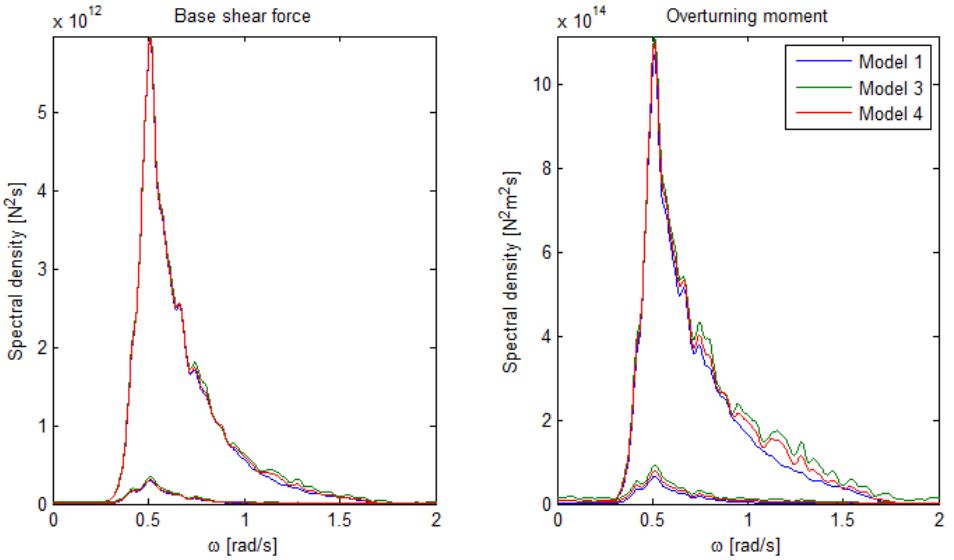

Figure 6.12: Load and moment spectra of inertia and drag from model 1, 3 and 4

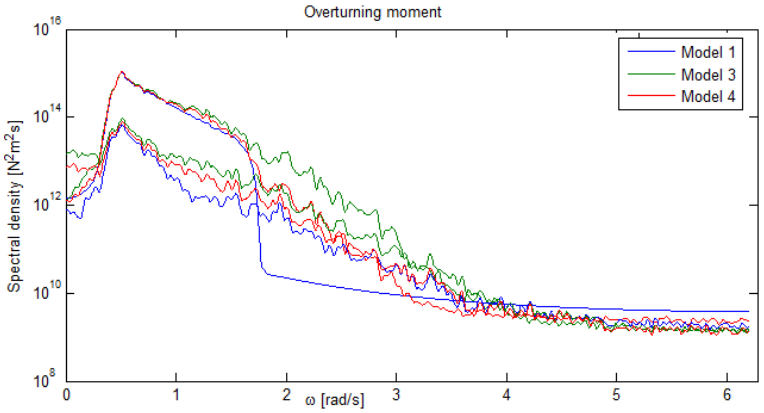

Figure 6.13: Logarithmic load spectra of inertia and drag from model 1, 3 and 4

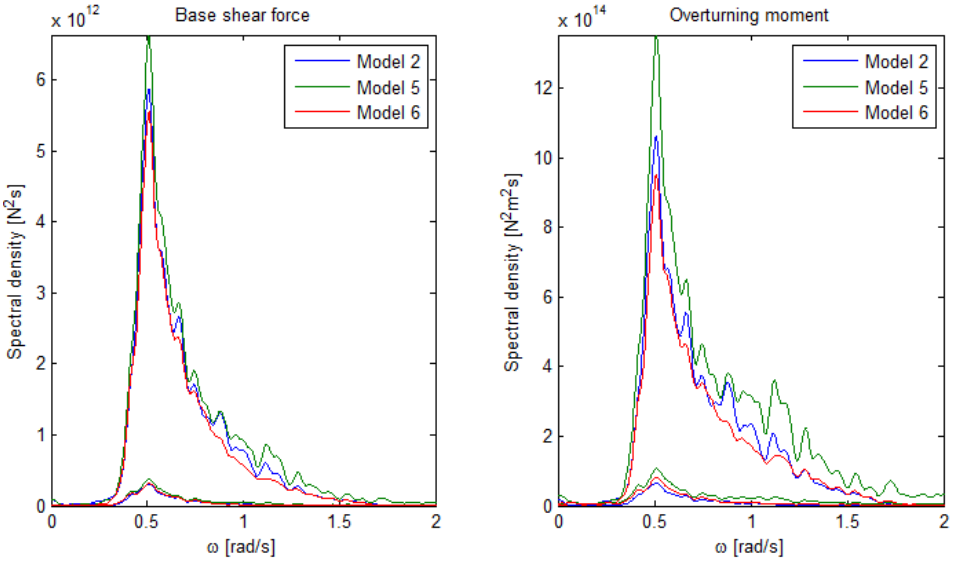

Figure 6.14: Load and moment spectra of inertia and drag from model 2, 5 and 6

model 1, which is linear, shows to follow the acceleration spectra as a straight line without disturbances. The tail of the moment spectrum can be studied in detail in figure 6.13, where the y-axis is logarithmic. A sudden drop can be seen in the linear tail (blue line), where the fading ends. The spectral value is zero after this, which the numeric calculation has captures very well, taking the ratio of 10^5 to the peak value into consideration. There is much disturbance in the tail of all the other models.

Model 2 and 5 using the 2nd order kinematics shows significantly more higher order energy. The peak value in the shear spectrum was similar in model 1, 3 and 4. This has now changed. Model 2 is consistent with these models, but model 5 is significantly higher, and model 6 lower. The reason is not clear, but the spectrum calculated from a longer time duration might even out the differences. However, it is through time realizations seen that model 6 actually gives lower peaks compared to model 4 (wheeler to linear surface). *The only explanation must be the more narrow wave crests which is out of phase with the inertia load.*

The large difference between model 5 and 6 is not consistent with the theoretical investigation in chapter 3 (see Stansberg [20]), which relied on measurements from wave tank experiments.

It is seen in general how non-linearity is most present in the specter of overturning moment. The drag component is in all the models seen to be small.

Discussion of time step in load calculations
The energy in the tail of model 3, linear extrapolation, show significant non-linear

effects. The moment spectrum for this model shows to die out around $\omega = 2$ in figure 6.12, and the disturbances in the logarithmic plot seem to stabilize around $\omega = 3$. The required time step for load calculations is then given by The Nyquist frequency. A time step of $\pi/3.14 = 1$s should be small enough to capture all significant non-linear effects.

It was shown in the presentation of load models, that force and moment contribution of 4th and higher order was possible. The spectra are calculated with H_S and T_P according to sea state 1 in table 5.3. This gives $\omega_P = 0.4924$. If higher order load will be visible, they must be created by interaction between frequencies of high energy content. A 5th order load will then give a frequency around $5\omega_P = 2.462$. The corresponding time step becomes according to Nyquist becomes $\Delta t = 1.276$. Again, a time step of 1s will be enough to represent all higher order loads.

The time step in load calculations is not CPU demanding as the generation of wave kinematics discussed in chapter 3. Load calculations will therefore be done with time step 0.5s. The wave kinematics is created with $\Delta t = 1$, and will be interpolated with the MATLAB function "spline.m". This works fine as already demonstrated in figure 3.15 (chapter 3).

However, for short dynamic analysis of only one seed, the generation of 2nd order kinematics will not be too CPU demanding, and the time step of 0.5s will be used, equal to the analysis in this chapter.

6.2.4 Effect of non-linearity at different water depth

The same seed has been calculated for model 3 applied to the wind mill structure at 45m water depth. The loads are significantly increased as shown in figure 6.15. The loads are larger, but the importance of non-linear components might be changed due to the lower ratio between wave elevation and water depth. The spectra of moment from each load series is shown in figure 6.16. The spectra has been scaled so that the peak is set to 1. The ratio between the peak component and components at higher order can then be compared. It show clearly how the ratio is significantly lower at 45m water depth.

6.3 Higher order load model - FNV

The so far presented load models builds on sophisticated kinematic formulation, but the goodness must still be questioned. The models contains higher order contributions, but they are not consistent, even not to the second order.

The drag term in Morison equation is based on an empirical formulation and will not be questioned. The problem is the inertia term which is derived analytically from equation 6.2 and 6.3. The 2nd order pressure $\frac{\rho}{2}(\nabla\phi)^2$ has been neglected, because Morison equation is only valid to 1st order. The term is found in the drag

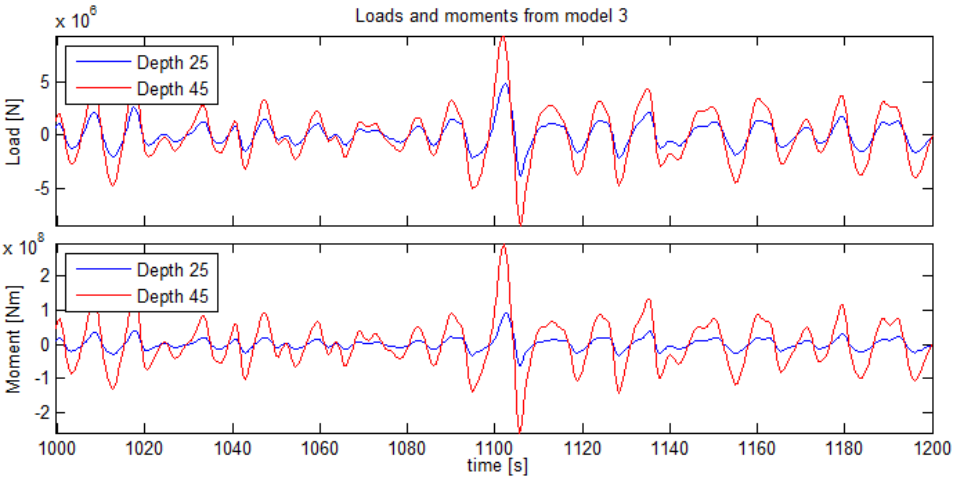

Figure 6.15: Load and moment from model 3 at both wind mill structures

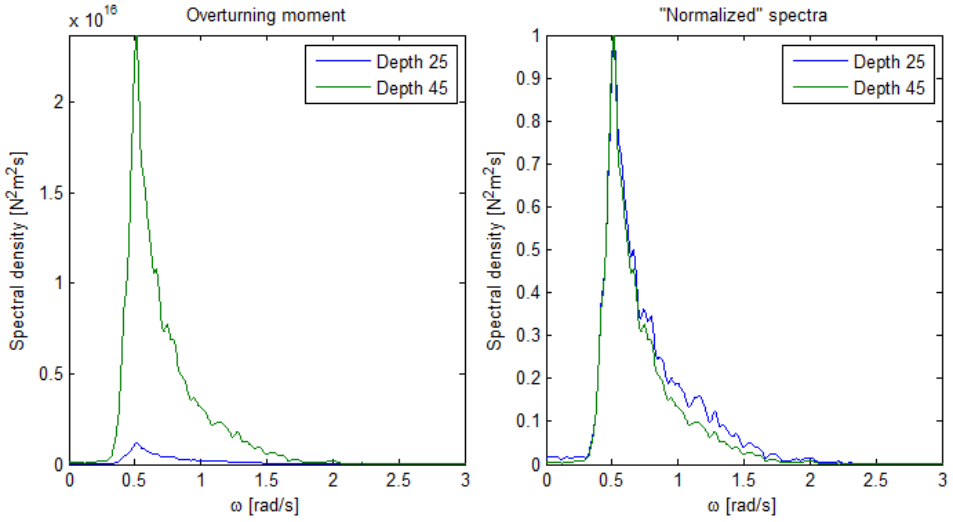

Figure 6.16: Moment spectra from model 3, "normalized" spectra to the left for comparison

load, but is included for another reason: The load on a body is zero in a stationary flow, because the velocity squared term creates an even velocity distribution around the body. This is unphysical due to viscous effect and is therefore corrected by the drag term. In the oscillating flow field, the velocity changes around the body and the second order dynamic pressure must be included!

The FNV theory is a sophisticated load model which describes the inertia load consistent to 3rd order, with the input of 1st and 2nd order regular waves. The

theory was developed by Faltinsen, Newman and Vinje.

$$
\begin{aligned}
F_{FNV} =& 2\pi a^2 \int_{-h}^{0} u_t(z)dz \\
&+ \pi\rho a^2 \int_{-h}^{0} wu_z dz + 2\pi a^2 u_t\Big|_{z=0} \zeta_1 \\
&+ \pi\rho a^2 \zeta_{I1}[u_{tz}\zeta_1 + wu_z - \frac{2}{g}u_t w_t]\Big|_{z=0} \\
&+ \pi\rho a^2/g u^2 u_t\Big|_{z=0} \beta(h/a)
\end{aligned}
\tag{6.15}
$$

Overturning moment:

$$
\begin{aligned}
M_{FNV} =& 2\pi a^2 \int_{-h}^{0} u_t(z)zdz \\
&+ \pi\rho a^2 \int_{-h}^{0} wu_z zdz + 2\pi a^2 u_t\big|_{z=0}\zeta_1(h+\zeta_1/2) \\
&+ 2\pi\rho a^2 u_{tz}\big|_{z=0}\zeta_1^2(h/2+\zeta_1/3) \\
&+ \pi\rho a^2 wu_z\big|_{z=0}\zeta_1(h+\zeta_1/2) \\
&+ 2\pi\rho a^2 u_t\big|_{z=0}\zeta_2\big|_{z=0}(h+\zeta_1) \\
&+ \pi\rho\frac{a^2}{g}u^2 u_t\big|_{z=0}\beta(h/a)(h+\zeta_1) \\
&- \frac{\pi\rho}{g}a^3 u^2 u_t\big|_{z=0}\gamma(h/a)
\end{aligned}
\tag{6.16}
$$

FNV might give larger loads compared to the Load models outlined previously. Load model 5 has shown to give much larger loads compared to the other models. The inertia component of this model has been compared to FNV for the same time series as used in the sections above. The result is shown in figure 6.17, and the specter for each model is shown in figure 6.18. The models follow each other quite well, but model 5 create still the largest load. The spectra of load models in figure 6.14 and 6.13 showed that model 5 contained significantly more energy in the tail created by non-linearity and that the peak at ω_P was significantly larger. The specter of model 5 is compared to FNV in figure 6.18. It shows clearly that FNV gives the same high peak at ω_P, and that in fact FNV contains significantly more energy at the non-linear components. We can imagine how FNV to a larger degree will give energy to excite the natural frequency of the structure.

Model 5 gave the largest load in this specific cut around a peak event through a 20min realization. Model 5 is expected to always give the largest peak when comparing model 1 to 6, because these build on the same load model. The result might change when comparing model 5 against FNV at longer time series. This

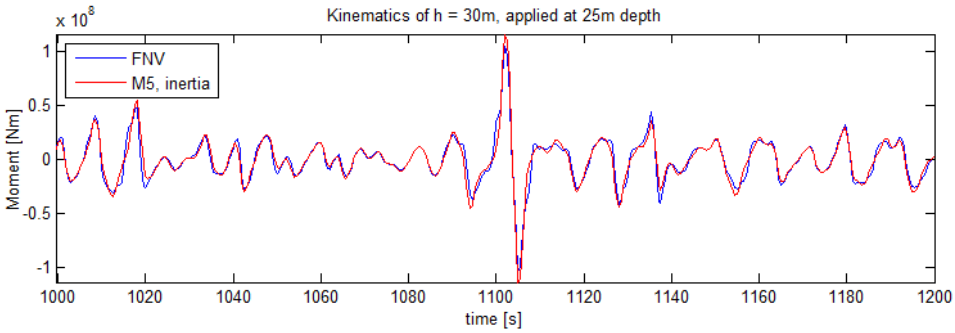

Figure 6.17: Overturning moment from FNV and inertia load by model 5

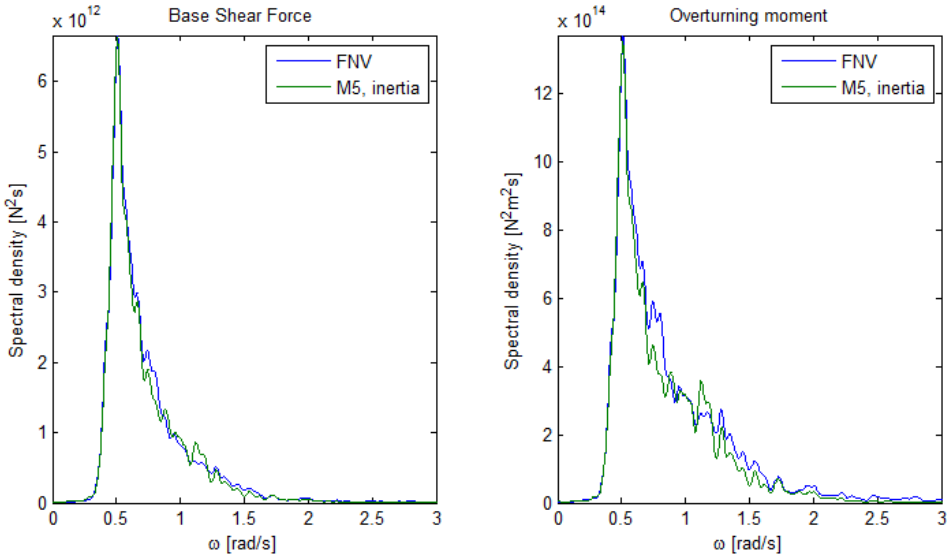

Figure 6.18: Specter of FNV and inertia load by model 5, both base shear and overturning moment

is because the physics behind the two models are quite different. Model 5 use extrapolated 2nd order irregular kinematics, with a first order load model.

Applying FNV to the wind mill structure has been complicated, and understanding of the different load terms listed in equation 6.15 and 6.16 has been required. Table 6.2 show how each term in the load and moment equation is given due to a distributed load and its area of integration. The moment is given about the MWL and is not the overturning as in equation 6.16. Each term is given a number, which now will be explained shortly. A more detailed explanation is found in my project thesis from fall 2013, [28].

- 1.1) The linear inertia load in morison integrated to MWL, equal to Model 1. 1st order load.
- 1.2) Morison equation applied around the free surface, as in model 3 (extrapolation), but consistent to the Stokes kinematics given by Taylor expansion (see eq. 2.12). 2nd order load.
- 1.3) The same as in term 1.2 but now using the 2nd order term in the Taylor expansion. This is also used in model 5, but then only consistent with the expansion above the MWL. 3 order load.
- 1.4) Morison equation applied between the linear and 2nd order surface elevation. This might be seen as the difference between model 4 and 6. The load is close to work as a point load at the linear surface elevation. 3rd order load.
- 2.1) 2nd order load term applied to the MWL. 2nd order load.
- 2.2) 2nd order load term applied around the free surface. 3rd order load.
- 3) 3rd order load term applied to the MWL. This is found to work mainly at the MWL as a 3rd order point load. The distributed load create a moment on the structure of 3rd order. The point load in 3a is in fact working close to the free surface, and gives a 4th order moment due to the linear wave elevation.

Figure 6.16 showed how the non-linear effect of model 3 changed from 25m to 45m water depth. Figure 6.19 show the same applied to FNV. It is easy to see how non-linear components gives less contribution to the total loads at deeper water.

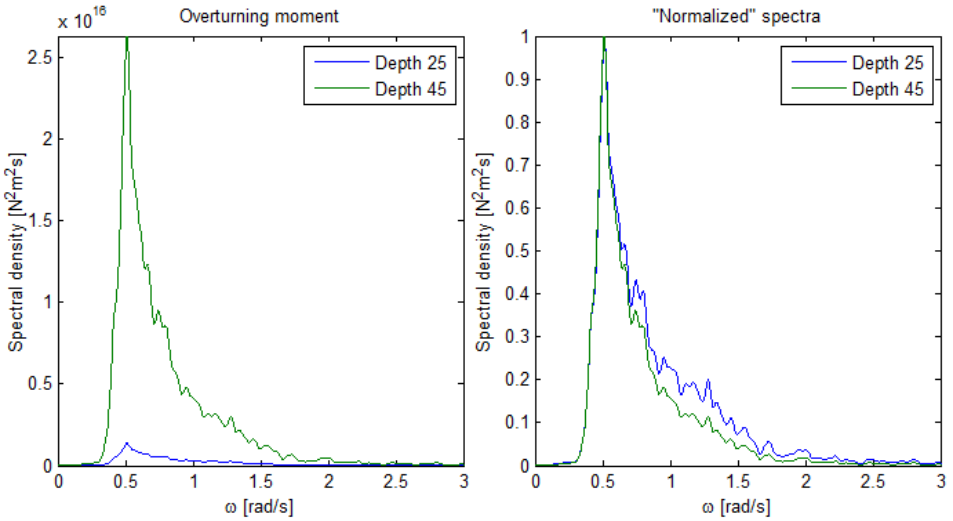

Figure 6.19: Specter of FNV model at depth 25m and 45m (scaled to get the same peak magnitude

FNV is only valid at deeper water. We can then imagine how the non-linear components might have become disproportional large. Testing the design for loads created by FNV might even though give important results for design considerations, since it might reveal load events that is not captured by the other load models.

6.4 Fedem/MATLAB-connection - Load lumping system

The distributed loads calculated in MATLAB must be applied to the Fedem model as point loads in the nodal points along the substructure model (see figure 5.6). The term "lump" is used to describe this process, and a "load lumping system" has been created that is consistent with the previous load integration method in the function "morison2.m" (figure 6.6). The system is shown in figure 6.20 and implemented in the function "morisonL.m".

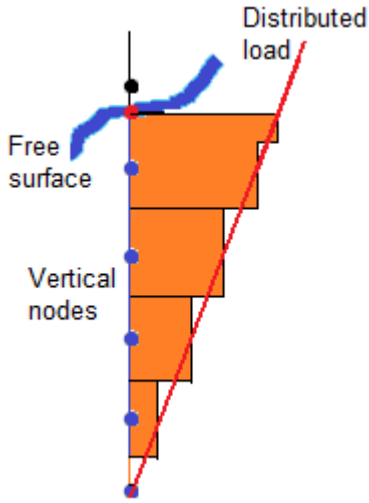

Figure 6.20: Lumping a distributed load according to the trapezoidal rule

A plot of the resulting force from the two integration methods will completely overlap, because they are identical. The ratio between the standard deviation calculated from each method, will always be 1. This is not the case for moment calculation. The lumping method cannot both describe base shear force and overturning moment correct. This is because the overturning moment depends on the vertical coordinates on the structure, which is fixed. The accuracy of moment calculation will increase when the distance between vertical coordinates decreases. We do not need to worry about this. The vertical coordinates at the Fedem model described in chapter 5, will give a standard deviation from the overturning moment

that is 0.02-0.05% lower then the other method. We see that there is very good agreement between the two methods!

In fact, the moment could be correct represented if the added load from the free surface kinematics (red point) was weighted to the node above (which is not submerged). However, this has not been implemented, due to the neglecting change in standard deviation.

Another, much more sophisticated method is developed to match the interpolated load integration which is implemented in the function "morisonS2.m" explained previously. This load lumping method uses interpolation in the same way, but the vertical points on the structure do not need to correspond to the vertical coordinates of calculated wave kinematics. The structure in Fedem can then be created without concern for the available kinematics This function is called "morisonSL.m".

6.4.1 Load Lumping of FNV model

Term	Load	Moment	dF	Domain
1.1	$2\pi\rho a^2 \int_{-h}^{0} u_t(z)dz$	$2\pi\rho a^2 \int_{-h}^{0} z u_t(z)dz$	$C_M \pi\rho a^2 u_t(z)dz$	$[-h, 0]$
1.2	$2\pi\rho a^2 u_t\|_{z=0}\zeta_1$	$\pi a^2 u_t\|_{z=0}\zeta_1^2$	$C_M \pi\rho a^2 u_t(0)dz$	$[0, \zeta(t)]$
1.3	$\pi\rho a^2 u_{tz}\|_{z=0}\zeta_1^2$	$\frac{2}{3}\pi a^2 u_{tz}\|_{z=0}\zeta_1^3$	$C_M \pi\rho a^2 u_{tz}(0)zdz$	$[0, \zeta(t)]$
1.4	$2\pi\rho a^2 u_t\|_{z=0}\zeta_2$	$2\pi\rho a^2 u_t\|_{z=0}\zeta_2\zeta_1$	$C_M \pi\rho a^2 u_t(0)\zeta_2$	$\zeta(t)$
2.1	$\pi\rho a^2 \int_{-h}^{0} w u_z dz$	$\pi\rho a^2 \int_{-h}^{0} z w u_z dz$	$\pi\rho a^2 w u_z dz$	$[-h, 0]$
2.2	$\pi\rho a^2 w u_z\|_{z=0}\zeta_1$	$\frac{1}{2}\pi\rho a^2 w u_z\|_{z=0}\zeta_1^2$	$\pi\rho a^2 w(0) u_z(0)dz$	$[0, \zeta(t)]$
$3a$	$\frac{\pi\rho a^2}{g} u^2 u_t\|_{z=0}\beta(a/h)$	$-\frac{\pi\rho}{g} a^3 u^2 u_t\|_{z=0}\gamma(h/a)$	$\sim (3\Psi_1(z) + 4\Psi_2(z))dz$	[-h,0]
$3b$	$\frac{\pi\rho a^2}{g} u^2 u_t\|_{z=0}\beta(a/h)$	$\frac{\pi\rho a^2}{g} u^2 u_t\|_{z=0}\beta(a/h)\zeta_1$	$\frac{\pi\rho a^2}{g} u^2(0) u_t(0)\beta(a/h)$	$\zeta(t)$

Table 6.2: Loads, term by term, in the FNV model

ζ_1 is the first order undisturbed wave elevation, and ζ_2 the second order contribution, so that the total undisturbed wave elevation becomes $\zeta = \zeta_1 + \zeta_2$.

Load term 3a is NOT implemented in the MATLAB calculations. This is because the involved Ψ-functions of the distributed load is rather complicated to express mathematically. Functions γ and β are the integral value of the distribution, with a/h as a dimensionless depth as input parameter. The load distribution is found to concentrate at the free surface, described as load 3b. This is included in the MATLAB implementation, and the deep water limits of γ and β are used:

- $\beta = 4.00$
- $\gamma = 4.95037$

6.4.2 Verification

The system has been verified by looking at the response generated by a regular linear wave. Both drag and mass load, with wheeler stretching of the kinematics (load model 4), was applied to be consistent with Fedem. The result is quite convincing, as shown in figure 6.21.

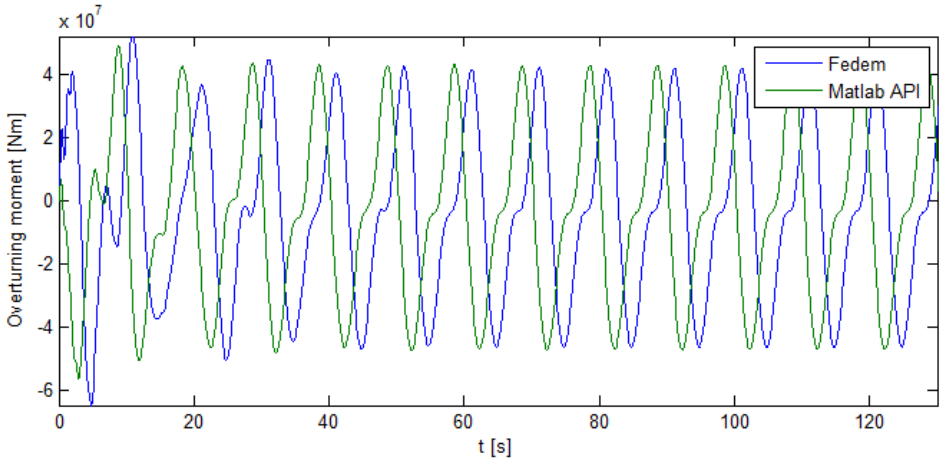

Figure 6.21: Dynamic overturning moment by regular wave directly from Fedem, and externally using MATLAB

The ratio between peak loads are found to be:

$$\frac{F_{Mat}}{F_{Fed}} = 0.9782 \tag{6.17}$$

Fedem includes the structural motions in the load calculation, as given in equation 6.9. From the same calculation, figure 6.22 give the kinematics at MWL by the wave and the body strip. The ratio between velocities are found to be 0.0121, and for the acceleration 0.0256.

The differences between Fedem and MATLAB will not be further assessed.

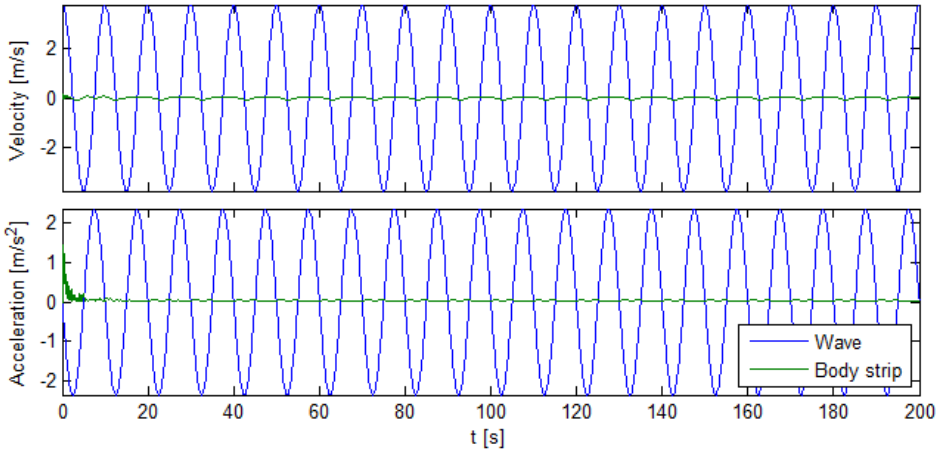

Figure 6.22: Kinematics at MWL by wave and body strip

Chapter 7

Dynamic analysis

The verification of loads applied through MATLAB in chapter 6, showed very good agreement with the loads applied directly through FEDEM. The resulting response was similar.

The only strange thing to consider was the shape of the response itself. The applied static overturning moment was sine shaped, because there was a neglecting influence from the drag component. This is obviously not the case at response level, where the second order effects are seen to be significant.

Figure 7.1 show an arbitrary irregular load history, with loads calculated from both drag and inertia by Wheeler stretching (model 4). It shows that the excitation of the first mode is extremely large, even though the energy from the static moment is very low at this frequency.

The reason for studying non-linear loads is to increase the realism in the models, for then to see if higher order loads might increase the structural response through dynamic amplification. This has been an issue for oil and gas installations when the natural frequency of a structure has been in the magnitude of 3 times ω_P. This is also the case for monopile substructures, and the dynamical effect to the structural model in Fedem, by the different load models, should now be compared.

More and more sophisticated models were outlined through chapter 3 and 6, which in different ways included non-linearity to trigger the effect of dynamic amplification. The effect is already very much triggered by a rather simple load model, and does totally dominate the response picture. Further comparison of load models seems to be pointless, but the extreme excitation might indicate that there is something wrong with the chosen parameters to the wind mill model.

A short section introducing some concepts of structural dynamics is given, then followed by an investigation of the parameter sensitivity, both structural and hydrodynamical. Parameters and the reason for the large amplification will be discussed, then followed by static and dynamic energy spectra of base shear load and

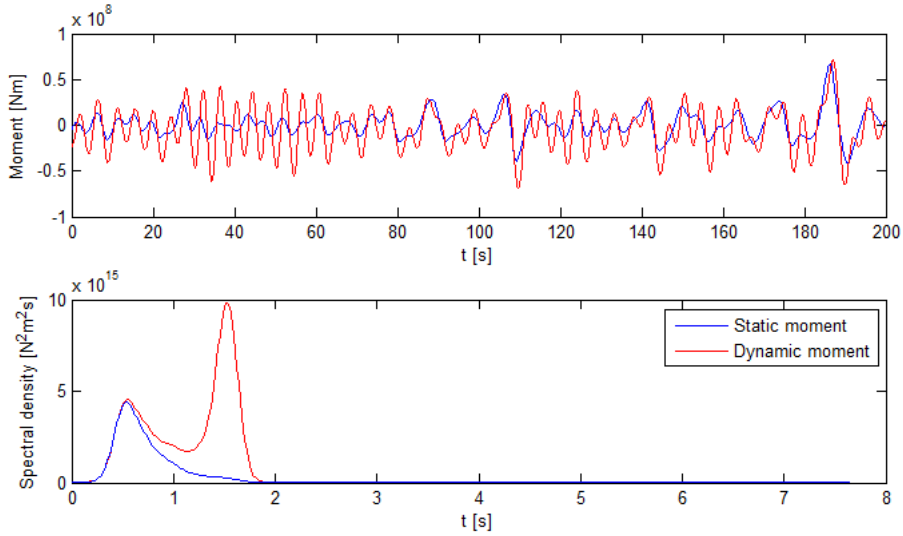

Figure 7.1: Dynamic and static moment from model 4

overturning moment resulting from the different load models outlined in chapter 6.

Only the wind mill model at 25m water depth will be considered for dynamic calculations. All sea state calculation in the chapter use parameters of sea state 1 in table 5.3. All static spectra is calculated directly from the applied loads by MATLAB.

7.1 Dynamic amplification

A dynamical system has a natural frequency, ω_N, which is the frequency of free oscillation. This frequency is determined by the mass and stiffness of the system. An oscillating force applied to the system will create a response motion, where the amplitude depends on the force amplitude and the ratio, β, between the load frequency and ω_N. The following relation is useful:

$$r = HF = \frac{DAF}{k}F = DAF \times r_0 \tag{7.1}$$

F is the applied force, r is the response displacement, H is the transferfunction between load and response, r_0 is the resulting response displacement if the system was static, and DAF is the ratio between dynamic and static response. DAF is the dynamic amplification factor. A dynamic system subject to a force with $\beta = 1$, and no damping, will get an infinite large response. This is known as resonance.

The effect of resonance decreases for increasing damping in the system. Figure 7.2 shows DAF as a function of β for different damping ratios, ζ.

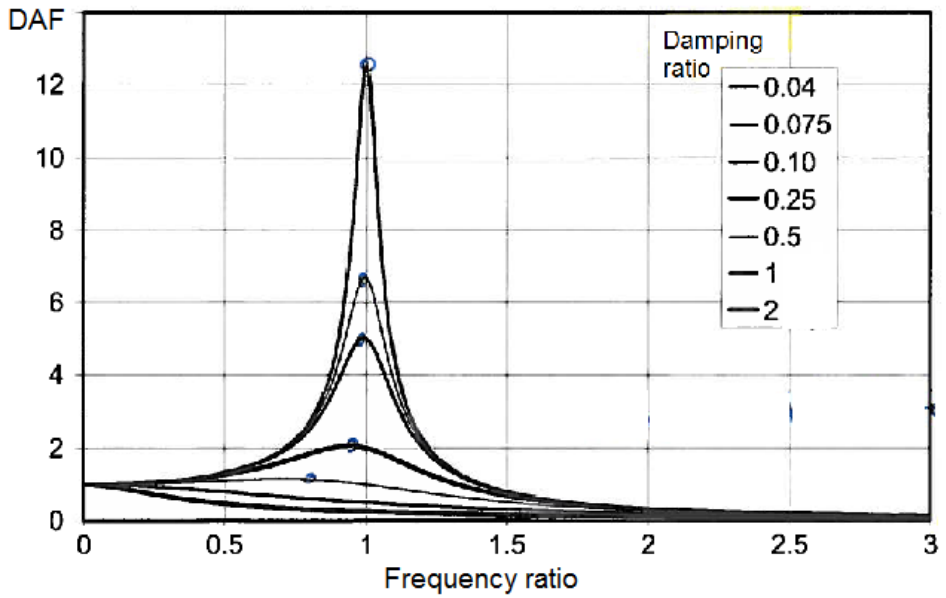

Figure 7.2: Dynamic Amplification factor, taken from Larsen [7]

Stiff structures have a rather high natural frequency compared to the excitation loads, giving a low β. DAF is then close to 1, and the system behave as quasi-static. This is the case for the monopile when subject to energetic linear loads, creating the first peak in the response spectra shown in figure 7.1.

The **damping** ratio of different parts in the structure must be chosen in the Fedem model. They must express the soil and material properties in a realistic way. The damping, c, is in Fedem set to be a proportion of the mass (m) and stiffness (k) in the system. The mass and stiffness proportional damping coefficients, v_m and v_k, are used

$$c = m \times v_m + k \times v_k \tag{7.2}$$

The damping ratio used in figure 7.2, is the ratio between damping and critical damping, c_{cr}. The critical damping is defined as the lowest damping that can be in the system without oscillations to be created after an impulse excitation. There is a simple relation between ζ and the proportional damping coefficients.

$$\zeta = \frac{v_m}{2\omega_N} + \frac{v_k \omega_N}{2} \tag{7.3}$$

7.2 Parameter sensitivity to overturning moment

The effect of load from drag and inertia, versus only inertia is shown in figure 7.3. The difference in static moment is not even visible in the plot with use of a logarithmic y-axis. But there is obviously a difference when looking at the dynamic response. To reduce the DAF, and to have a better control of the excitation frequencies, drag will be turned off in the following analysis. Load model 1 (linear kinematics integrated to MSL) will be used.

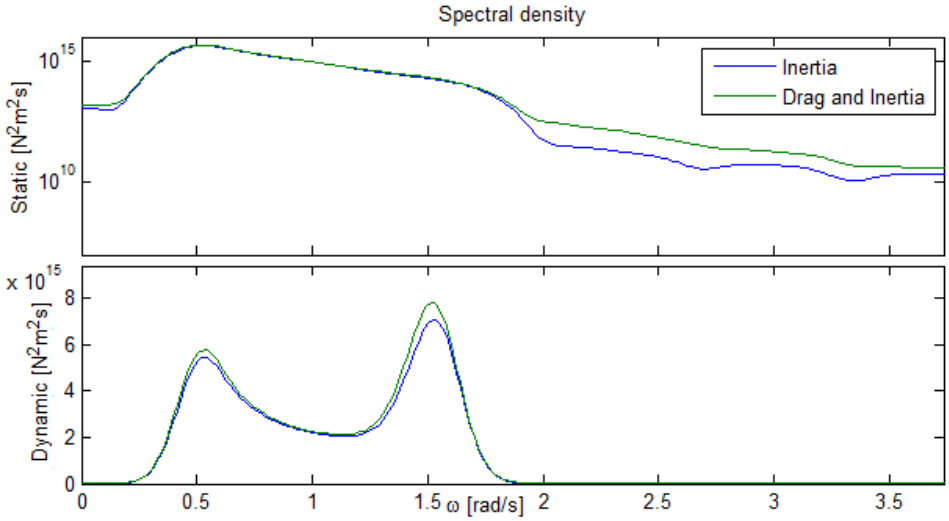

Figure 7.3: Spectra of static and dynamic moment from model 1, with and without drag.

7.2.1 Analysis by load model 1, $C_D = 0$

Peak-enhancement factor
A study of the effect of changing peak-enhancement factor, γ, has been performed. This is input to the JONSWAP specter given in eq. 3.4. Figure 7.4 shows how the wave spectrum changes with the $\gamma-$factors to consider. Increasing the factor moves energy to the peak frequency, and reduces the energy level at the natural frequency of the structure.

The resulting spectra of static and dynamic overturning moment for the different $\gamma-$factors are given in figure 7.5. We see how the reduced tail decreases the 1st mode excitation significantly.

Substructure damping ratio
Then, the effect of changing structural damping ratio in the monopile substructure

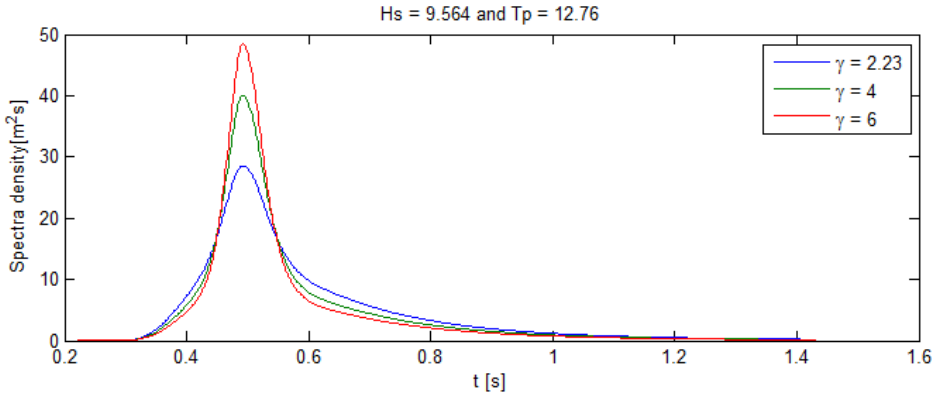

Figure 7.4: Wave spectra at different peak-enhancement factors

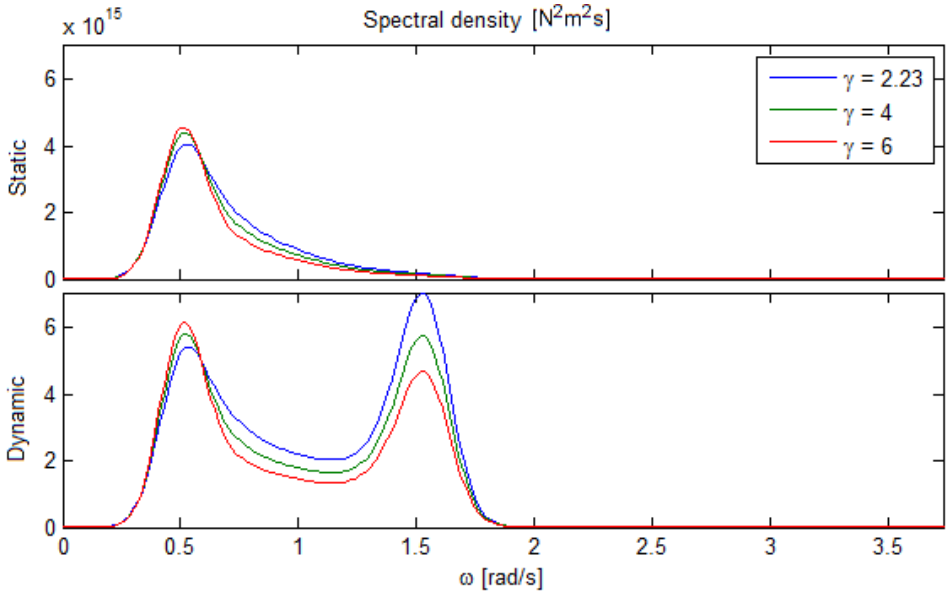

Figure 7.5: Spectra of static and dynamic moment from linear inertia load for different peak-enhancement factors.

has been analyzed at $\gamma = 6$. The result is given in figure 7.6. We see clearly how the increased damping gives less 1st mode excitation, but also that the dynamic effect of changing the peak-enhancement factor was more significant.

Soil pile damping ratio

The effect of damping ratio in the soil pile model has been investigated. The damping used in the previous calculations have been $v_k = 0.005$. Figure 7.7 gives the OM static and dynamic specter of two different structural damping ratios

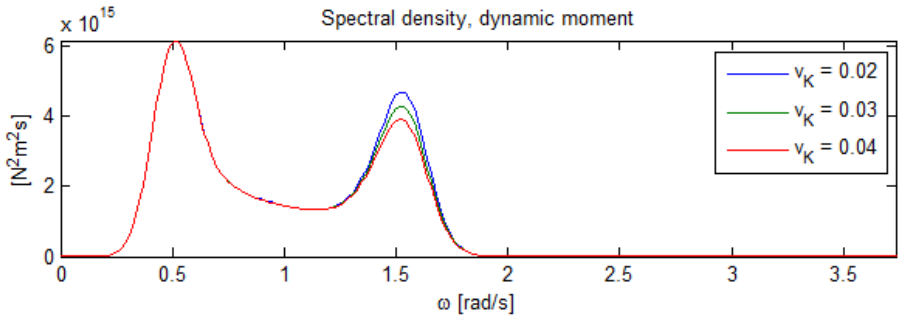

Figure 7.6: Spectra of dynamic overturning moment by linear inertia load for different damping ratios, v_k

applied to the beams in the soil pile model. The result is shown to be significant. The substructure damping ratio has been set to $v_k = 0.04$, the high value from the previous investigation.

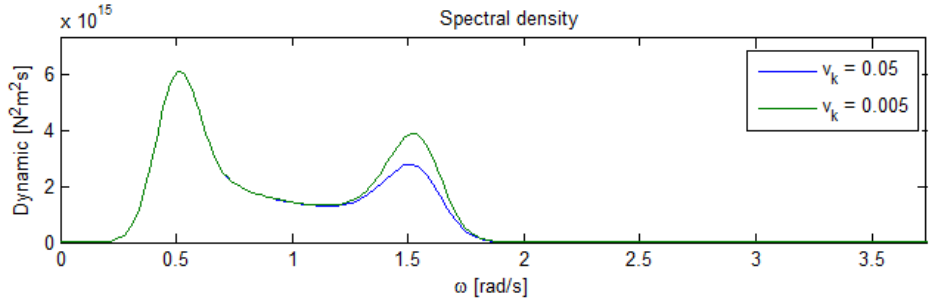

Figure 7.7: Spectra of static and dynamic moment by linear inertia load for different soilpile damping

Regular waves by Load model 1 and 4
Regular sea at $H = 0.7Hs$ and $T = Tp$ has been studied for model 1 (Linear) and 4 (Wheeler stretching), given in figure 7.8. The left picture shows static OM, and a little hump is indicated for model 4 around $2\omega_P$. The right figure shows dynamic excitation. There is no 1st mode excitation in model 1, but the hump in model 4 has become enlarged. Looking closely at model 4, a little hump is also seen at $3\omega_P \simeq \omega_N$, even though this is not visible in the static specter. Remember that the spectra is smoothed out, and that the specter created directly from FFT give more narrow peaks.

Specter Fading ON/OFF
Figure 7.5 to 7.7 show the specter created from a linear load with cut-off frequency significantly lower than the natural frequency. NO dynamic excitation should be

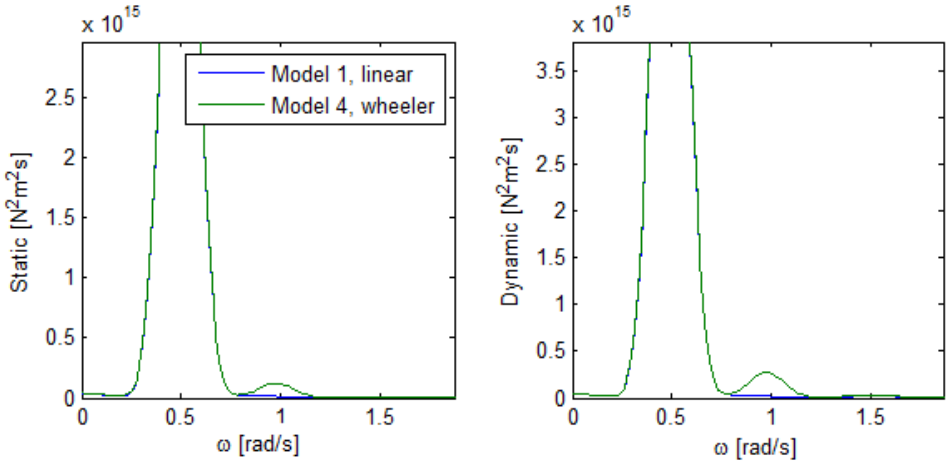

Figure 7.8: Spectra of static and dynamic moment from linear inertia load by regular wave, from model 1 and 4.

expected, equal to the result created by the regular wave in figure 7.8 by model 1. The reason for the excitation is that all the analysis has been performed with a wave spectra that is faded at the cut-off frequency, which gives a little tail of low energy that stretches beyond the natural frequency.

- 1st natural frequency: $\omega_{1st} = 1.556$
- Cut off frequency: $\omega_{cut} = \sqrt{2g/H_S} = 1.44$
- Highest frequency with fading: $\omega_{max} = 1.8212$

Figure 7.9 show the spectra for static and dynamic moment where the fading at cut-off is switched ON/OFF. High damping values are applied, $v_k = 0.05$ (soil pile) and $v_k = 0.04$ (substructure). The switch is shown to be successful, no excitation is created.

7.2.2 Influence of top mass

The parameter sensitivity analysis indicates that the dynamic output spectra is completely consistent with the static input spectra. There is no reason to believe anything wrong with the model. The large DAF must instead be explained by the nature of the wind mill structure.

The horizontal top mass displacement (TMD) creates a moment at the base given by the following relation:

$$M = m_{Top} \times g \times x_{disp} \tag{7.4}$$

The top mass, m_{Top}, in the model is 226 tons. The spectra of TMD and the resulting moment given eq. 7.4 is shown in figure 7.10. Load model 1,3 and 4 have

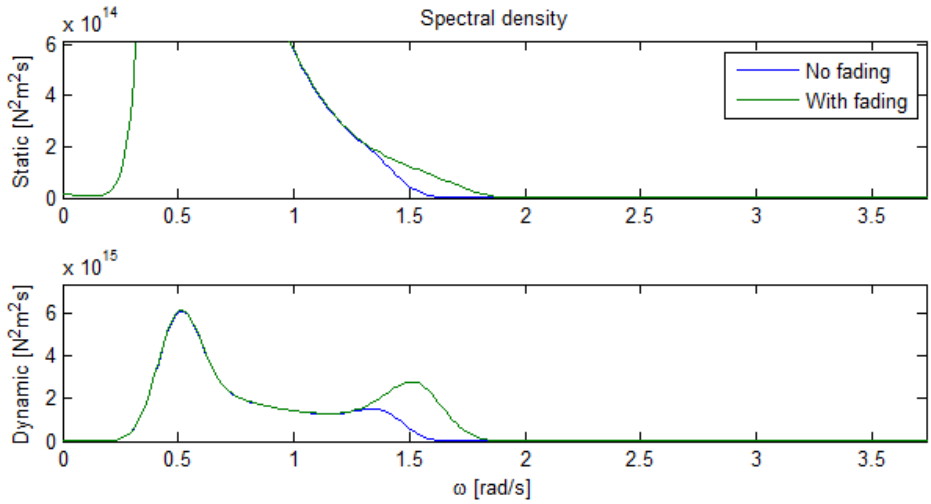

Figure 7.9: Spectra of static and dynamic moment from linear inertia, fading on and off.

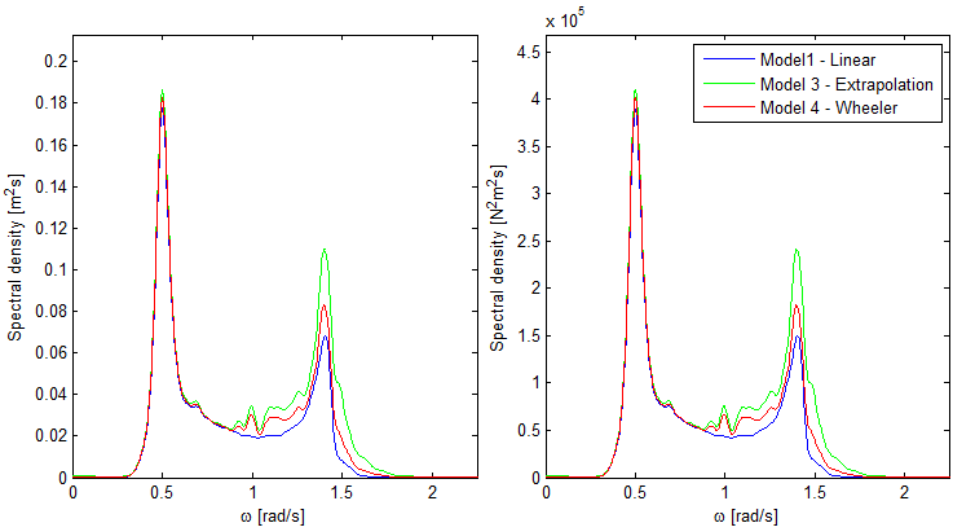

Figure 7.10: Dynamic top mass displacement and resulting OM eq. 7.4 at high damping values

been applied and high damping values are used, $v_k = 0.05$ (soil pile damping) and $v_k = 0.04$ (substructure damping). The **fading** is turned OFF, but the **drag** load is turned ON. We see again that the first mode is highly excited, which now is only due to the drag component (the only change in the load from the blue line in figure 7.9). The moment created by TMD will work as an external load and the

contribution is highly significant compared to the static moment created by drag load.

If TMD shall be a reason for the high excitation, then TMD must be highly sensitive to loads at the natural frequency. Figure 7.11 shows three pictures (TMD, OM and BSF) calculated from three cases.

- Case 1: High substructure damping, $v_k = 0.04$
- Case 2: Low substructure damping, $v_k = 0.01$
- Case 3: Low substructure damping, $v_k = 0.01$, with gravity turned OFF

The left picture show how the TMD is significant even with no gravity. Then, turning the gravity ON, the moment shown in figure 7.10 works as an external force which again will create dynamic amplification to the overturning moment. This will then also increase the TMD which creates an even larger load component at the natural frequency. This process will stabilize, and will highly contribute to the unexpected large dynamic amplification.

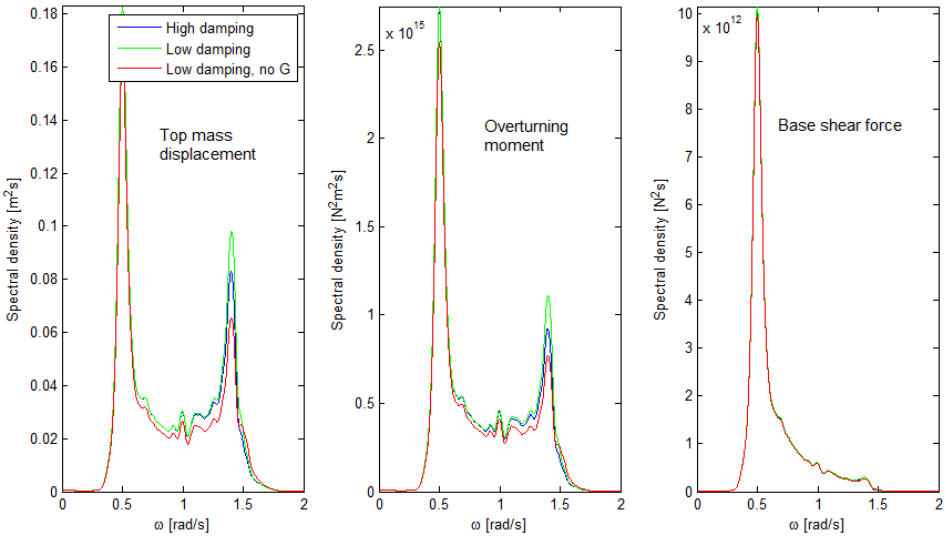

Figure 7.11: Dynamic top mass displacement, overturning moment and base shear force

The figure shows that the BSF is much less sensitive to excitation at the first mode, and that the increased external moment from the top mass displacement has no influence. Base shear force is then a much better response parameter to study when comparing the sensitivity to different load models.

7.3 Dynamic excitation by load models (with modified parameters)

Load model 1 to 6 including FNV has been analyzed using Fedem. To increase the sensitivity to the choice of load model, parameters that minimize the excitation of the 1st mode are chosen. The high substructure damping ratio of $v_k = 0.05$, that are used in some calculations above is not realistic and will be changed. The chosen parameters are given in the table. Drag is included.

v_k, substructure	$= 0.01$
v_k, soilpile	0.05
γ	6
Fading	OFF

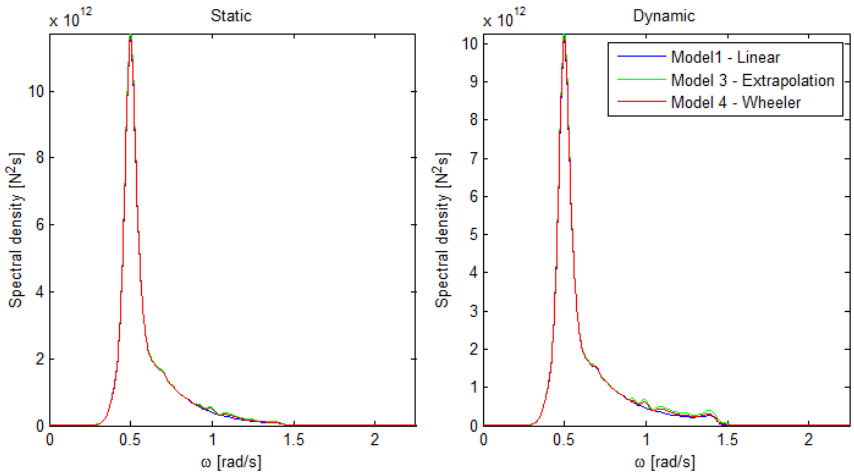

Figure 7.12: Spectra of static and dynamic BSF from model 1, 3 and 4.

Model 1, 3 and 4 (linear, extrapolation and wheeler) are shown to be quite consistent in terms of energy at ω_P, but model 3 shows slightly higher energy. The dynamic shear is shown to be significantly less then the static, but this relation is turned around when looking at overturning moment. The top mass effect (discussed in the previous section) might be the explanation. Model 3 is shown to give higher dynamic excitation than the other. Note that the higher γ-value is the reason for larger spectral peaks in this chapter compared to the analysis of load models in chapter 6. The spectra are calculated from time series of **50 minutes**, and $\Delta t = 0.5$**s**.

The spectra of **load model 2, 5 and 6**, that will be presented next, is based on a **20 minute** realization. The reason for a shorter duration is that the models

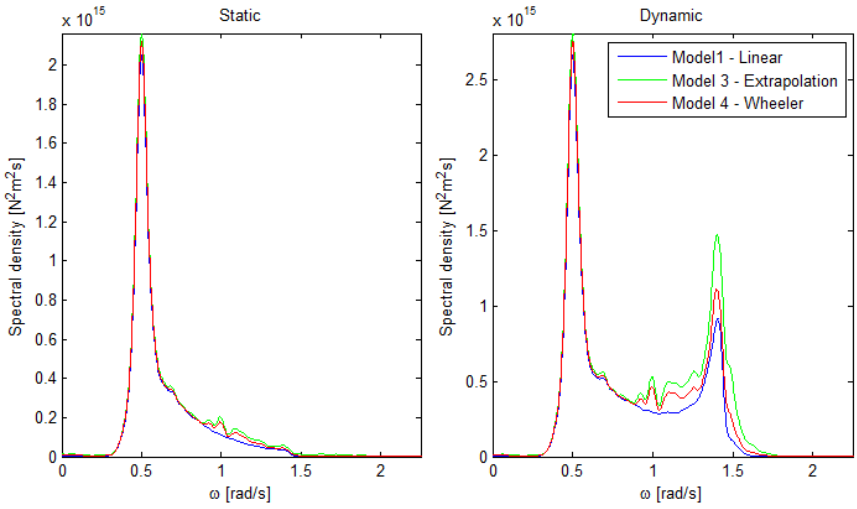

Figure 7.13: Spectra of static and dynamic OM from model 1, 3 and 4.

involve 2nd order irregular wave theory, which is very time consuming to calculate for long time series (as discussed in chapter 3).

All load models should be compared, and to be able to do this, we must compare the realizations using the same load model. Response spectra calculated by model 3 (extrapolation), for both shear and OM, is given in figure 7.14. We notice that

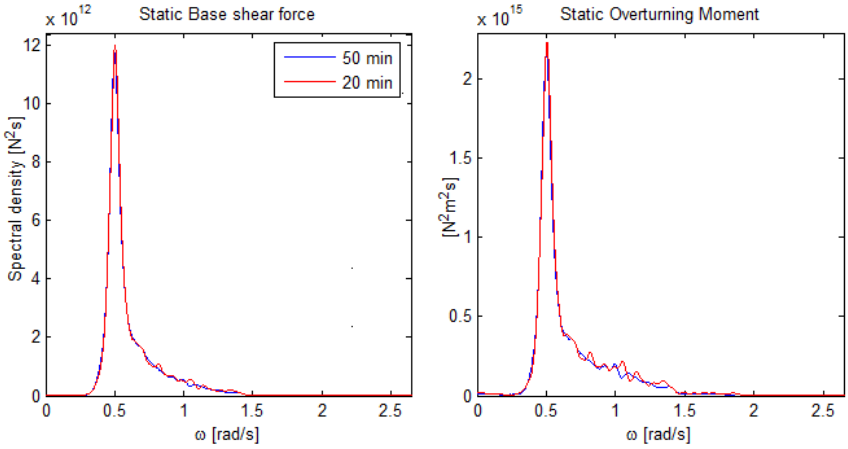

Figure 7.14: Spectra of dynamic BSF and OM from model 3 by 20 and 50 minute realizations

the 20 minute realization shows slightly more energy, both at first and second order (around $2\omega_P \simeq 1$). Keep in mind that the spectra are less reliable when calculated

from a shorter time duration.

Due to the unphysical enlargement of difference-frequency components in the second order irregular model at 25 meter water depth, a safe depth parameter of 30 meter was found in chapter 3. Spectra of model 2, 5 and 6 (models involving 2nd order theory) were calculated at 30 meter, but were found to give about 20% less energy at the ω_P-peak compared to model 1, 3 and 4. This was unexpected, and an investigation of how the water depth affects the scaling of kinematics were carried out. Figure 7.15 shows model 3 (extrapolation) calculated at the 25m wind turbine model, using both 25 and 30 meter water depth kinematics. The figure illustrate the lower energy used at the same model and seed. The way of choosing differ-

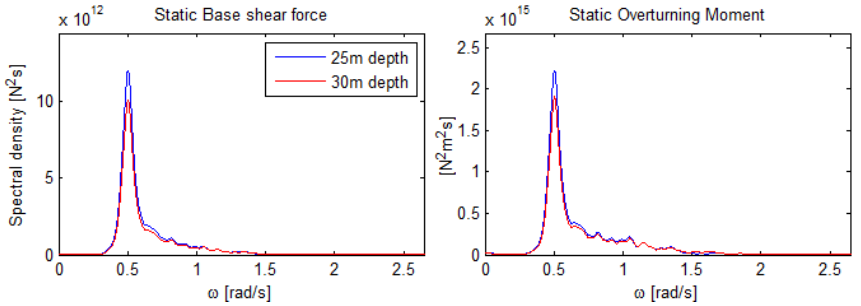

Figure 7.15: Spectra of dynamic BSF and OM from model 3 by 20 minute realization with kinematics calculated from 25 and 30 meter water depth.

ent water depths was obviously a mistake. Figure 7.16 shows the depth scaling of kinematics, given by the following relation (which is found both in the velocity and acceleration component):

$$\frac{\cosh k(z+h)}{\sinh kh}$$

The different pictures show how the scaling change for different wave periods. The

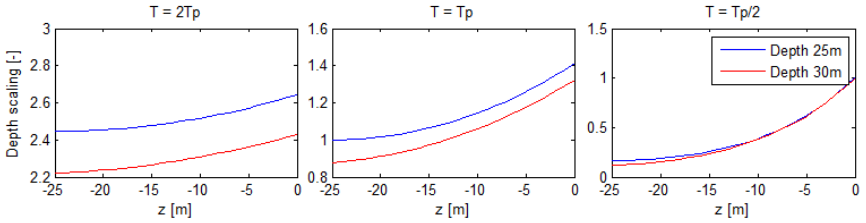

Figure 7.16: Depth scaling of kinematics with Tp = 12.76 at depth 25 and 30 meter

wave period determine the wave number through the linear dispersion relation, eq. 2.16.

The figure shows how the higher order spectral components is unaffected by depth scaling, because they propagate at deep water. But higher order loads at $2\omega_P$

and $3\omega_P$ are mainly created by the high energy waves, which are affected by the depth.

New time realizations were then calculated to create a peak at ω_P that is consistent with the previous calculations. The calculation of model 2, 5 and 6 were now done in a slightly more complicated way:

- The linear part of the model, $\phi^{(1)}$ and $\eta^{(1)}$, use 25m water depth
- The 2nd order part of the model, $\phi^{(2)}$ and $\eta^{(2)}$, use 30m water depth

This results in different depth scaling of order one and two, but the sum components in the 2nd order part will be unaffected because they anyway propagate at deep water.

The resulting spectra are shown in figure 7.17 and 7.18.

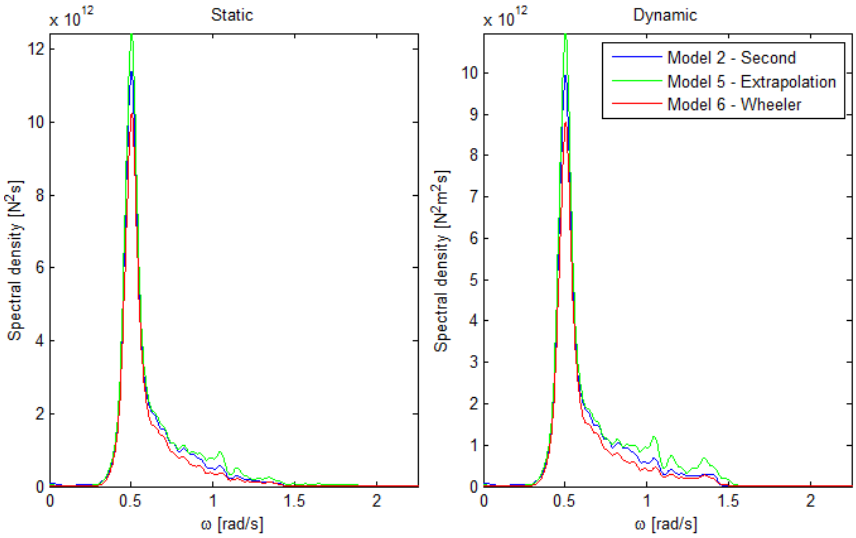

Figure 7.17: Spectra of static and dynamic base shear force from model 2, 5 and 6.

The trend of lower peak in the dynamic BSF spectrum compared to the static, observed in load model 1, 3 and 4, continues in these load models. The opposite relation for the peaks in the OM spectra has also continued.

The peak at model 5 is most consistent with model 1, 3 and 4, but is slightly increased above 12×10^{12}. Model 2 has become significantly lower, which is difficult to explain, but the same trend was found in chapter 6. The result from model 6 is surprisingly low, but this was also observed and discussed in chapter 6. Model 5 gives more energy at ω_N which results in large amplification in the OM-spectra.

The **FNV model** has also been calculated at 25 meter water depth. The time

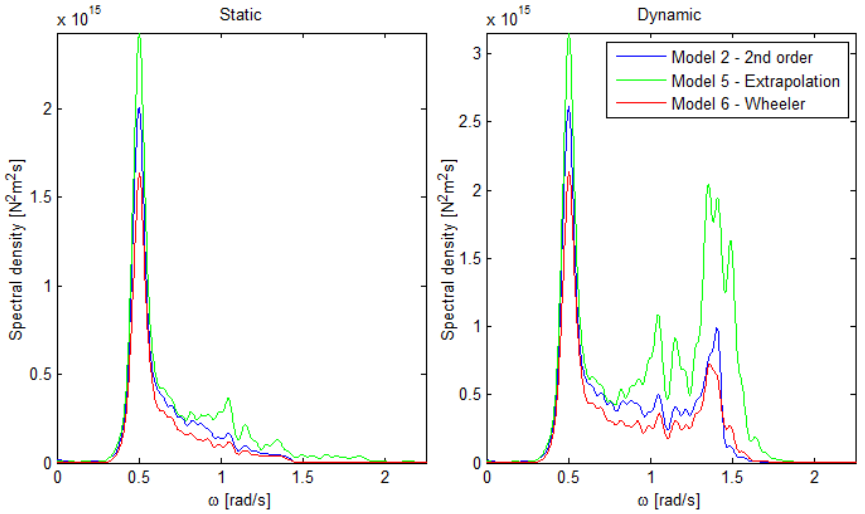

Figure 7.18: Spectra of static and dynamic moment from model 2, 5 and 6.

duration of 20 minutes has been applied. This model is most similar to the extrapolation models, model 3 and 5, which we have seen to contain most energy. In section 6.3, the FNV model was found to give the same peak at ω_P as the inertia load from model 5. The specter of the models is shown in figure 7.19 and 7.20. Keep in mind that the extrapolation models now also include drag load. The figures show that model 3 and 5 contains more second order energy, but that FNV gives more dynamic amplification because it contains more energy at $3\omega_P$. The peaks at ω_P is completely consistent between model 5 and FNV.

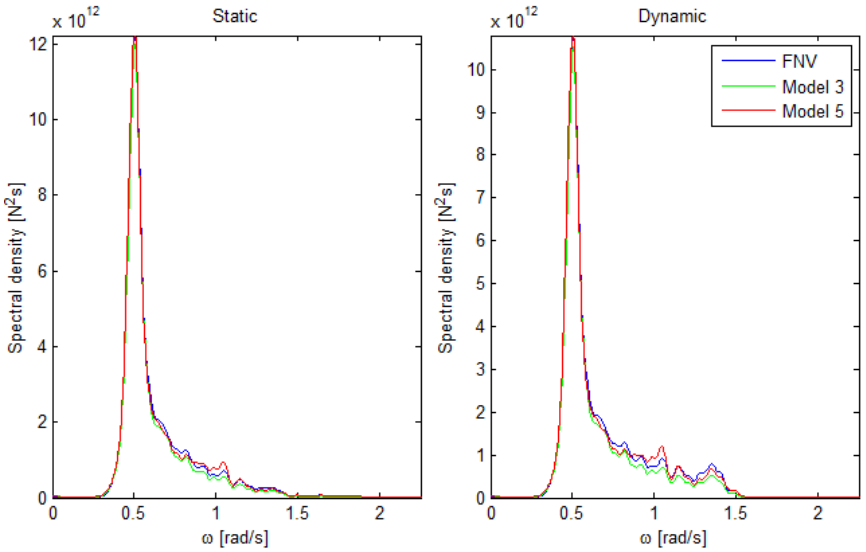

Figure 7.19: Spectra of static and dynamic base shear force from FNV and model 3 and 5.

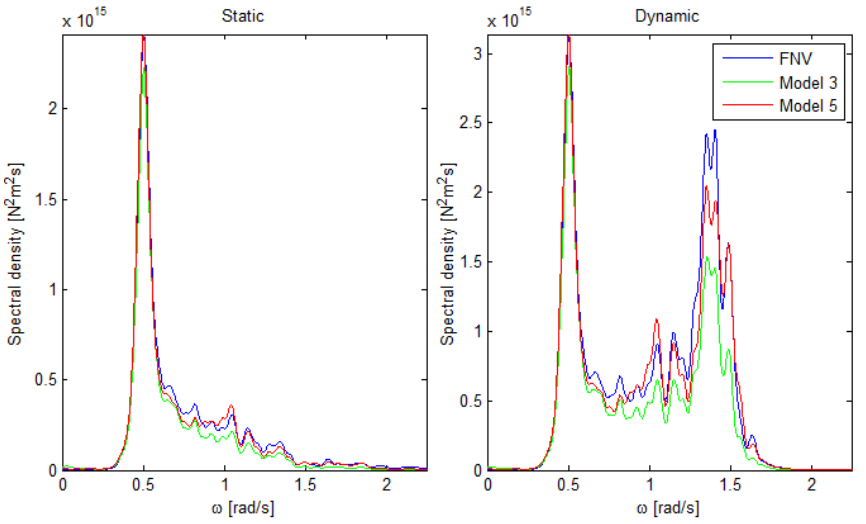

Figure 7.20: Spectra of static and dynamic moment from FNV and model 3 and 5.

Chapter 8

Embedded Stream Function

The Stream function wave theory was given a short presentation in chapter 2.4 to give the reader a theoretical background for the subject of this chapter. Large waves at the sites of bottom fixed wind mill structures will be limited by the water depth, and only the Stream function wave theory does give a valid physical description of the wave kinematics. Embedding is an important tool for applying the large waves that is required by load case 6.2a, and the usage in the verification process is discussed in the next section. The method has been implemented in MATLAB and this is described in the sections after, including different methods.

8.1 The use of Stream function waves

The waves of 50 year return period were determined in chapter 5 about site conditions. Values given by Næss at $Hs = 12m$ is found in table 5.5, but these wave heights were found to be unphysical due to the depth limiting factor. The design waves according to $Hs = 12m$ at $T_{low} = 12.28s$ from table 5.7 is given by the wave breaking limit determined by Stream function. The waves can be studied in the view of figure 2.3, that shows the applicability of different theories. The values on the figure axis is calculated:

- Depth 25m: $\frac{h}{gT^2} = 0.0169$
- Depth 45m: $\frac{h}{gT^2} = 0.0304$
- Stream function H = 18.1: $\frac{H}{gT^2} = 0.0122$
- Næss H = 22.66: $\frac{H}{gT^2} = 0.0153$

The figure tells us that the wave determined by Næss at 25m is in the wave breaking region, but that the wave height from Stream function is exactly at the breaking limit and can be described by a 9th to 11th order Stream function wave. The value from Næss is unchanged at 45 meter, and is safely below the wave breaking limit. This will at least require a 9th order description.

Linear waves are symmetric about the still water level, with equal size of crests and trough. When the water depth is a limiting factor and the order of wave theory is increased, the crest will grow and become more narrow, and the trough gets wider and less deep. The need of a 9th order wave indicates that this horizontal anti-symmetric profile is highly present. Only the stream function can provide such a high order, and the usefulness of stream function is then demonstrated. In addition, the kinematic is described correctly to the free surface as shown in chapter 2.4.

Offshore wind mills have been developed in the last decades, but at more shallow water depths and where the wave environment has been much less extreme then at Dogger Bank. The turbines have also been smaller, with the following reduced substructure dimensions. As shown in figure 6.3 and 6.2, the reduction of dimensions increases the significance of drag loads. Drag is calculated from the horizontal velocity, which has a profile that is similar to the profile of surface elevation. When the surface is anti-symmetric, the velocity will get the same shape, and a stream function is required to create a true representation. When drag loads dominate, this true representation is very important when searching for extreme loads. The velocity in the crest will be much larger then compared to linear theory, and linear waves will be highly non-conservative.

The largest wave according to load case 6.2a, H_{50yr}, will happen once through the design period. Then, testing the dynamic response of the structure with regular waves of H_{50yr} applied, will be unrealistic. To apply a linear or second order realization process containing H_{50yr} will on the other hand also be unrealistic, because the non-linearity of H_{50yr} is not captured. The validity of these irregular models are in addition restricted due to the water depth. The available kinematic models, stretching and extrapolation, might also be insufficient to create a true representation in the crest of the very largest waves, even in deep water when the theories are completely valid.

The problem has been overcome by a practical engineering approach, which is not founded in any theoretical perspective. The method is to create an **embedded stream function**, a stream function wave put into a stochastic irregular wave model. The method is widely applied in the verification process of wind turbines. The stochastic nature of the surface will be violated, but the idea is that this does not matter when looking at extreme values according to ULS

The method is not available in any commercial software, but has been implemented in MATLAB as a part of this thesis and is available for application to Fedem in the same way as the other kinematic models described in chapter 6. The next chapters will introduce how the implementation is done, and the different ways

available of creating the embedded wave model. The goodness of the model related to dominating drag versus inertia load will be discussed.

8.2 Matlab Implementation

8.2.1 Kinematics

The proposed solution to the stream function was given in equation 2.36 in chapter 2.4. The wave kinematics is derived directly from this expression. The horizontal wave particle velocity in the fixed coordinate system (not moving with the wave), is found to be:

$$u = -\sum_{n=1}^{N} kX(n)\cosh nk(z+h)\cos nk(-c_r t + x) \tag{8.1}$$

Material derivative is found in Kundu [15], and is the total derivative including both time and spatial derivatives. This must be used to calculate the acceleration when higher order terms are included.

$$\frac{du}{dt} = \frac{\partial u}{\partial t} + u\frac{\partial u}{\partial x} + w\frac{\partial u}{\partial z} \tag{8.2}$$

$$w = -\sum_{n=1}^{N} nkX(n)\sinh nk(z+h)\cos nk(-c_r t + x) \tag{8.3}$$

$$\frac{\partial u}{\partial t} = -c_r k u(x,z,t) = -c_r u_x$$

$$\frac{\partial u}{\partial x} = \sum_{n=1}^{N} (nk)^2 X(n)\cosh nk(z+h)\sin nk(-c_r t + x)$$

$$\frac{\partial u}{\partial z} = -\sum_{n=1}^{N} (nk)^2 X(n)\sinh nk(z+h)\cos nk(-c_r t + x)$$

N is the order of theory, $X(n)$ is the n'th Fourier coefficient, and c_r is the phase velocity. The total wave acceleration can be written as:

$$\frac{du}{dt} = (-c_r + u)u_x + wu_z \tag{8.4}$$

Figure 8.1 is created by MATLAB at 25 meter water depth. We see how the depth increases the non-linearity of larger waves. It is easy to see how the surface elevation and velocity moves towards cosine curves for shorter waves, and the acceleration moves towards a sine curve. We also see that the velocity get a very sharp top at the breaking limit, and that the acceleration is close to become discontinuous at the crest.

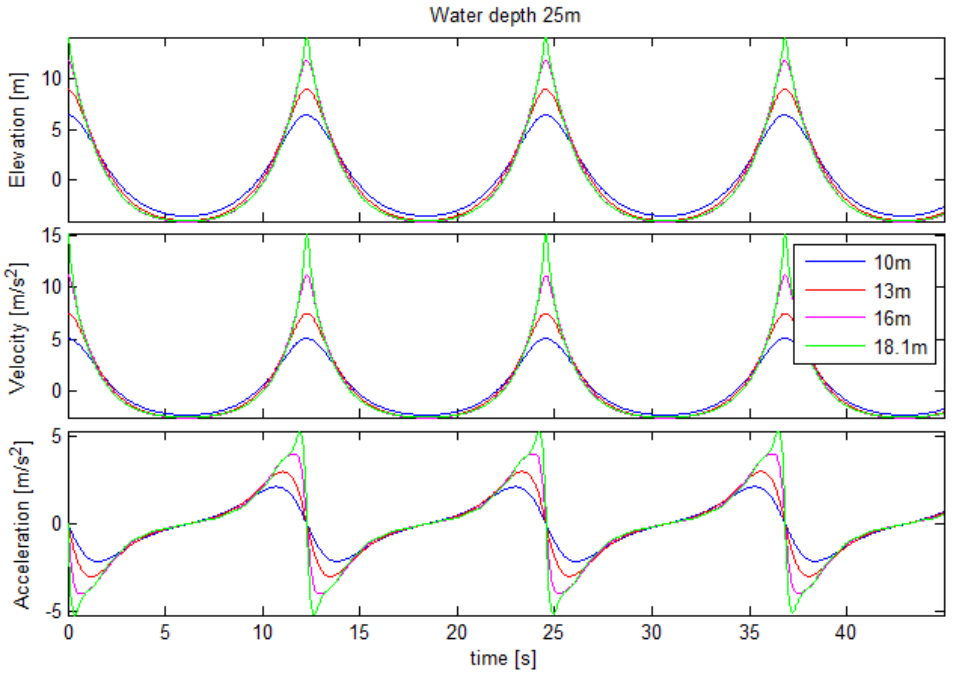

Figure 8.1: Surface elevation, velocity and acceleration for different wave heights

8.2.2 Calculation of the system of equations - Fortran routine

The system of equations described in chapter 2.4 is difficult to solve and require insight in numeric iteration procedures used to solve non-linear systems. A Fortran routine written by J. G. Dalrymple (see reference [29]) is available on the internet, and has been used for the calculation. The routine has been modified and compiled, and is implemented in MATLAB as a call to an external executable function.

The surface elevation is not given in any equation, but is a part of the solution in the equation system. The elevation is solved in a number of points along the x-axis, a number that is given as user input. Other input parameters to the solution process is the number of iterations, damping and theory order. In the modified Fortran routine delivered with this master thesis, some number are set:

- The number of iterations is set to 10
- The number surface points is set to 41
- The damping is 0.3

The parameters is easy to change by looking into the text file of the program. The damping is a numeric parameter included in the solution process and is advised to

be the given number. The user is also able to specify water current, but this has been set to 0.

The user specifies theory order, depth, wave height and wave period. The output coefficients from the routine are given as follows:

- Coefficient 1: Wave length [ft]
- Coefficient 2: First Fourier coefficient, X(1) [ft^2]
- Coefficient N+1: Last Fourier coefficient, X(N) [ft^2]
- Coefficient N+2: Volume flux under the wave Q [ft^2/s], but given with a negative sign.

The volume flux is given as defined in equation 2.34, ans is completely consistent with the flux found by numerical integration in MATLAB of the resulting velocity field.

Input and output between MATLAB and FORTRAN is done by using text files. The interface between the programs change from meter to feet automatically, and the user does not need to think about this.

8.3 Forced Embedding

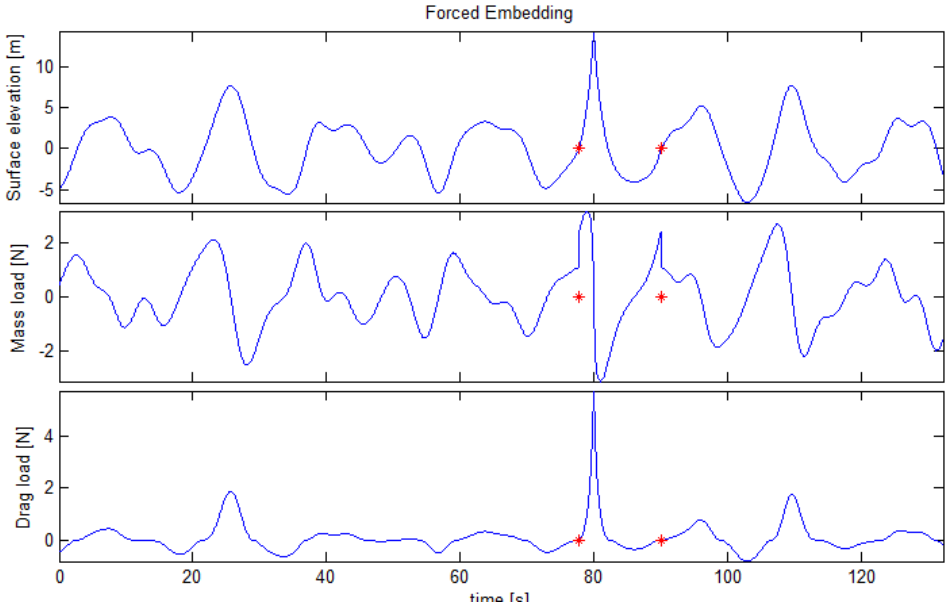

Figure 8.2: Forced embedding, plot of wave elevation, mass and drag load from morison equation

A simple way to create the embedded stream function is to find an arbitrary zero up-crossing in the realization of linear irregular waves. Then the realization can be split apart at this point, and a stream function wave of the wanted height can be substituted in. The red points in figure 8.2 was connected in the original time realization.

The consideration to neighboring waves with respect to height or period is not taken care of. The wave elevation and velocity will be continuous in the embedded realization, but the acceleration will not. This method will be refered to as **forced embedding** because the change in the wave field is sudden and the position of substitution is completely arbitrary. Figure 8.2 shows the wave elevation, inertia load and drag load for a forced embedded realization at depth 25m. The Stream wave is created as the design wave determined by wave breaking at 25m with $T = 12.28s$, giving H = 18.1m (from table 5.7). The sea state parameters are Hs = 12m, Tp = 15.8s and $\gamma = 4$.

We see that the drag load given by stream function is extremely large, and that it actually becomes larger then the inertia load. The discontinuity created by acceleration is not physical and gives a bad representation of the loads on the structure.

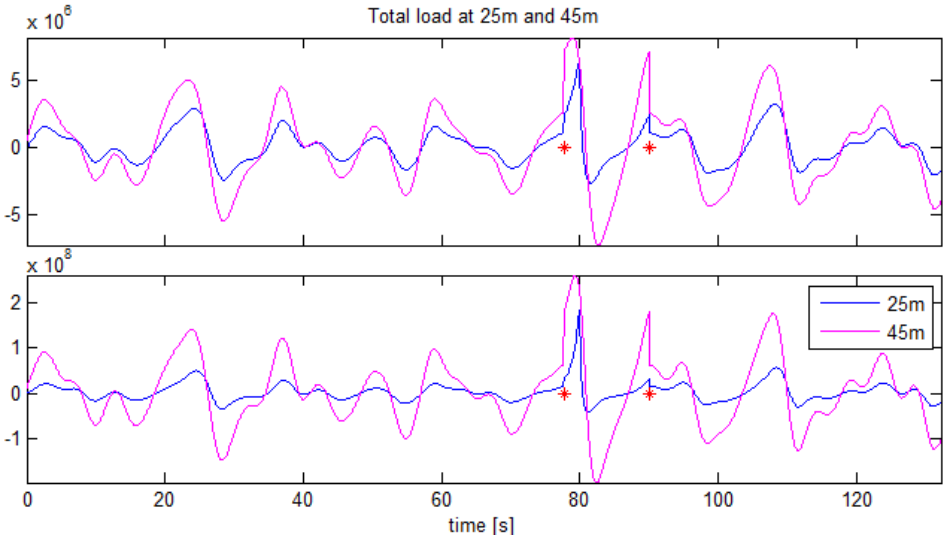

Figure 8.3: Forced embedding with H = 18.1m, load from drag and inertia at the two wind mill structures

Figure 8.3 show the total load (drag and inertia), both base shear force and moment, at the two wind mill structure designs at water depth 25 and 45 meter. It show how the spike created by acceleration becomes even larger when the structure dimension increases from 6m to 8m. The load graphs touches at the peak of the 25 meter load. This is where acceleration is zero, and velocity is at maximum. The drag has

not increased as much as inertia, remember that inertia load increases with D^2 but that drag only has a linear relation.

8.4 Smooth Embedding

Embedded stream function can also be created in a more sophisticated way. A long time realization can be carried out to find the largest wave height or crest that can be chosen as the location to put the stream function. Instead of cutting the time series apart and substituting a predefined wave in to a zero up-crossing as done above, the stream function wave will be blended in to the realization and replacing the original wave. This method is described in reference [8], and is the only reference to embedding found through a comprehensive literature study. Figure 8.4 shows

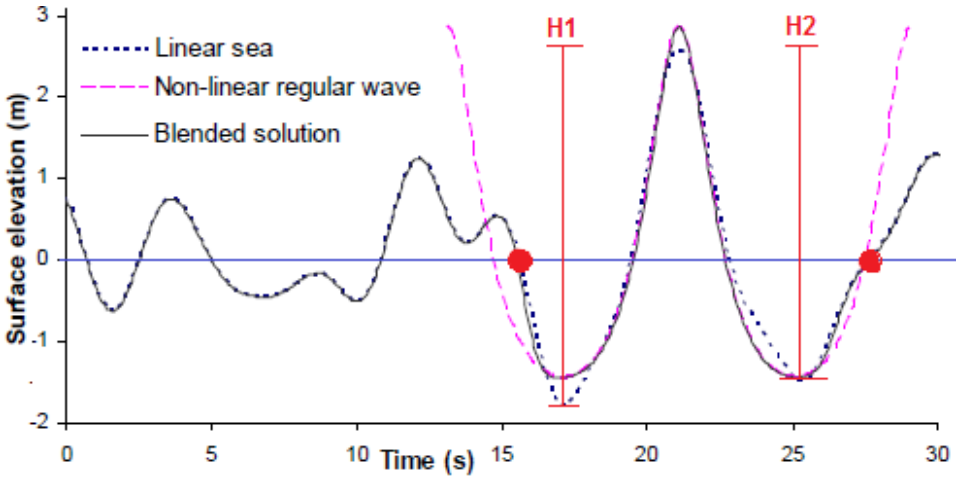

Figure 8.4: Implementation of embedding with smoothing functions, builds on [8]

how the stream function is embedded in to the stochastic time history. The large stochastic wave is asymmetric with different depth of the succeeding troughs. The embedded wave is regular and symmetric, and will violate the stochastic nature of the time realization. Table 8.1 shows the smoothing functions proposed in reference [8]. T_0 denotes the time at the crest, t is the running time, and T the wave period of the wave in the stochastic time series. The stream function must be chosen with the same wave period and height as the original wave to give a best fit into the realization. The blending parameters are created with a cosine function which gives a continuous surface and surface time derivative through the transition. The same blending parameters will be used for the kinematics.

Figure 8.4 shows how the wave period and wave height of the wave is calculated. The wave period is found by the time difference between the red points, which is spaced 1.5 times the wave period. The wave is either picked out as the largest wave

Time	Stream function	Stochastic time history
$\lvert t-T_0\rvert > 3T/4$	0	1
$T/2 \leq \lvert t-T_0\rvert \leq \frac{3}{4}T$	$\frac{1}{2}+\frac{1}{2}\cos\left(4\pi\left(\frac{\lvert t-T_0\rvert}{T}-\frac{1}{2}\right)\right)$	$\frac{1}{2}-\frac{1}{2}\cos\left(4\pi\left(\frac{\lvert t-T_0\rvert}{T}-\frac{1}{2}\right)\right)$
$\lvert t-T_0\rvert < T/2$	1	0

Table 8.1: Smoothing functions to blend a regular wave in to a stochastic time history

height or crest in the realization. When finding the largest height, every wave is given two wave heights, given as H1 and H2 in the figure. The wave that gives the largest H1 or H2 becomes the chosen wave.

This process becomes more easy when defining the largest crest. But which trough shall define the wave height? Two methods have been implemented, one use the mean trough depth, the other use the deepest.

8.4.1 Statistic consequences

An analysis of the statistic consequences of embedded stream function has been performed. The embedded wave replaces the wave of the largest height or crest in a long time realization. The wave will be assumed to create the largest load through the realization. A study of how the extremal value changes from the stochastic wave to the stream function wave can then be studied by creating a Gumbel plot from a number of realizations.

The analysis has been carried out with the following parameters:

- Depth, $h = 25$m
- time duration: 30min
- Tp = 16.2s
- Hs = 12m

The program search for the highest wave, and find its wave period. At the original Tp = 15.8s, sea state 5 from table 5.3, the program indicate many occurrences of wave breaking: The stream function wave can not be calculated with the obtained values of H and T. The solution is to slightly increase Tp, so that large waves in general get a longer wave period which has a higher breaking limit.

As mentioned above, there are methods to pick out the largest wave:

- Method 1: Largest wave height
- Method 2: Largest wave crest, height defined to the mean trough depth
- Method 3: Largest wave crest, height defined to the deepest trough

40 realizations of linear waves was carried out, which gave 28 successful embedded waves by method 2. The resulting base shear between original wave and embedded wave, is presented in Gumbel plots.

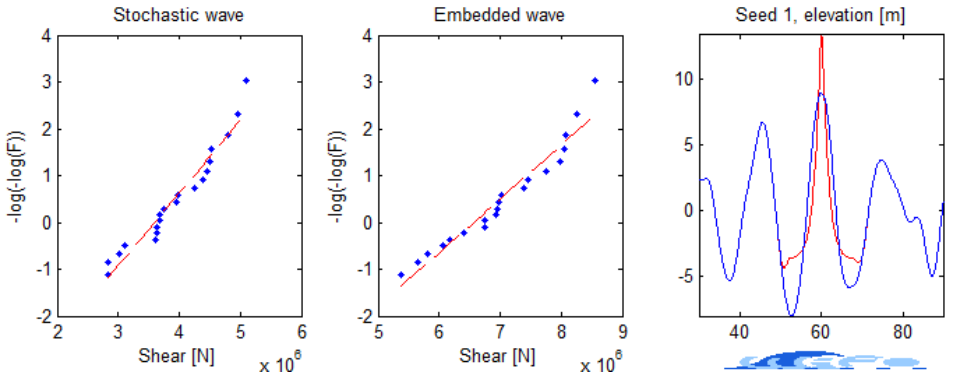

Figure 8.5: Embedding at the largest wave heigh in realizations of 30 minutes

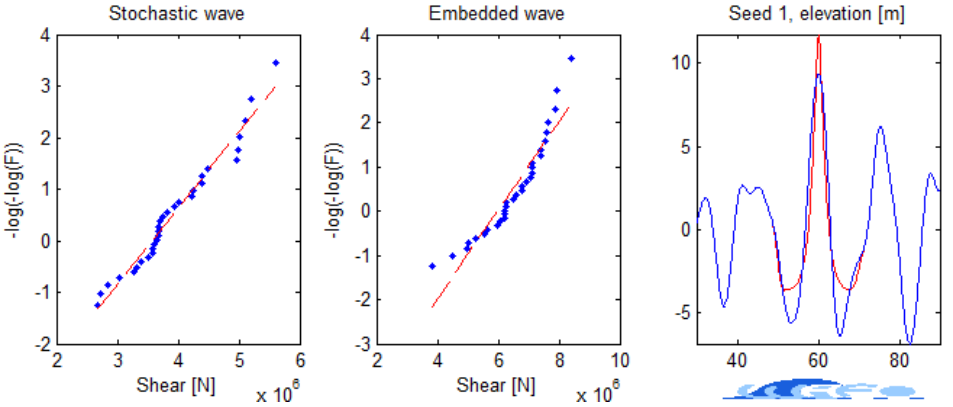

Figure 8.6: Embedding at the largest wave crest, method 2, in realizations of 30 minutes

Comments:
It must be emphasized that load model 3, extrapolation, is used in the irregular waves. The loads are found to be large when compared to the result of shear load at the 25m structure given by the design wave in figure 8.3. The reason is related to time step and the sharp peak of acceleration, shown in figure 8.2. The topic will be discussed in the end of chapter 9 about load case 6.2a.

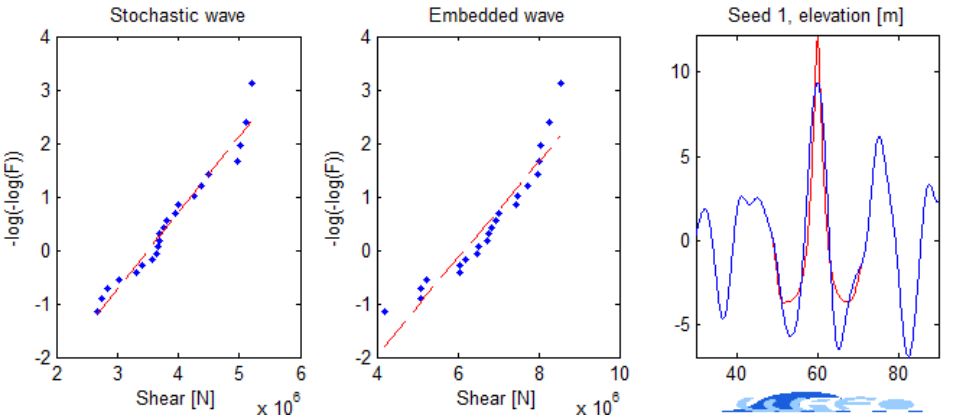

Figure 8.7: Embedding at the largest wave crest, method 3, in realizations of 30 minutes

8.4.2 Mixed approach between forced and smooth embedding

A combined method between the forced and smooth embedding has been created. A wave according to the design parameters can be predefined. Then a time series can be created where the suitable wave is picked out with one of the three methods outlined above. The only problem now, is that the period of the chosen wave in the realization might be smaller than the predefined wave period. What we want, is that the crest of the embedded wave shall replace the original. This is ensured, and the stochastic time series is extended at the wave crest, where it is weighted by the blending parameters to zero! The wave period used in the smoothing functions (T in table 8.1) is now the predefined period. Figure 8.8 shows the implementation. The red circles show the area of transition.

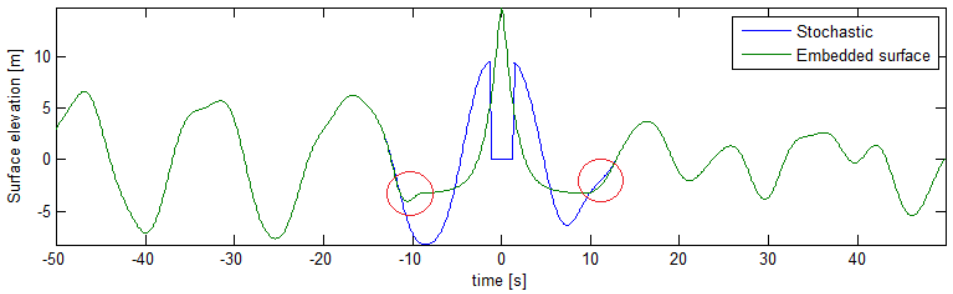

Figure 8.8: Implementation of mixed approach embedding

The shear force resulting from this surface elevation is found in figure 8.9. The method can be compared to forced embedding at 25m water depth found in fig-

ure 8.3. Both use the same design wave of $H = 18.1m$ and $T = 12.28s$. The discontinuity created by acceleration is not present anymore.

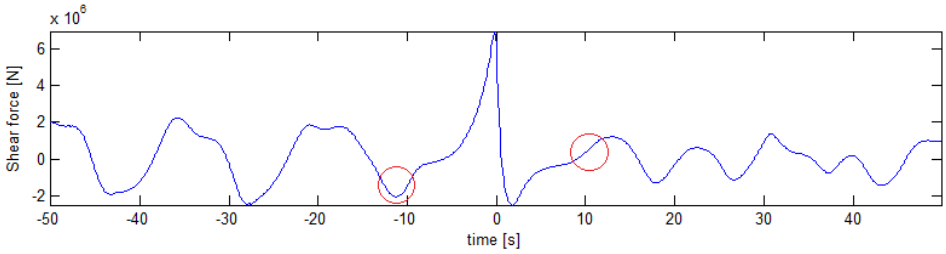

Figure 8.9: Shear froce from the mixed approach embedding

Chapter 9

Non-linear loads in design calculations

9.1 Load case 6.1a, Dynamic calculation

9.1.1 Assessment of Load models in extreme wave events

Running the dynamic structural analysis, as required by the standards discussed in chapter 4, is time consuming and needs powerful computer resources. The goal is to assess the use of different non-linear models in design load calculations, rather than actually find statistical answerable design values.

The standard require many seeds of calculation at different points on the 50-year contour line. The realizations should last between 30 minutes and 3 hours, preferably 3 hours as the duration of a sea state.

The models were compared in chapter 6 around the peak load in an arbitrary time realization. This method will also be used in this section, but now the event will be chosen more carefully. Linear irregular waves are used to calculate realizations of 20 minutes using 9×20 different seeds. This should be equal to run a 3 hour analysis (3 hour $= 9 \times 20$min), at 20 different seeds. 20 minute realizations is chosen instead of 3 hours, because the CPU time then is much reduced due to less spectral components (as discussed in section 3.2.1). Two seeds were picked out: The realization containing the largest crest, and the realization containing the largest positive acceleration.

The analysis use the parameters in section 7.3, dynamic calculation:

- The wave specter is calculated with $\gamma = 6$, and with the use of Hs $= 9.56$ and Tp $= 12.76$ given by sea state 1 in table 5.3

- Fading is turned OFF
- Linear kinematics: $\phi^{(1)}$ and $\eta^{(1)}$, use 25m water depth
- 2nd order kinematics: $\phi^{(2)}$ and $\eta^{(2)}$, use 30m water depth
- Damping values are realistic: $v_k = 0.05$ (soil pile) and $v_k = 0.01$ (substructure)

The sea state of the lowest Hs-value is chosen, because it is the most interesting sea state in a dynamic perspective, with $3\omega_P \simeq \omega_N$.

The realizations have been applied to the Fedem model. The maximum base shear force and overturning moment, both static and dynamic, have been found in each realization and are presented in tables. The time of occurrence, and the dynamic amplification at that specific point is also given. The maximum DAF through the realization is also found by dividing the dynamic response by the static load at each time step. The location of this occurrence is also given. All the static loads presented, is the loads applied through MATLAB, and not output from quasi-static analysis on the model.

Seed giving the largest acceleration
Table 9.1 shows the result of base shear force given by the 20 minute realization containing the largest positive acceleration. This occur at $t = 983$s and all the models are found to give the largest loads around this event. The loads are positive in all models because the peak acceleration is positive. The largest dynamic and

Model	F^{dyn}_{max} [MN]	DAF	time [s]	F^{stat}_{max} [MN]	DAF	time [s]	DAF_{max}	time [s]
1	3.66	1.01	983	3.6	1.01	983	119.11	607.5
2	3.65	1.04	983.5	3.67	0.99	983	397.78	1027
3	4.7	0.96	983.5	4.89	0.96	983.5	581.31	201
4	4.2	0.98	983.5	4.29	0.98	983.5	1259.89	607.5
5	5.45	0.98	984	5.54	0.98	984	82.36	1033
6	3.34	0.94	983.5	3.56	0.94	983.5	82.95	545
FNV	5.29	0.97	983.5	5.48	0.97	983.5	249.36	601.5

Table 9.1: Maximum base shear, DAF and time of event in the sea state of maximal acceleration

static shear occur at the same time step in each model, but there is a variation of 1 second between them. The DAF is found to be about 1 in all models. The results of largest DAF in the realization, does not seem to provide any valuable information. The ratio between models are found to be consistent with the results in chapter 6 and 7. Model 5 is the largest, followed by FNV and model 3. A cut of the realization showing these models are given around the peak event in figure 9.1. Model 6, stretching to the 2nd order wave elevation, is again found to be smallest.

Table 9.2 and figure 9.2 show the same data of overturning moment. The same trends are found, but the DAF-values are increased significantly. However, this is

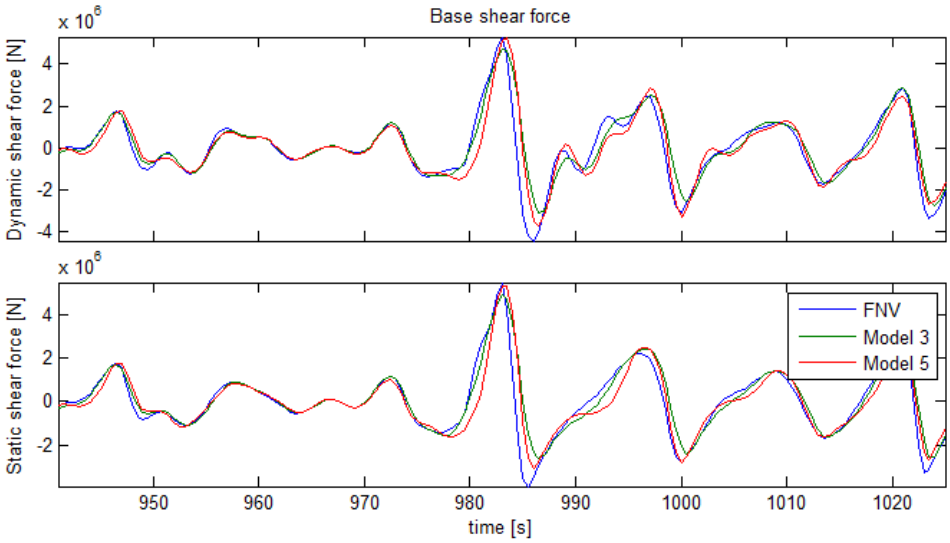

Figure 9.1: Time series around maximum event from table 9.1, FNV and model 3 and 5

no surprise, comparing the spectra of static and dynamic OM provided in chapter 7. The static OM in each model is found at the same time step as the BSF in the previous table, and is positive in each model as the case with BSF. The same ratio between magnitudes are again observed. The dynamic result is now more

Model	M_{max}^{dyn} [MNm]	DAF	time [s]	M_{max}^{stat} [MNm]	DAF	time [s]	DAF_{max}	time [s]
1	76.51	1.47	983	52.03	1.47	983	4208.88	138.5
2	-81.68	1.92	83	54.77	1.22	983	439.76	354.5
3	-105.11	3	987.5	91.03	1.06	984	391.87	703.5
4	85.15	1.13	984	76.64	1.11	983.5	2715.3	138.5
5	-150.72	3.38	987	119.1	1.02	984	3026.62	273.5
6	-64.35	3.23	83.5	52.38	0.9	983.5	2277.81	1056.5
FNV	-174.65	2.67	986.5	116.75	0.93	983.5	795.28	195

Table 9.2: Maximum overturning moment, DAF and time of event in the sea state of maximal acceleration

interesting, due to much larger dynamic amplifications. This is consistent with the results provided in chapter 7, considering the ratio between the peaks in static and dynamic OM spectra. The largest response is now found to be at the preceding trough on the graphs, and that is why negative moment values are listed in the table. This is also the case in model 3, but not in model 1 and 4.

Notice that large dynamic amplification has triggered at another location, $t = 83$s, in model 2 and 6. The static moment at this location is about 85% of the listed M_{max}^{stat} in the table, but dynamic amplification has for some reason triggered. We

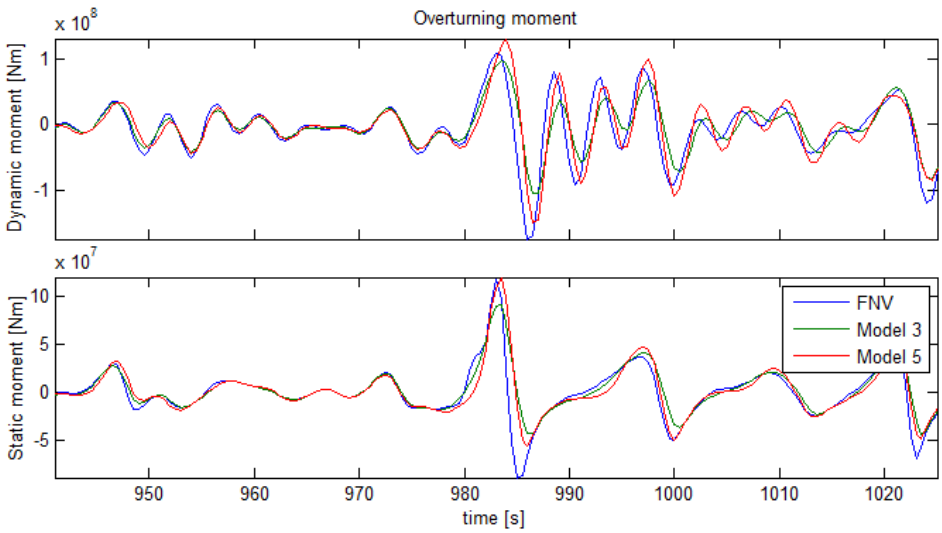

Figure 9.2: Time series around maximum event from table 9.2, FNV and model 3 and 5

must be aware of that dynamic amplification trigger of non-linearity which do not necessary coincide with the largest acceleration created by a linear model. This illustrate the importance of running dynamic simulations in the time domain.

Seed giving the largest crest

Table 9.3 shows the result of base shear force given by the 20 minute realization containing the largest crest.

Model	F_{max}^{dyn} [MN]	DAF	time [s]	F_{max}^{stat} [MN]	DAF	time [s]	DAF_{max}	time [s]
1	-3.92	1.02	691	3.9	0.91	686.5	85.33	51.5
2	-4.59	1.01	691	-4.55	1.01	691	18390.35	938
3	5.42	0.96	687.5	5.73	0.88	687	71.73	708
4	4.64	0.95	687.5	5.11	0.89	687	85.98	51.5
5	-6.87	1.29	690.5	6.21	0.91	687	348.99	185
6	3.54	0.89	687	4.01	0.86	686.5	169.67	551.5
FNV	-6.87	1.22	690	-5.71	1.02	689.5	362.96	860.5

Table 9.3: Maximum base shear, DAF and time of event in the sea state of maximal acceleration

The crest occur at $t = 686.5$s and all the models are found to give the largest loads around this. A cut of the realization around the event is given in figure 9.3 and 9.4 showing the dynamic and static BSF given by model 1-6. The largest dynamic and static shear occur around the peak crest in each model, but there is now observed a delay, in contrast to the previous realization. Dynamic amplification has moved F_{max}^{dyn} to the preceding trough (negative signs). The values is increased, especially

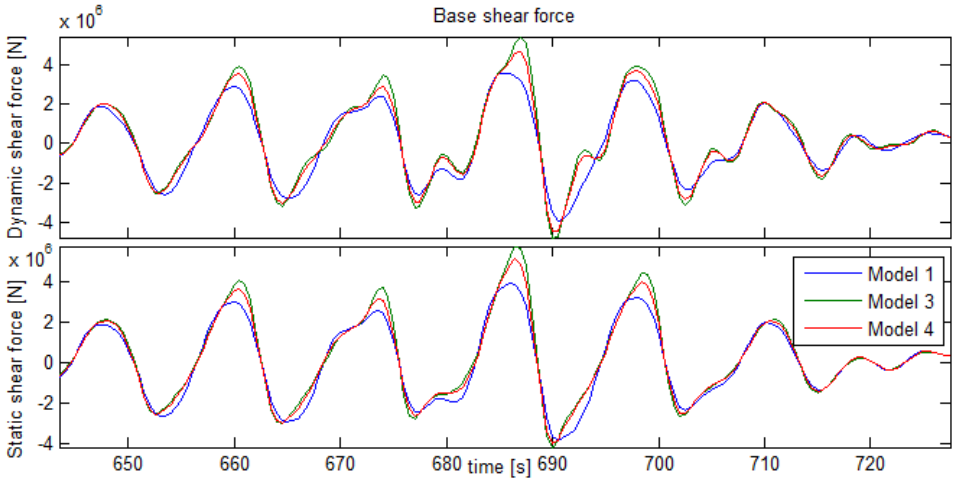

Figure 9.3: Time series around maximum event from table 9.3, model 1, 3 and 4

in model 3, 4 and 5, which integrates to the linear surface and is increased by the high crest. The DAF is found to be mostly the same compared to the previous realization, but the value in model 5 and FNV is significantly increased. The largest static load in FNV is at the negative value and trigger large amplification at this point. The resulting F_{max}^{dyn} of the two models are by coincidence the same. FNV is not included in the figures due to over-complexity to the reader. It does to a large extent follow model 5, except that the value is significantly lower at the occurrence of the largest crest.

Model	M_{max}^{dyn} [MNm]	DAF	time [s]	M_{max}^{stat} [MNm]	DAF	time [s]	DAF_{max}	time [s]
1	-97.09	1.93	691.5	53.93	0.63	687	11923.16	1062
2	-107.92	1.68	690.5	-64.27	1.68	690.5	4552.69	327.5
3	-175.45	3.39	691	113.79	0.96	687.5	1201.19	853
4	-149.69	2.88	691	95.74	0.96	687.5	32436.92	1062
5	-270.28	3.11	690.5	138.5	1.17	687.5	1918.78	1072.5
6	-87.61	4.08	691	56.88	0.69	687	1660.32	276
FNV	-272.17	3.6	690.5	126.59	1.27	689.5	3132.69	1062

Table 9.4: Maximum overturning moment, DAF and time of event in the sea state of maximal acceleration

Table 9.4 and figure 9.5 and 9.6 show the same data of overturning moment. The same trends are found, and the DAF-values are again increased significantly. The $M_{max}^{stat}-$value in each model is found within 0.5s from the respective listed occurrence of F_{max}^{stat}. The same ratio between magnitudes are again observed to continue. M_{max}^{dyn} is now found to be at the preceding trough in each model, except in model 2 where M_{max}^{stat} coincide with the trough. FNV does again create the largest M_{max}^{dyn}, and model 5 the largest M_{max}^{stat}. The FNV model is seen to trigger dynamic excita-

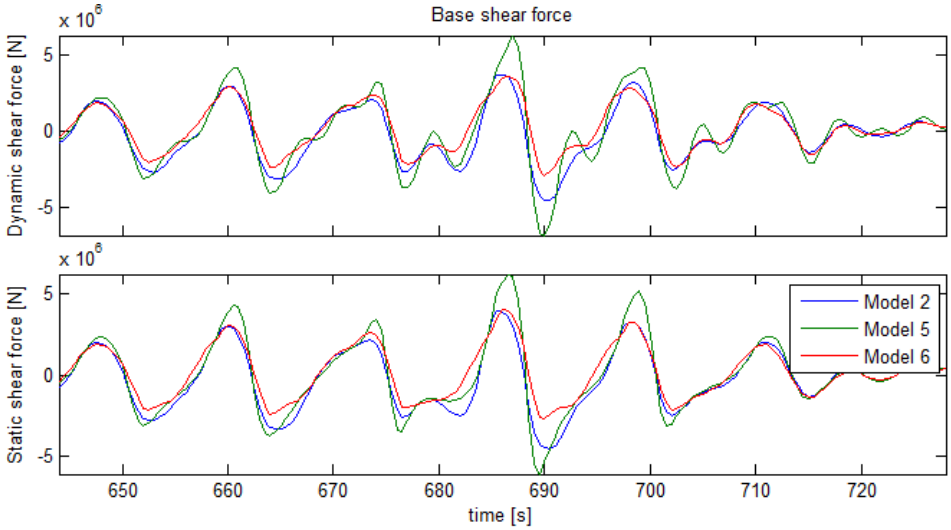

Figure 9.4: Time series around maximum event from table 9.3, model 2, 5 and 6

tion which the other models cannot capture.

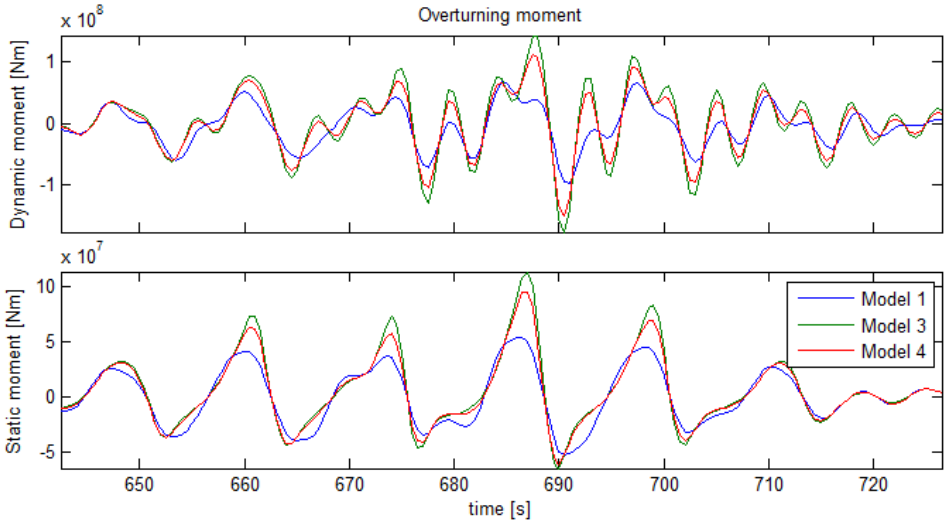

Figure 9.5: Time series around maximum event from table 9.4, model 1, 3 and 4

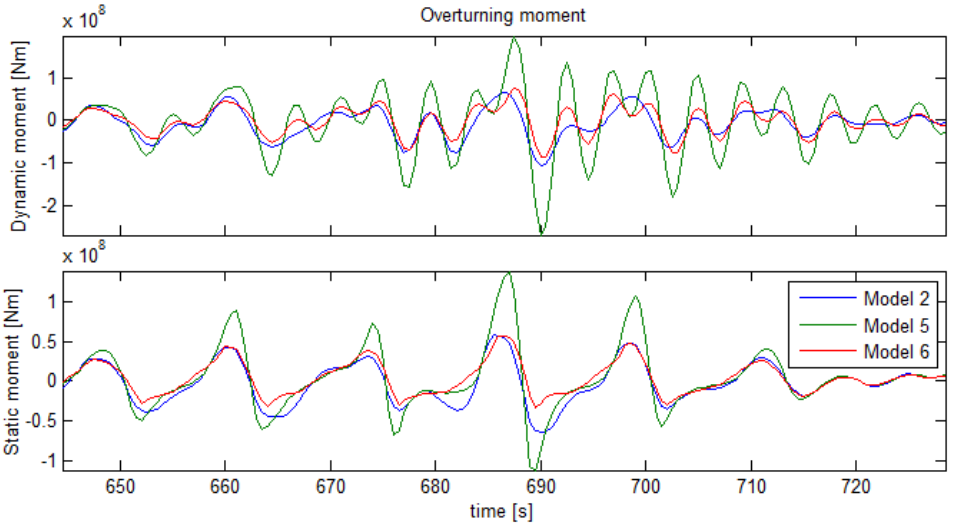

Figure 9.6: Time series around maximum event from table 9.4, model 2, 5 and 6

9.1.2 Assessment of using Contour line versus Tp variation at Hs_{50yr}

As presented and discussed in chapter 4, load case 6.1a require us to search for extreme loads with sea state parameters given by a reasonable Tp variation at the 50 year significant wave height, H_{S50yr}. This is different to the practice given in NORSOK [21], which require the analysis to follow the 50 year contour line. The use of 50 year contour line for design purposes is well reasoned on a statistical basis. The Tp variation at H_{S50yr} is not, and the following study in this section will assess the conservatism between the model.

The analysis use load model 4, wheeler stretching to the linear surface elevation, which is the most applied model for analysis in the industry. The chosen sea states from the contour line is given in table 5.3. Due to time limitations, only sea state 1, 3 and 5 will be included in the analysis. Then two Tp-variations at sea state 5 will be analyzed, given and discussed around table 5.4 and figure 5.3. This is fewer sea states compared to what would be considered in the industry, but it will still illustrate the difference between the methods. 20 seeds is considered in each analysis to create Gumbel plots and account for the short term variability. The following parameters are used in the study:

- The wave specter is calculated with $\gamma = 4$
- Fading is turned ON
- Damping values are realistic: $v_k = 0.05$ (soil pile) and $v_k = 0.01$ (substructure)
- $\Delta t = 0.5$
- Time duration: 30min

Figure 9.7 and 9.8 shows the Gumbel plots of base shear force by the analysis. The resulting 90% values are given in table 9.5.

90%−values	State 1	State 3	State 5	Tp-var. 1	Tp-var 2
F_{dyn} [MN]	4.55	5.59	6.25	6.67	6.15
M_{dyn} [MNm]	126.36	141.38	156.21	166.86	146.23

Table 9.5: Design values from contour line versus Tp variation at maximum Hs

Design loads are now found as the mean value of the result in the table. Design loads according to the contour line variation:

- $F_{design} = 5.4636$ MN
- $M_{design} = 141.32$ MNm

Design loads according to the Tp variation, around sea state 5:

- $F_{design} = 6.3551$ MN

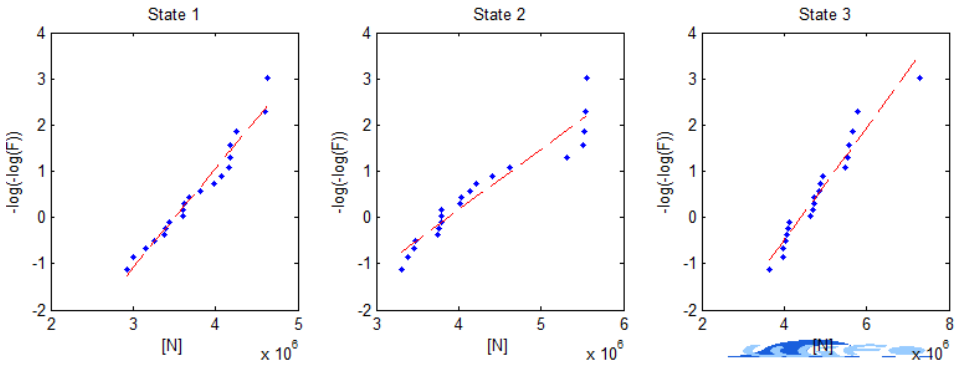

Figure 9.7: Gumbel plot of BSF from sea state 1, 3 and 5 in table 5.3

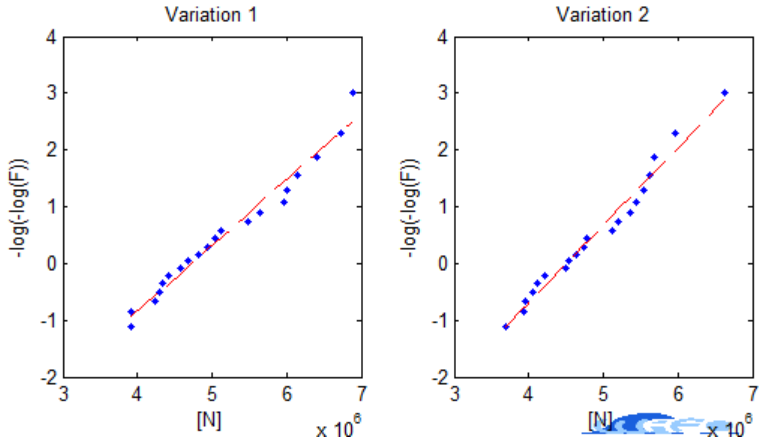

Figure 9.8: Gumbel plot of BSF from Tp-variations at sea state number 5

- $M_{design} = 156.44$ MNm

It is clear that the method required in the load case is more conservative. It seems unnecessary to follow this conservative approach. The method should be questioned because it is not reasoned on a statistical basis as the contour line variation.

Comment
The overturning moment was shown in chapter 7 to be highly sensitive to excitation around ω_N. The fading of the spectra was turned ON through the analysis, which might have been a mistake. The gumbel plots of OM were not included because the analysis regarding this design parameter might be corrupted. The fading should have been turned OFF, because the cut-off frequency vary according to the Hs-value, and will stretch beyond ω_N in sea state 1 and 3, but stop right before in the Tp-variation using sea state 5. To assess the validity of the result, spectra of dynamic OM by the first seed in each analysis, including the respective wave spectra

with logarithmic y-axis, is shown in figure 9.9 and 9.10. The figures illustrate the

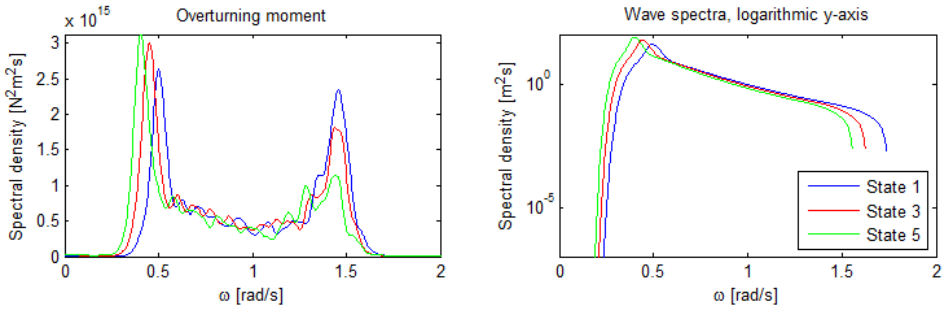

Figure 9.9: Dynamic OM spectra and logarithmic Wave spectra of contour line variation

strong consistency between wave spectra and dynamic OM. They illustrate that OM given by sea state 1 and 3 might be out of proportion compared to the values by sea state 5. Then, the final design values of OM according to the contour line variation should be lower, which will indicate that the method of Tp variaton at sea state 5 is even more conservative.

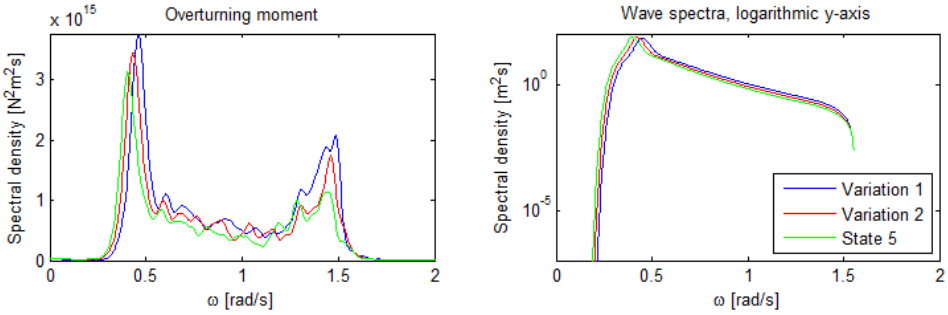

Figure 9.10: Dynamic OM spectra and logarithmic Wave spectra of Tp variation at sea state 5

9.2 Load case 6.1a, assessment of load models by Static analysis

Design loads according to Load Case 6.1a, will as seen in section 9.1.1, largely depend on the choice of load model. The study showed how the models behaved static and dynamic at two seeds, chosen to contain extreme linear events.

The next study will look at extreme static values by each model. This is done to get a better impression of the different models for design purposes. According to Load

Case 6.1a, many seeds have been applied to a long time realization. As discussed in chapter 4, a Gumbel plot is created and the 90%-value found to account for the short term variability.

Wave kinematics is calculated according to the static calculation parameters outlined in section 3.3.4. The safe depth parameter for 2nd order kinematics is 29m and 45m. The kinematics is calculated using $\Delta t = 1$s, then interpolated to a time step 0.5s before the load integration is applied. This method has been discussed and reasoned in chapter 3 and 6, and will halve the CPU time. Realizations of 50 minutes have been created, but split into durations of 3×1000s to speed up the calculation significantly due to almost 3 times less spectral components.

To simplify the calculations, all the wave kinematics at the 25m depth wind mill structure is performed with the depth parameter $h = 29$m (instead of splitting 1st and 2nd order components as done in chapter 7 and section 9.1.1).

The wave spectra is calculated according to sea state 1 in table 5.3 (Hs = 9.56 and Tp = 12.76) and with the use of $\gamma = 2.23$ (as in the spectra in chapter 6). The fading is turned ON.

The results of base shear force and overturning moment is presented in table 9.2 at both wind mill structures.

	Depth 25m		Depth 45m	
Model	$F_{90\%}$ [MN]	$M_{90\%}$ [MNm]	$F_{90\%}$[MN]	$M_{90\%}$ [MNm]
1	3.816	70.38	8.547	235.0
2	4.431	85.07	8.817	250.7
3	5.295	124.1	9.976	320.8
4	4.553	102.6	8.873	273.9
5	6.976	183.0	12.28	387.6
6	4.280	100.5	8.341	243.5
FNV	6.324	140.8	11.63	426.4
μ	*5.10*	*115.21*	*9.78*	*305.41*

Table 9.6: 90% value of Gumbel plot for all load models including the mean value at water depth 25 and 45 meter

There are large differences between the models, and the largest loads are again given by the extrapolation models and FNV. The mean value is given in the last row, which is seen to be somewhere between model 3 and 4 in all cases. The same observation can be seen when taking the mean value of all the tables in the dynamic comparison in section 9.1.1.

The difference between models is shown to be largest for the overturning moment, but it is shown to be reduced at depth 45m. To better study these differences, the values in each column have been divided by the value obtained from model 1. Then, the mean of these "normalized" values in each column is calculated: These

	Depth 25m	Depth 45m
Base Shear Load	1.3355	1.1443
Overturning Moment	1.6369	1.2996

Table 9.7: Mean of normalized results

values illustrate the differences.

The Gumbel plots, giving the values in the table, did in general show that the peak values follow the Gumbel distribution quite well. 3×20 seeds were calculated, and the first extremal value is taken as the largest value found in the 3 first seeds. Then, the 2nd value is taken from the three next, and so on. The values obtained from Load model 1 and 6 did show a bit more spreading around the fitted distribution, but the result is regarded to be statistical answerable.

The Gumbel plots is presented for the keen reader. The first figure show FNV at both water depths. Then load model 1 to 6 follows at the two next pages, first at depth 25 meter, then at 45.

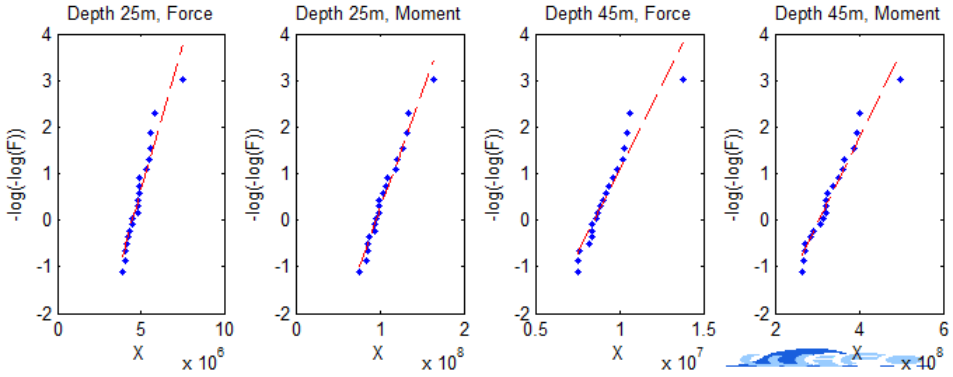

Figure 9.11: Gumbel plot of 50 min time series, FNV at depth 25 and 45 meter

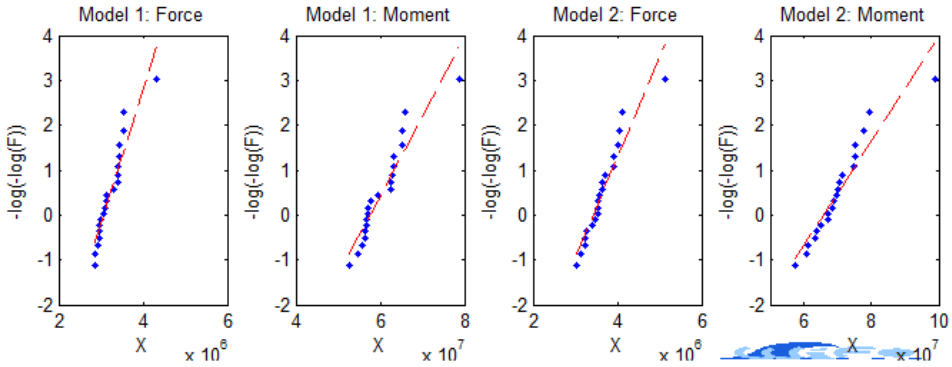

Figure 9.12: Gumbel plot of 50 min time series, model 1 and 2 at depth 25 meter

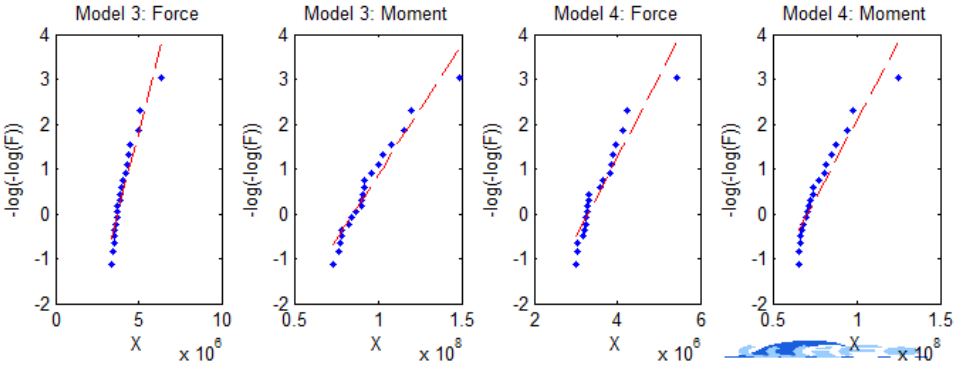

Figure 9.13: Gumbel plot of 50 min time series, model 3 and 4 at depth 25 meter

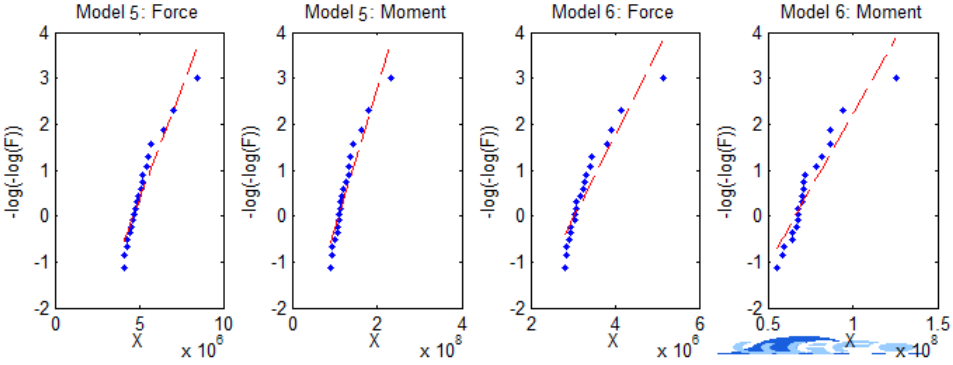

Figure 9.14: Gumbel plot of 50 min time series, model 5 and 6 at depth 25 meter

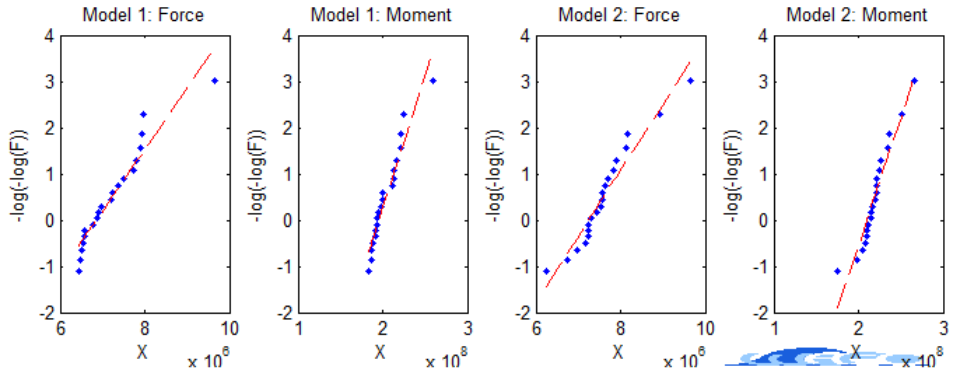

Figure 9.15: Gumbel plot of 50 min time series, model 1 and 2 at depth 45 meter

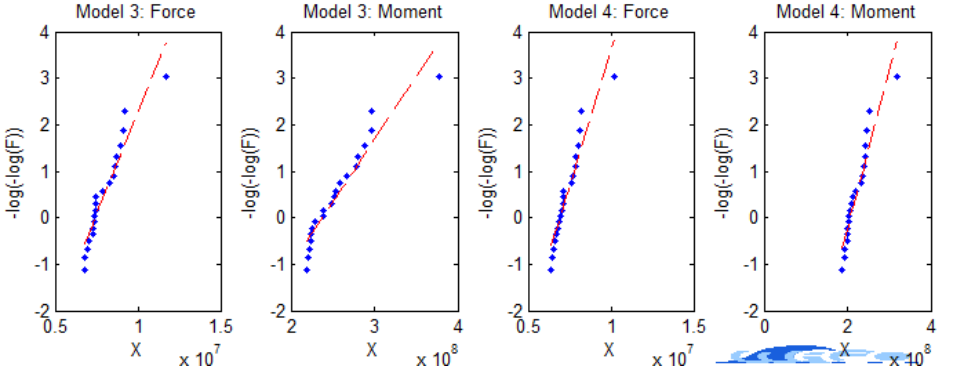

Figure 9.16: Gumbel plot of 50 min time series, model 3 and 4 at depth 45 meter

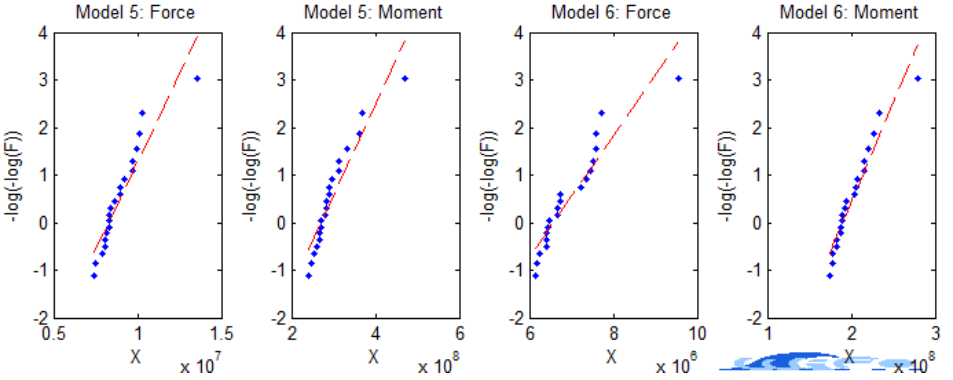

Figure 9.17: Gumbel plot of 50 min time series, model 5 and 6 at depth 45 meter

9.3 Load case 6.2a

In load case 6.2a, as presented in chapter 4, the structure shall be analyzed using the largest wave that must be expected through the design period. A complete analysis consistent with the given requirements in the DNV standard [6] has been performed, except that loads due to wind and current is not included. The parameters of the design wave were discussed in chapter 5, and the need for a non-linear wave model due to the effect of depth limitations were presented in chapter 8. The analysis is rather simple to perform, because the design wave should be applied to the structure as a regular wave. However, the standard does not specify exactly how this shall be done, but a wave theory according to the depth limitations must be chosen.

The method of embedded stream function will be given an assessment. Then, design loads obtained from different methods will be calculated. These methods are:

- Linear regular waves
- Stream function regular waves
- Forced Embedding, outlined in section 8.3
- Mixed approach Embedding, outlined in section 8.4.2

Finally, these methods are discussed in the view conservatism based on presented results.

Parameters in the analysis

- The wave spectra is calculated with $\gamma = 4$, and with the use of Hs = 12 and Tp = 14.8 given by sea state 5 in table 5.3. Fading is turned ON.
- Damping values are realistic: $v_k = 0.05$ (soil pile) and $v_k = 0.01$ (substructure)
- Design wave parameters: H = 18.1m and wave period variation according to equation 4.17, 12.28s, 14.05s and 15.82s.

9.3.1 Assessment of Embedded stream function

Forced embedding is the method that is applied for verification. The stream function wave is applied at an arbitrary location without the use of smoothing functions. The wave period variation is done, and the largest loads are found. Different locations for embedding at each wave period are not considered.

The following study assess the dynamic loads given by the embedded stream function wave at the first wave period variation, $T = 12.28$s. The wave is embedded at 20 locations, and the result of base shear force and overturning moment are presented in Gumbel plots. The response is also given in time series including the

static loads, to illustrate the dynamic consequences of the method. Both the forced embedding, and the mixed approach is considered.

Forced embedding
Figure 9.18 presents the result of the dynamic analysis using forced embedding. The variation is significant. To ensure that the result provided is meaningful, the peak static BSF and OM is controlled to be the same at each realization:

- $F_{max}^{stat} = 5.9156$ MN
- $M_{max}^{stat} = 150.60$ MNm

Figure 9.19 shows BSF, static and dynamic, given by embedding at three different locations. Figure 9.20 shows the same result with overturning moment. The load event is found to create a transient response effect both in shear and moment.

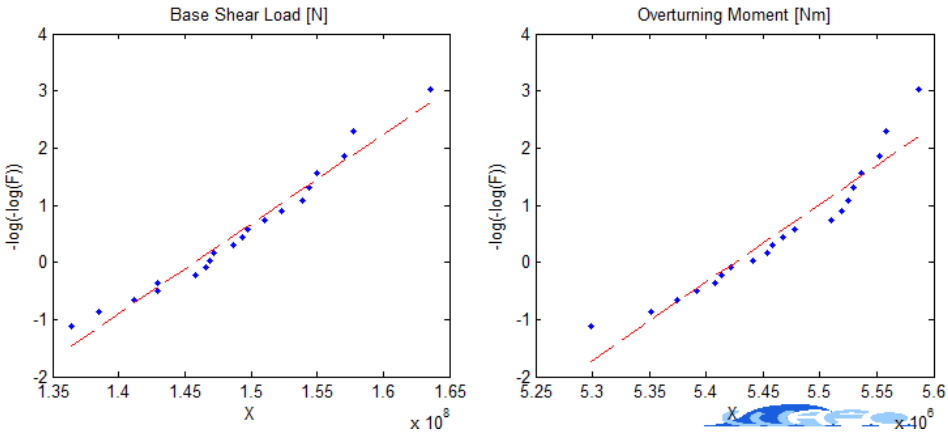

Figure 9.18: Gumbel plot of maximum base shear and overturning moment from forced embedding at different locations

Mixed approach embedding
Figure 9.21 presents the result of the dynamic analysis using the Mixed approach. The variation is significant, and the peak static BSF and OM are again controlled to be the same at each realization:

- $F_{max}^{stat} = 5.7391$ MN
- $M_{max}^{stat} = 162.87$ MNm

Figure 9.22 shows BSF, static and dynamic, given by embedding at three different locations. Figure 9.23 shows the same result with overturning moment. The load event is again found to create a transient response effect both in shear and moment.

Dynamic response variation
The coefficient of variation, given as $C_V = \sigma/\mu$ (calculated from the extreme values), is included to investigate if there is any difference between the models in

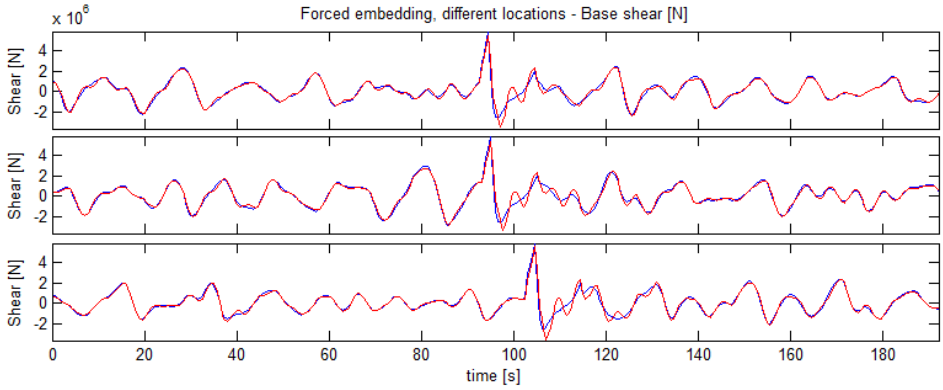

Figure 9.19: Forced embedding at different locations, dynamic and static base shear force

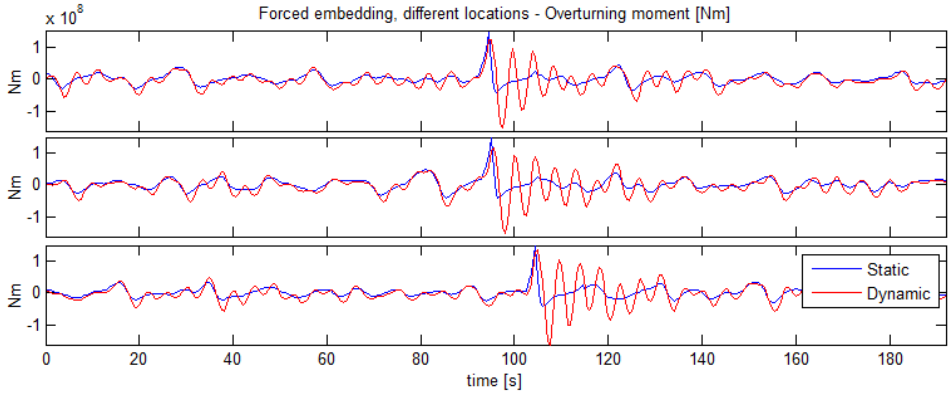

Figure 9.20: Forced embedding at different locations, dynamic and static overturning moment

terms of dynamic response variation. Calculated values are given in table 9.8. The dynamic response variation is seen to be reduced with the Mexed Approach model. This might be obvious because the original structural motions by the stochastic load series is not any longer maintained to the embedding location (as in Forced embedding), but adapted by the stream wave. The method is then more reliable since only 1 location will be used in the design calculation.

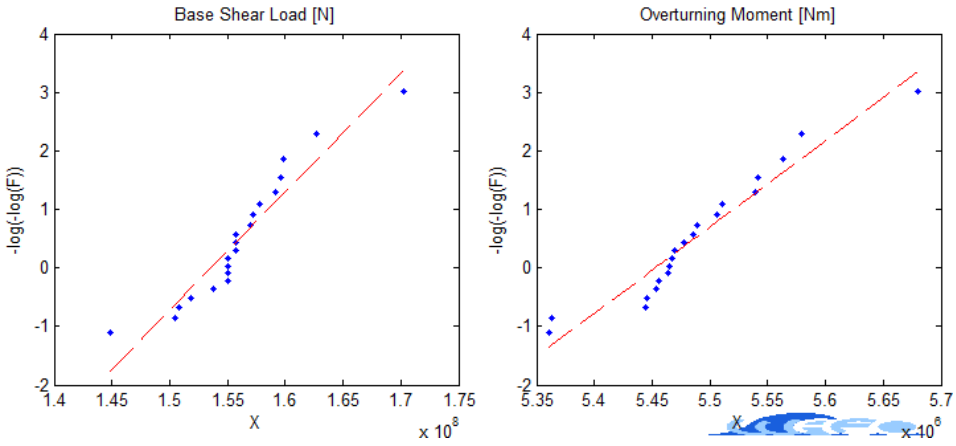

Figure 9.21: Gumbel plot of maximum base shear and overturning moment from Mixed approach embedding at different locations

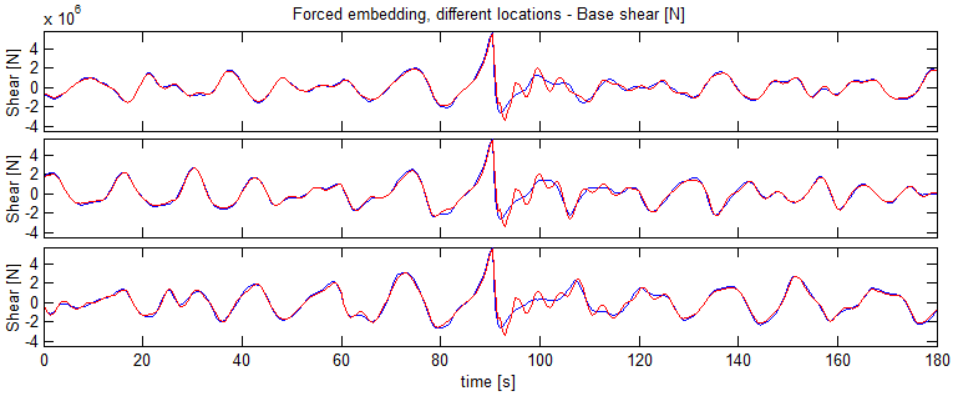

Figure 9.22: Mixed approach embedding at different locations, dynamic and static base shear force

	C_V of F_{max}^{dyn}	C_V of M_{max}^{dyn}
Forced	0.0140	0.0457
Mixed Approach	0.0130	0.0329

Table 9.8: The coefficient of variation to dynamic extreme response by embedded stream function models

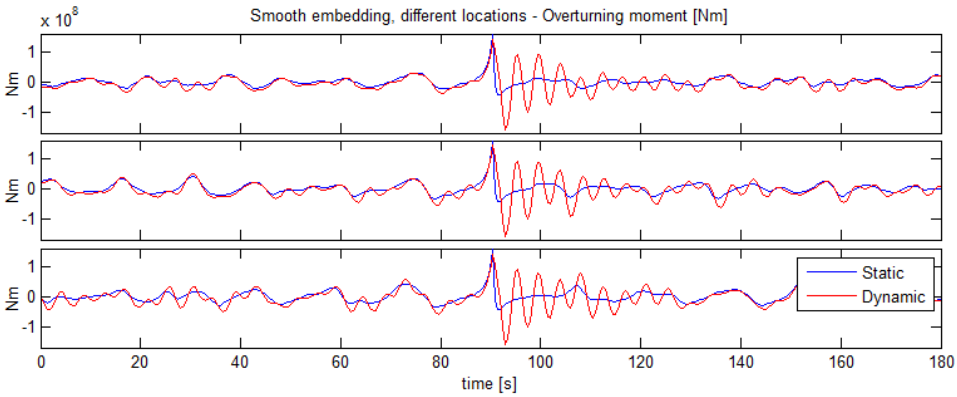

Figure 9.23: Mixed approach embedding at different locations, dynamic and static overturning moment

9.3.2 Results and assessment of Design load calculation

Table 9.9 show the result from the dynamic load calculation. Negative value is given when the largest response occurred at the preceding trough, and not at the large load itself which from figure 9.19 to 9.23 is seen to always be positive.

The values obtained from embedding at the first wave period variation, are taken from the first seed used in the Gumbel plot. This is because different seeds are not required by the standard, and using an complete arbitrary embedding location will give a result most equal to what would be obtained through the verification procedure by industrial practice. The results in table 9.9 should then be the true results obtained in load case 6.2a, except that wind and current is excluded from the calculation. The linear regular wave is only included for comparison.

T [s]	Max load $\times 10^{-6}$	Regular Linear	Regular Stream F.	Forced Embedding	Mixed app. embedding
12.28	F_{dyn}	4.14	6.19	5.51	5.54
	M_{dyn}	-96.61	-193.86	-154.97	-159.85
14.05	F_{dyn}	3.86	7.24	6.24	5.83
	M_{dyn}	-93.42	195.26	-171	-162.54
15.82	F_{dyn}	3.77	6.68	6.42	6.13
	M_{dyn}	81.36	-160.07	-171.64	-167.27

Table 9.9: Dynamic response values by different methods in Load case 6.2a

The linear regular waves gives clearly much lower values compared to stream function methods. The linear values are also seen to decrease for larger wave period, but a similar conclusion of stream function methods can not be taken.

The largest load is given at the 2nd wave period variation at regular stream waves:

- $F_{max}^{dyn} = 7.24$ MN
- $M_{max}^{dyn} = 195.26$ MNm

These largest values would be the design loads of shear and overturning moment according to the load case.

The value of OM does in this case differ from all the other, because it is found to be positive. The results in the table must be further assessed by looking at the largest static loads given in each load analysis. The static loads are given in table 9.10. The linear load is again seen to decrease for larger wave period. The opposite relation is found in the stream wave for BSF, but not for OM. It is still to early to make conclusions. The results of static values from the different methods using stream function, at the same wave period variation, show in addition no consistency. This is strange, because the same stream wave is put in to each method. The values must be analyzed further.

T [s]	Max load $\times 10^{-6}$	Regular Linear	Regular Stream F.	Forced Embedding	Mixed app. embedding
12.28	F_{stat}	4.22	7.35	5.92	5.74
	M_{stat}	74.59	209.25	150.59	162.87
14.05	F_{stat}	4.09	7.47	6.42	5.96
	M_{stat}	71.55	205.2	178.01	165.21
15.82	F_{stat}	3.88	7.71	6.89	6.38
	M_{stat}	68	209.35	173.95	166.91

Table 9.10: Static load values by different methods in Load case 6.2a

The velocity and acceleration profile of the stream wave function gives very sharp peaks which is shown in figure 8.1. These peaks is difficult to capture even with a small time step. The chosen time step in the analysis show to be very significant in capturing the peak value. The problem has been aware of, and the figure 8.1 was created with a time step of $\Delta t = 0.03$s to give a good impression of the profiles. The peak variation is not easy to see on the figure, but it is still highly present even with this small time step. It is difficult to see because only a few wave periods are included. Figure 9.24 shows velocity and acceleration at the crest. The same wave is plotted for $\Delta t = 0.001$ and $\Delta t = 0.5$. It shows how the acceleration is

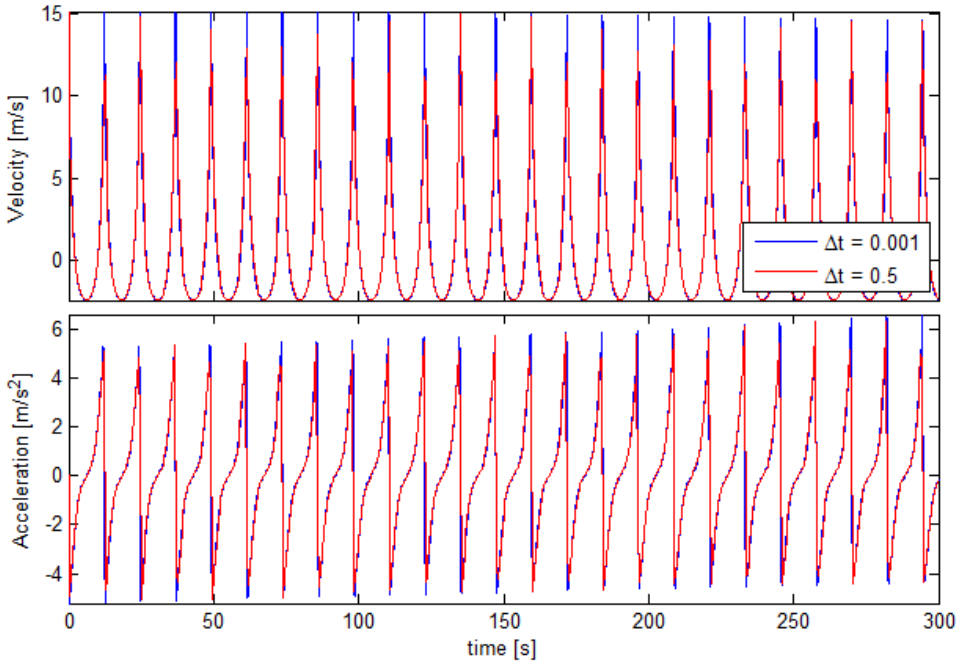

Figure 9.24: Kinematics by stream function given by wave of H = 18.1m at time steps $\Delta t = 0.001$ and $\Delta t = 0.5$

most sensitive to the time step, and that the very small time step still give large variation in the peak value. The wave period used in the visualization is the first wave period variation, T = 12.28s. The exact value is T = 12.2766s which is the reason why the maximum values change for each peak. The time step hit a new value in the wave period for each round.

The effect is largely captured in the inertia load, and the reason for no consistency between the loads given in table 9.10. A discussion of the validity of loads obtained by Stream function waves is placed in the last section in the chapter.

9.3.3 Discussion on conservatism

The dynamic amplification factor, DAF, has been calculated as the ratio between the dynamic and respective static load taken from the tables above. The result is presented in table 9.11. It is difficult to base any conclusions of these values.

T [s]	DAF	Regular Linear	Regular Linear	Smooth Embedding	Mixed app. embedding
12.28	F	0.98	0.84	0.93	0.97
	M	-1.30	-0.93	-1.03	-0.98
14.05	F	0.94	0.97	0.97	0.98
	M	-1.31	0.95	-0.96	-0.98
15.82	F	0.97	0.87	0.93	0.96
	M	1.20	-0.76	-0.99	-1.00

Table 9.11: DAF given by dynamic load in table 9.9 divided by respective value in table 9.10

The amplification factors for the linear regular wave is found to be consistent with earlier analysis. The dynamic BSF has been reduced, and the dynamic OM has been increased (see spectra calculated in section 7.3). Surprisingly, the DAF-values of overturning moment is found to be less then 1 in the other methods. The values by regular stream waves is particularly low, but with the largest values at the 2nd T-variation. This is where the largest loads did occur. A further investigation of the DAF-values by regular stream waves seems necessary.

The ratio of wave frequency (1/T) to the natural frequency of the structure has been found for each T-variation:

- 1st variation: 3.0402
- 2nd variation: 3.4785
- 3rd variation: 3.9167

The applied stream function is of the 10th order, and consists of 10 frequency components of decreasing amplitude from $\omega_1 = 1/T$ to $\omega_{10} = 10\omega_1$. We see that the first T-variation will hit the natural frequency with the 3rd component, and the

3rd variation with the 4th. From this result, high dynamic amplification should be expected at the 1st and 3rd variation. But this is not the case. It is discussed in chapter 6 how the load integration to the free surface affects the order of resulting moment. However, this will not change the frequency components other than creating more energy at each of them.

The problem must be assessed in the time domain. Figure 9.25 shows static and dynamic moment from the 1st and 2nd T-variation. The start up of the simulation is included to show how the dynamic moment develop in to the response pattern. The 1st variation show in fact large dynamic amplification at the 3rd wave compo-

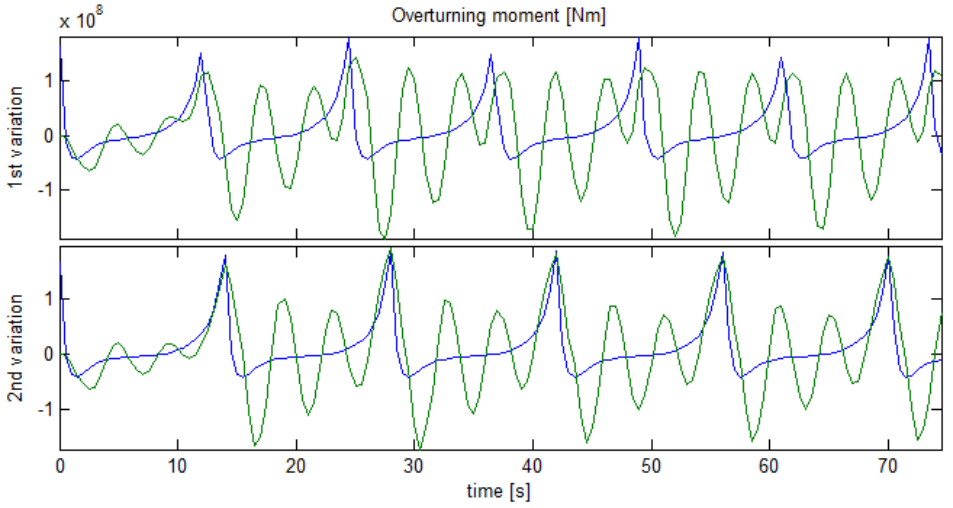

Figure 9.25: Time series of dynamic and static OM by stream function wave at the 1st and 2nd T-variation

nent, which creates the dominating response. This is out of phase with the shape of the total load, and result in a lower DAF given as $M_{max}^{dyn}/M_{max}^{stat}$. The natural frequency is in the middle between the 3rd and 4th frequency component of the 2nd T-variation. There is then very little dynamic amplification. The response has a more quasi-static pattern which follow the static moment. This conclusion might be to simple, but it explains the very large moment, and also why it is positive opposed to all other cases.

The surprising result of this discussion, is that the largest load occur when there is no excitation at the natural frequency. This occur when $\omega_N \simeq \frac{2n+1}{2}\omega$, where n is an even number. Regarding conservatism, the most conservative case must be to apply a regular stream function wave as in the 2nd T-variation.

However, as discussed in chapter 8, to apply a wave train of the design wave has no statistical basis. The method of embedded stream function might in fact give a better result. It is also observed how the regular linear waves is highly non-conservative.

9.4 Discussion of analysis using stream function through the thesis

The previous section showed how variation in the loads given by stream function waves occur. The sharp peaks in the kinematics are only captured by a very fine time step.

This will create a rather arbitrary maximum load created by the variation of peak kinematics, mainly acceleration, shown in figure 9.24. This is the reason for no consistency between the loads by equal stream function waves in table 9.9. The load variation for this wave is extreme, because the wave parameters is determined by wave breaking. Figure 8.1 show how the kinematic profiles changes for less steep waves. The problem of peak load variability will in other words only occur close to wave breaking.

A time step small enough to capture the actual peak load is not possible when close to wave breaking. This was shown in figure 9.24, giving large acceleration variability even by using $\Delta t = 0.001$. However, it is the dynamic loads that are of interest. Sharp load peaks contain little energy due to the short duration. It is then important to use a small time step. This mainly to apply the large load as a spike, and not risk the chance of hitting the large load with a time step of $\Delta t = 0.5$. These two ways to apply the large load on the structure is highly different in terms of dynamic response. The spike will only introduce transient effects in the structure, and will force the structure much less compared to a load of longer duration. Based on the experiences through the thesis, the applied time step in dynamic calculations should be low. But an analysis of the effect has not been carried out.

The different analyzes using stream function through the thesis must now be summarized to leave no questions about their validity.

Statistical consequences of stream function were analyzed in section 8.4. The problem of peak variation had come to attention, and a small time step of $\Delta t = 0.1$s were chosen. As seen, lower time step cannot exclude the problem of peak variation to the static loads. However, the problem is not a consideration in this analysis. The design wave used in load case 6.2a is determined by wave breaking at 25m depth with wave period T = 12.28s. Wave breaking was also a problem when embedding the wave automatically by the MATLAB routine. 40 seeds of time realization were created to embed waves. The number of wave breaking out of 40 seeds, the mean wave height and the mean wave period for the embedded waves is given for comparison:

- Method 1: 20 breaking waves, H =18.21m, T = 15.49s
- Method 2: 9 breaking waves, H =17.43m, T = 15.77s
- Method 3: 18 breaking waves, H = 17.8m, T = 15.62s

The result do in fact explain how the wave loads is much larger in these analysis compared to the values in table 9.10. The waves are in general not close to wave breaking, and the load created by the true acceleration peak is in fact captured. The conclusion of this analysis, is that the true maximal value is captured. Even if this was violated, the analysis would still be valid, showing the change in maximal loads given by irregular wave versus stream function.

The **assessment of embedded stream function** in section 9.3.1 is also highly valid. This time, the embedded wave is the design wave that is close to breaking. The peak load is not captured and the time step is large: $\Delta t = 0.5$s. However, this does not matter because in each method separately, the exactly same wave is embedded in all realizations. The stream function wave kinematics is calculated once, then embedded at different locations. Every realization, in each method separately, contain the same peak load. The study do then provide the valuable information for how the embedding location affects the dynamic loads.

The conclusion given by the change in the coefficient of variation, C_V, that the mixed approach method reduces the dynamic response variation should also be valid. The different peaks could corrupt the result, but since the first model give largest F_{max}^{stat}, and the other largest M_{max}^{stat}, the conclusion is most likely to be valid.

The result of **load case 6.2a** in section 9.3.2 is also highly valid as an assessment of the industrial practice and the standard requirements. The design wave close to wave breaking is again applied, and the coarse time step of 0.5s is used. It is not known what time step that is used in the industry, but the result show large variation in both static and dynamic loads at the applied Δt. The result indicates that a shorter time step should be used, to reduce the peak variability. The result would then probably be more even, and the resulting design loads more reliable. The assessment of conservatism would then also be more meaningful. The true static load is most likely close to the maximum value obtained by regular waves, because many peaks are included and not just one as in the embedding methods.

Chapter 10

Summary and conclusions

This thesis has widely assessed non-linear wave loads for the use in design calculations against ULS. The conclusions are many, some might be obvious and well known, but other might be useful and create new attention.

1st and 2nd order irregular wave models are presented, including stretching and extrapolation which is methods to account for the surface elevation. The wave spectra was shown to give a slow decay to the tail of the acceleration spectrum. This is unphysical and the spectrum had to be truncated. A cut-off value proposed to 2nd order theory was chosen to be used for all kinematic models, so that the later comparison would be more meaningful.

The 2nd order irregular wave model at deep water is known to reduce the crest velocity due to difference-frequency components. The sum-frequency components increases to intermediate water depths, and the increased crest kinematics as given by the regular wave theory will again be observed. However, the theory becomes unphysical due to enlargement of the difference frequency terms at more shallow water. This problem is highly visible at 25m water depth, but not an issue at 45m. The physical reasons has not been assessed, but it was found that the problem is numerical and can be avoided by analyzing the depth dependent enlargement at a given set of frequency components. A safe input parameter of 30m was found in realizations of 20min using $\Delta t = 0.5$s, and 29m when applying 1000s using $\Delta t = 1$s.

The irregular load models are compared, and the 2nd order extrapolation was found to give the largest loads and contain most energy in the spectrum. Stretching to the 2nd order surface gave the smallest loads, and contained the least energy. This is not consistent with the theoretical investigation from regular waves in chapter 3, which indicated that these two models should be more equal. FNV gave almost the same large load as extrapolation, but contained even more energy at $3\omega_P$. Non-linearity was seen to create a higher portion of the total energy at 25m compared to 45m. Inertia loads are found to dominate completely and the effects of drag are

not significant.

Overturning moment was found to be highly sensitive to dynamic excitation due to the top mass displacement. Parameters were modified to be able to analyze the sensitivity to load models and not only show resonance at ω_N. Fading of the wave spectra was turned off so that $\omega_{max} < \omega_N$. The soilpile damping and γ were in addition significantly increased.

Dynamic spectra showed in general large energy increase at ω_P, and dynamic excitation at $2\omega_P$ and $3\omega_P$ were clearly most present in the 2nd order extrapolation model. FNV gave further increase at $3\omega_P$. Ringing events get low attention in DNV [6], but is much more addressed in NORSOK [21]. FNV is the only load model consistent to higher order and was found to reveal dynamic effects. However, the model is not necessary valid at 25m depth.

Base shear load was not sensitive to the first mode excitation. The peak spectral value at ω_P was actually lower compared to static, but closer to $3\omega_P$ the values became slightly higher.

Energy at ω_P was found to decrease significantly with kinematics calculated at 30m compared to 25m, due to the effect of depth in the vertical scaling of ϕ. With extreme sea state parameters Hs= 9.56m and Tp= 12.76s, depth 25m starts to become rather shallow and the energy at ω_P might be unphysical large. It is the energy at ω_P which mainly creates the load effects at $2\omega_P$ and $3\omega_P$, and these effects might then also be unphysical large.

The contributions from $\phi_{(2)}$ and $\eta_{(2)}$ were calculated with 30m as depth parameter. The sum-components propagate at deep water and will not be affected by depth scaling, but the difference-terms will be significantly reduced. However, these terms are anyway considered from a theoretical basis to be unphysical large.

Extreme wave load cases were presented in chapter 4. Design sea state parameters according to DNV [6] should be found only by the PDF of Hs alone, without considering Tp-values as the case in NORSOK [21]. A Tp-variation shall be done, but it is not specified how. Dynamic analysis were performed using both methods. A Tp-variation were chosen using $f_{Tp|Hs}(t)$ from the contour line, and using Tp corresponding to 2.5% as the lower limit. This sea state indicated wave breaking by the use of embedded stream function. 25 out of 40 embedding locations gave wave breaking. Design values from the Tp-variation showed to be highly conservative compared to the contour line method. Also the many occurrences of wave breaking must be seen as a critique to the method of Tp-variation.

Load models were compared in the time domain at two different seeds giving respective extreme crest and extreme acceleration. 2nd order extrapolation were again found to give the largest static loads, but FNV the largest dynamic. The linear load model gave the smallest static loads, but stretching to the 2nd order surface the smallest dynamic. Wheeler stretching to the linear surface, which is applied in the industry, give loads which is closest to the average between all models.

Static loads by each model is analyzed by 20 seeds of 50min time duration. The same trends are shown, the largest loads are created by 2nd order extrapolation. However, FNV creates the absolute largest OM at 45m. The average value between models has been calculated, and it is shown to be given somewhere between linear extrapolation and stretching to $\zeta^{(1)}$. The differences are largest to the OM, but all differences becomes less at 45m. This shows again how the effects of non-linearity are reduced in deeper water.

The embedded stream function is created to improve the design load calculation according to load case 6.2a. The method is widely applied, but to areas of less demanding site conditions where the structures have smaller dimensions. The method as applied in the industry creates a discontinuity in the acceleration time series, which creates a jump in the load series at the inertia dominated structure. The jump is even more present at 45m, where the dimensions are even larger.

An improved embedding method is created, which finds the best location to embed the wave. Blending functions are applied to smooth the transition. The two methods are studied in dynamic analysis by Fedem to investigate how the embedding location affects the response. The coefficient of variation is about 1.5% to BSF and 3.3-4.6% to OM, and can not be neglected. The improved embedding showed 1.1% less C_V which gives the conclusion of less dynamic response variation. The method is then more reliable since only 1 location will be used in the design calculation.

An embedded wave will violate the stochastic nature of the time series. This has been analyzed by performing extreme value analysis to the loads at large crests, compared to the resulting loads by the embedded stream function wave at that specific location. The embedded wave creates a significant increase to both force and moment. The coefficient of variation between extreme values seems to be maintained.

The stream function wave is shown to create sharp load peaks when the wave is close to the breaking limit. This corrupts the result by different load models in load case 6.2a. A variation in peak load is introduced, and depends on Δt. However, even $\Delta t = 0.001$s gives a significant peak load variation, so the problem cannot be eliminated this way. A small Δt will be required in dynamic analysis to simulate the short load duration. The problem does *only* occur close to breaking, and is *only* a problem to embedding (where the sharp load peak happen once).

The surprising result of the analysis by regular stream waves, is that the largest load occur when there is no excitation at the natural frequency. This occur when $\omega_N \simeq \frac{2n+1}{2}\omega$, where n is an even number. These regular waves did also show to be most conservative.

10.1 Recommendations for further work

The following recommendations are based on the work of this thesis:

- The different load models are found to give large variation to the design loads. Results from model tests should be analyzed to improve the understanding of what model that is most realistic.
- The MATLAB routines computing 2nd order wave kinematics should be implemented in FORTRAN to speed up the calculations and make it possible to generate longer time series. The extreme value calculations for Load case 6.1a can then be better assessed.
- The load models has only been analyzed dynamically in Fedem for a short time duration. Extensive analysis according to load case 6.1a should be done to get reliable design values and assess the dynamics in each model.
- Only the Gumbel distribution has been considered for the extreme value statistics. Based on longer analysis, more general extreme value distributions could be tried fitted to the realizations.
- A new assessment of load case 6.2a in the view of different wave models should be done. The result was corrupted in the stream function wave models, due to the sharp load peaks. A new analysis should be done with a less steep wave and with a smaller time step. The effect of sharp peaks to the dynamic response should be analyzed with different time steps.
- The method of embedded stream function has been improved in the Mixed Approach method. The blending parameters could be studied closer and improved to create a smoother transition to the embedded wave. The location for embedding is found by a linear stochastic surface. It should be studied if the 2nd order surface might improve the location due to sharper crests and create a better transition which gives less transient effects. Before the transition starts, the kinematic model could be changed to the 2nd order extrapolation which might be closer to the nature of stream function. This could also improve the transition.
- A study of how the embedded wave changes the extreme load statistics has been performed, but the result was only visualized. C_V should be calculated. In addition, analysis was only to the static loads: A new analysis to explore the changes in dynamic response could be carried out in Fedem. The true dynamic effects from the stochastic series can then be compared to the transient effects which seems to occur artificially by the embedding. The suggested analysis to improve the transition could be studied this way.
- The implemented FNV model in MATLAB has not been compared to the built in model in Fedem.
- Load integration using interpolation of the calculated kinematics along the structure has been implemented, but not been verified. Se functions "morisonS2.m"

and "morisonSL.m"

The developed MATLAB routines and the interface to Fedem should be used to realize these suggestions for further work. The MATLAB routine

Bibliography

[1] E. A. Engebretsen. Wave conditions for offshore wind turbine foundations in intermediate water depths. Master's thesis, NTNU, June 2012.

[2] Michael Brorson. Non-linear waves. Technical report, Department of Civil Engineering, Aalborg University, March 2008. DCE Lecture Notes No. 9.

[3] *USFOS Hydrodynamics, Theory, Description of use, Verification.*

[4] Thomas B Johannessen. Nonlinear superposition methods applied to continuous ocean wave spectra. *Journal of Offshore Mechanics and Arctic Engineering*, 134(1):011302, 2012.

[5] http://www.theengineer.co.uk/in-depth/the-big-story/wind-energy-gets-serial/1012449.article, April 2012. Article at the Engineer.

[6] DNV-OS-J101. Design of offshore wind turbine structures. Technical report, Det Norske Veritas, January 2013.

[7] C. M. Larsen. *Marin Dynamikk.* Dept. of Marin Techn. NTNU, Trondheim, Norway, 2012.

[8] PJ Rainey and TR Camp. Constrained non-linear waves for offshore wind turbine design. In *Journal of Physics: Conference Series*, volume 75, page 012067. IOP Publishing, 2007.

[9] George B. Thomas Jr. J. Hass, Maurice D. Weir. *Calculus 2.* 2009.

[10] Odd Faltinsen. *Sea loads on ships and offshore structures.* Cambridge university press, 1993.

[11] B. Pettersen. *Marin Teknikk 3 Hydrodynamikk.* Dept. of Marin Techn. NTNU, Trondheim, Norway, January 2007.

[12] DNV-RP-C205. Environmental conditions and environmental loads. Technical report, Det Norske Veritas, October 2010.

[13] J. Birknes. Skjevhet av tyngdeblger og ekstrem overflatehevning. Master's thesis, Universitetet i Oslo, May 1999.

[14] D. Myrhaug. *Marin Dynamikk - Uregelmessig sjø*. Dept. of Marin Techn. NTNU, Trondheim, Norway, 2007.

[15] P.K. Kundu and Ira M. Cohen. *Fluid Mechanics*. Academic press, 4 edition, 2008.

[16] M. J. Tucker and E. G. Pitt. Waves in ocean engineering. Elsevier Ocean Engineering book series, 2001.

[17] D. E Newman. *An introduction to random vibration, spectral and wavelet analysis*. 3 edition, 1993.

[18] WAFO group. *Tutorial for a Matlab Toolbox for Analysis of Random Waves and Loads version 2.5*. Lund, Sweden, March 2011.

[19] Thomas B Johannessen. Calculations of kinematics underneath measured time histories of steep water waves. *Applied Ocean Research*, 32(4):391–403, 2010.

[20] Carl Trygve Stansberg, Ove T Gudmestad, and Sverre K Haver. Kinematics under extreme waves. *Journal of Offshore Mechanics and Arctic Engineering*, 130(2):021010, 2008.

[21] NORSOK Standard N-003. Action and action effect. Technical report, Det Norske Veritas, 2007.

[22] S. Haver. *Prediction of Characteristic Response for Design Purposes*. Statoil, 2011.

[23] G. S. Baarholm S. Haver, K. Bruserud. Lecture notes tmr4195 - design of offshore structures, February 2014.

[24] Statkraft. Confidential internal report, 2011.

[25] E. A. Svangstu. An investigation of wave conditions and wave induced loads for design of wind turbine foundations at 1540m depth. Master's thesis, NTNU, June 2011.

[26] T. Fischer, W. de Vries, and B. Schmidt. *Offshore Foundations and Support Structures*. Stuttgart, Germany, October 2010.

[27] Fedem Technology AS, Trondheim, Norway. *FEDEM User's guide release 7.0.1*, January 2013.

[28] Øivind Paulshus. Sensitivity of load models in extreme wave conditions, 2013.

[29] R. A. Dalrymple. Fortran routine at authors personal page at johns hopkins university. http://www.ce.jhu.edu/dalrymple/stream.f.

Appendices

Appendix A

User manual to load calculation in MATLAB

A.1 General

Sheets are created to give user input. These are given names starting with "UI". The following sheets are available:

- **UI_mainIrregular.m**: User input to irregular wave calculation
- **UI_mainRegular.m**: User input to regular wave calculation
- **UI_FNV.m**: User input to FNV load model
- **UI_embedDNV.m**: User input to forced embedding (see section 8.3)
- **UI_embedFIT.m**: User input to smooth embedding (see section 8.4.1)
- **UI_embedMIX.m**: User input to mixed approach embedding (see section 8.4.2)

Each input sheet should be run as a script. It will automatically call the main function of the actual program, and everything is computed automatically. The output will be stored in .mat-files and appear in the same folders as the input sheets. The main-functions are called from the folder "main_functions". The names of the folders must NOT be changed, because Matlab will change between directories in the calculation process.

All programs will first calculate wave kinematics. Then the load integration is performed automatically.

All the different input values are listed and explained below. The required input to each program is specified at the actual input sheet.

Input values

- rho = water density
- g = gravity
- h = water depth. (Note: Two depths can be given. The first value defines the depth in all linear components $\zeta^{(1)}$ and $\phi^{(1)}$. This is the assumed true water depth, and will be given as input to the load integration routines. The second value defines the depth in all 2nd order components $\zeta^{(2)}$ and $\phi^{(2)}$.
- D = Monopile diameter
- Cm = Mass coefficient
- Cd = Drag coefficient
- gam = Peak enhancement factor to the JONSWAP specter
- Hs = significant wave height
- Tp = Peak spectral period
- seed = seeds to include in the calculation, given as a vector. The values are input to the built in "rng.m"-function before the random seeds are obtained
- H = Wave height of a regular wave
- T = Wave period of a regular wave
- ORDER = Order of the Stream function wave
- Zvec = Vertical coordinates on the structure, increasing order. First value should be the water depth
- time = time duration
- dt = time step
- optWave = option for wave elevation:
  1 = linear
  2 = 2nd order deep
  3 = 2nd order finite
- optKine = option for wave kinematics:
  0 = none
  1 = linear (named linear)
  2 = 2nd order deep (named 2nd_deep)
  3 = 2nd order finite (named second)
  4 = extrapolation to linear surface (named expol1)
  5 = extrapolation to 2nd order deep surface (named expol2)
  6 = extrapolation to 2nd order finite surface (named expol3)
  7 = stretching to linear surface (named wheel1)
  8 =stretching to 2nd order finite surface (named wheel2)

- Wmax = cut off value. (Note: model 2, 3, 5 and 6 involve 2nd order theory and is cut at $\sqrt{2g/H_S}$ automatically)

The names given at "optKine" are the names on the models that will appear in Matlab.

Output
All output will be saved automatically in a .mat file as a structure. The structure will contain the following fields in all the programs:

- INFO, contains all the input used for the calculation, including the values of the applied wave spectra (frequencies and spectral values)
- FM, contain base shear force (row 1) and overturning moment (row 2). Each seed is stored in its own run as FM.run1 and FM.run2. The integration method is "morison2.m"
- Fdist, contains a matrix of the nodal loads which can be applied to the Fedem model. Each seed is stored in its own run as Fdist.run1 and Fdist.run2. The integration method is "morisonL.m"
- Umat, contains the velocity matrix. Each seed is stored in its own run as Umat.run1 and Umat.run2.
- Amat, contains the acceleration matrix. Each seed is stored in its own run as Amat.run1 and Amat.run2.
- Zmat, contains the surface elevation matrix. Each seed is stored in its own row as Zmat(1,:) and Zmat(2,:).
- Type, specifies the kinematic that is calculated. The names listed under *"optKine"* will be used.

A.2 Extra

Irregular wave calculation and the FNV load model
Several values can be specified at **"optKine"** to create different kinematics at once. Each model will be saved in its own structure. During the calculation, all the given seeds will be saved as "run1.mat", "run2.mat" ... These can be deleted after the calculation is completed. The seeds calculated by the FNV model is also stored the same way. The final output is saved as FNV.m.

Regular wave calculation
The value **"optKine"** is defined different in this program. Only one model can now be chosen!

- optKine = option for wave kinematics:
  1 = linear to MWL (named linear)
  2 = stretched linear kinematics to the linear free surface (named linear_stretched)

3 = third order kinematics to MWL (named third)
4 = stretched 3rd order kinematics to the 3rd order free surface (named third_stretched)
5 = stream function wave (named stream_function)

The named values will appear as the name of the saved output.

Another output is created: "flux" is the calculated mean volumetric flux over one wave period per vertical meter.

Embedding methods
The input value **"optKine"** must be chosen 4 or higher, because the kinematics used for the stochastic time series is required to account for the free surface elevation. Only one model can now be chosen! Seeds are calculated in the same way as in irregular and FNV programs, but the result is not saved before the end.

Forced embedding use the specified time duration, and put the embedded wave at the first zero-up crossing found after the half duration.

Smooth and Mixed approach embedding require two new input values.

- optExtr = option for which method to pick the embedding location. This is described in section 8.4.1
  1 = Largest wave height
  2 = Largest wave crest, height defined to the mean trough depth
  3 = Largest wave crest, height defined to the deepest trough

- Tcutoff = surface elevation is calculated and the crest of the embedded wave is placed at a location. This value give the time duration before and after the embedded crest location, to be included for the further stochastic wave kinematic calculation.

More output is created in *smooth embedding*. The original surface elevation and kinematics are stored as "Zirr", "Uirr" and "Airr". The field "STAT" is another structure which give the information of embedding for all seeds calculated. The wave periods, heights, surface elevations and stream function coefficient are found here. The number of breaking waves will be stored in "INFO.BRW".

Remarks about the stream function wave calculation
A new output field is created when running calculation involving stream function. The field "STR" is a structure which again contain the wave elevation (STR.Z), kinematics (STR.U and STR.A) and stream function coefficient (STR.COEFF). The coefficients are explained in the end of section 8.2.2.

When applying the Stream function wave, wave breaking might be given as output. The wave breaking limit will be written, and the program will fail and write errors to the screen. A new calculation should be performed with the wave height below the given breaking limit.

The numeric error SIGFPE might also occur. The program will then crash, and Matlab might need to be turned off by the use of ctrl-alt-delete. Functions $\cosh(nh)$

is calculated, where n is the theory order and h the wave height. These become very large, and cannot be handled by the Fortran routine. The problem is avoided by selecting a lower order. Deep water cannot be handled, problems usually occur around $h > 50$m.

A.3 Interface to Fedem

The script "fedint.m" should be run. A graphical user interface will open, and let you pick a stored .mat file calculated from one of the programs described above. When selecting a file, the available seeds in that file will show on the screen. The selected seed will be written to Fedem.

When done, the program ask if you want to assign new text files to the triads in Fedem. This should only be done the first time a structural model are given loads from Matlab. To use this functionality, C# must be installed and the API system in Fedem must be available at your license.

The load files can also be linked manually through Fedem. It is important that each triad in the model correspond to the calculated kinematics. The vertical coordinates of the triads must be consistent with the user specified "Zvec" (see list of input values).

Appendix B

List of MATLAB code

The content in the attached .zip file will be explained in this appendix.

```
function OUT = CmCd(Hs,Tp,D,h)
OUT = CmCd(Hs,Tp,D,h)
Input:  Hs, Tp, structure diameter and water depth
Output: OUT is a structure with the given fields: Cm, Cd, KS,
      LAM, H
Calculates mass coefficient, drag coefficient and Keulagan
      Carpenter-number
Returns also the wave length and wave height used in the
      calculation.
Call: OUT = MaxWaves(Hs,Tp,h,dur)
      dur = 30
```

fedint.m
```
User interface to Fedem
Calls: FEDEMloads from directory Csharp
```

UI_embedDNV.m
```
User input %%%%%%%%%%%%%%%%%%%%%%%%%%%%%%%%%%%%%%%%%%%%%%%%%%%%%%%%
% Calls: embedDNV(UI) from directory main_functions
```

UI_embedFIT.m
```
User input %%%%%%%%%%%%%%%%%%%%%%%%%%%%%%%%%%%%%%%%%%%%%%%%%%%%%%%%
Calls: embedFIT(UI) from directory main_functions
```

UI_embedMIX.m
```
User input %%%%%%%%%%%%%%%%%%%%%%%%%%%%%%%%%%%%%%%%%%%%%%%%%%%%%%%%%%
Calls: embedMIX(UI) from directory main_functions
```

UI_mainRegular.m
```
User input %%%%%%%%%%%%%%%%%%%%%%%%%%%%%%%%%%%%%%%%%%%%%%%%%%%%%%%%%%
% Calls: mainRegular(UI) from directory main_functions
```

UI_mainIrregular.m
```
User input %%%%%%%%%%%%%%%%%%%%%%%%%%%%%%%%%%%%%%%%%%%%%%%%%%%%%%%%%%
% Calls: mainIrregular(UI) from directory main_functions
```

UI_FNV.m
```
User input %%%%%%%%%%%%%%%%%%%%%%%%%%%%%%%%%%%%%%%%%%%%%%%%%%%%%%%%%%
% Calls: mainFNV(UI) from directory main_functions
```

cd Csharp

```
function FEDEMloads(Fdist,dTstr)
Assign distributed load in Fdist to Fedem
dTstr = time step
```

```
fedem.sln
Script in Csharp that assign load files in directory force_files
to the triads in Fedem through API system. The script will open
automaticall i Csharp (must be innstalled). Then, it must be
compiled in C# befor it can be executed

directory fedem1
contains support files to fedem1.sln

directory force_files
contains the load files written by FEDEMloads
```

cd dean_fortran

```
embedding2
The Modified Fortran routine by Dalrymple [29]. Includes an
executable (.exe), fortran file (.f) and other support-files

embedding_input.dat
Input given to the executable from Matlab

embedding_output.dat
Output given from the executable to Matlab
```

cd diverse

```
function OUT = MaxWaves(Hs,Tp,h,dur)
OUT = MaxWaves(Hs,Tp,h,dur)
Input:  Hs, Tp, water depth, time duration
Output: OUT is a structure with the given fields: rayleigh,
      Naess, forristall
Calculate wave heights from different PDF, acoording to the most
      probable wave in a duration specified by "dur"
The wave is determined by Naess dist. as the most likely wave to
      occur
Call: [S,W] = WaveSpectra(Hs,Tp,Tvec,Wmax,2);
          K = wave_number(W,h);
```

```
function out = DistProperty(Zvec,Pdist,eta)
out = DistProperty(Zvec,Fdist,eta)
Input:  Vertical coordinates along structure, a matrix of
      distributed property, like velocity and acceleration
      matrix as used throughout the code
Output: out is matrix, with the property "lumped" to nodes by
      the trapezoidal rule, equal to "morisonL.m"


function FM = morison1(Cm,Cd,D,h,Zvec,U,A)
FM = morison1(Cm,Cd,D,h,Zvec,U,A)
Input: h = depth, U = velocity matrix, A = acceleration matrix,
      Zvec = coordinates corresponding to kinematic matrices
Output: FM(1,:) = base shear force, FM(2,:) = overturning moment
Calculates forces from wave kinematics using Morison:
Fdist = rho*Cm*pi*D^2/4*A + rho*D/2*Cd*U.*abs(U);
then trapezoidal rule, by FM(1,:)= trapz(Zvec,Fdist(:,i))  for
each time step i


function out = morison2(Cm,Cd,D,h,Zvec,eta,U,A)
out = morison2(Cm,Cd,D,h,Zvec,eta,U,A)
Input: h = depth, U = velocity matrix, A = acceleration matrix,
      Zvec = coordinates corresponding to kinematic matrices,
      eta = surface elevation
Output: out(1,:) = base shear force, out(2,:) = overturning
      moment
Calculates forces from wave kinematics using Morison with
      trapz(), includes the free surface elevation!


function out = mosionL(Cm,Cd,D,h,Zvec,eta,U,A)
out = mosionL(Cm,Cd,D,h,Zvec,eta,U,A)
See morison2.m
This function do the same, but the distributed loads is lumped
      to the nodes specified in Zvec


function out = morisonS2(Cm,Cd,D,h,Zvec,eta,U,A)
out = morisonS2(Cm,Cd,D,h,Zvec,eta,U,A)
See morison2.m
This function do the same, but the distributed loads will be
      interpolated by spline() before the trapz() is applied
```

```
function out = morisonSL(Cm,Cd,D,h,Zvec,eta,U,A,Zstr)
out = morisonSL(Cm,Cd,D,h,Zvec,eta,U,A,Zstr)
See morisonS2.m
This function do the same, but the distributed loads is lumped
      to the nodes specified in Zstr (which do not need to
      correspond to Zvec, the vertical coordinates of calculated
      kinematics


function Rvec = readFedemOutput(STR_FED)
Rvec = readFedemOutput(STR_FED)
Input:  string name of an ascii-file, without .asc
Output: Vector of data
Reads the output from Fedem


function K = wave_number(W,h)
K = wave_number(W,h)
Input:  Matrix Frequencies, water depth
Output: Matrix of Wave numbers corresponding to W
Calculation by iteration process, linear dispersion relation
```

cd embedding

```
function Znew = blend(Tvec,T,Zirr,Zemb)
Znew = blend(Tvec,T,Zirr,Zemb)
Input:  Time vector, Wave period, Irregular stochastic matrix,
      embedded matrix
Output: Matrix blended solution
Blend Zirr and Zemb, both have the embedding location (crest of
      wave) at time 0


function [Mnew Mirr] = blend2(Tvec,Tirr,Mirr,Tstr,Mstr)
Tvec = Time vector from irregular time series
[Mnew Mirr] = blend2(Tvec,Tirr,Mirr,Tstr,Mstr)
See blend.m  --> Input:  Mirr = Zirr, Mstr = Zemb
                 Output: Mew = Znew
This function do the same, but the Stream function wave period
      (Tstr) can now be different from the irregular Period
      (Tirr). Mirr is the stochastic matrix adapted to the wave
      period Tstr


Embedded stream function
function OUT = ExtractSeries(Tvec,Z,Tcutoff,dt,choice)
OUT = ExtractSeries(Tvec,Z,Tcutoff,dt,choice)
Input:  Time vector, Surface elevation vector, Time to include
      before and after the embedding location, time step,
```

```
      choice:
      1 = max crest to min through,
      2 = max crest to mean through,
      3 = max height
Output: OUT is a structure with the given fields: H, T, Tvec, Z
       H = wave height, T = wave period, Tvec = new time vector,
       Z corresponding surface elevation


Stream function coefficients
function STAT = read_output(NR,NORDER)
STAT = read_output(NR,NORDER)
Input:  number of run, order of theory
Output: STAT, structure containing Stream function coefficients
      and information about each embedding location as T and H
Reads the output given by the Fortran Routine


function STAT = read_output2(NR,NORDER)
Stream function coefficients
See "read_output.m"
This function do the same, but reads the output when Fortran is
      allowed to continue to the next embedding location, after
      the computation has failed due to wave breaking.
```

cd irregular_sea

```
function ETA = wave_profile(Tvec,W,S,hh,Hs,choice)
% Wave: Z = Za*cos(k*x - w*t + eps)
%  1           2                 3
% linear    %2nd order deep   %2nd order finite


function OUT = FNVcalc(Cm,Cd,D,h,S,W,Tvec,Zvec,seed)
OUT = FNVcalc(Cm,Cd,D,h,S,W,Tvec,Zvec,seed)
Input:  S = specter values, W = wave frequencies
Output: OUT is a structure with the given fields: LM, LF, Fdist,
      FM
Calculates the FNV load model
FM is consistent with FNV equation
Fdist is FNV "lumped" to nodes
LF = lumped force, sum of Fdist for each time step
LM = lumped moment, moment by Fdist for each time step
LF and LM can be compared to FM, which validate the "lumping"
      process
Call: K = wave_number(W,h)
```

```
function [VEL, ACC] = kinematics(Tvec,Zvec,hh,ETA,choice,nr)
%% Create irregular wave kinematics
% 1      2        3        4     5       6         7       8
%linear %deep2 %second %expol1 %expol2 %expol3 %wheel1 %wheel2

All the following routines will be called from this function:

function [U,A] = K1linear(LIN,Tvec,Zvec,h,nr)
Calculates linear kinematic

function [Utot,Atot,SEC] = K2deep2(SEC,U,A,Tvec,Zvec,h,nr)
Calculates second order kinematic at deep water

function [Utot,Atot,SEC] = K3second(SEC,U,A,Tvec,Zvec,hlin,nr)
Calculates second order kinematic at finite water

function [Utot,Atot] = K4extrapolation1(ETA,U,A,Tvec,Zvec,h,nr)
Extrapolation: linear kinematics under wave, finite water depth

K5extrapolation2.m
Extrapolation: second order kinematics under wave, finite  water
      depth

K6extrapolation3.m
Extrapolation: second order kinematics under wave, finite water
      depth

function [U,A] = Kwheeler(Tvec,Zvec,h,eta,U,A)
Script calculating Wheeler stretching to eta of kinematic
      U and A

function [Y,W] = WaveSpectra2nd(Y,W,Hs,opt)
Cut wave spectra sqrt(2g/Hs), used for 2nd order processess
opt = 1, Y = S-values
opt = 2, Y = Za-values
```

cd main_function

```
function embedDNV(UI)
% Forced embedding
% Calls: WaveSpectra.m
%        stream.m
%        wave_number.m
%        wave_profile.m
%        kinematics.m
%        morison2.m
```

```
%         morisonL.m
%         WaveSpectra.m


function embedFIT(UI)
% Smooth embedding
% Calls: !embedding2.exe
%         wave_number.m
%         wave_profile.m
%         kinematics.m
%         stream_kinematics.m
%         morison2.m
%         morisonL.m
%         ExtractSeries.m
%         read_output2.m
%         blend2.m
%         WaveSpectra.m



function embedMIX(UI)
% Mixed approach embedding
% Calls: stream.m
%         wave_number.m
%         wave_profile.m
%         kinematics.m
%         stream_kinematics.m
%         morison2.m
%         morisonL.m
%         ExtractSeries.m
%         blend2.m
%         WaveSpectra.m


function mainFNV(UI)
%% FNV load calculation
% Calls: FNVcalc.m
%         wave_number.m
%         WaveSpectra.m


function mainIrregular(UI)
% Irregular sea calculation
% Calls: WaveSpectra.m
%         wave_number.m
%         wave_profile.m
%         kinematics.m
%         morison2.m
%         morisonL.m
```

```
function mainRegular(UI)
% Wave: Z = Za*cos(k*x - w*t)
% Regular sea calculation
% Calls: WaveSpectra.m
%        wave_number.m
%        wave_linear.m
%        Kwheeler.m
%        morison2.m
%        morisonL.m
%        stokes3rd.m
%        DistProperty.m
%        stream.m
```

cd regular

```
function THI = stokes3rd(H,T,h,Tvec,Zvec)
Calculation of third order stokes kinematic
Calls: wave_number.m


function KIN = stream_kinematics(eta,coeff,T,Zvec,Tvec,h)
WAVE KINEMATICS FROM STREAM FUNCTION
This function use the output from dean-fortran, with output
      changed to metric!


function Z = stream_wave(Xvector,Yvector,Vpos)
Create periodic function of calculated stream function surface
      by Fortran
The function spline() is used


function LIN = wave_linear(H,T,h,Tvec,Zvec)
Linear Regular wave
Wave: Z = Za*cos(k*x - w*t)
Calls: wave_number.m


function STR = stream(Tvec,Zvec,H,T,h,NORDER)
Stream function wave
Wave: Z = Za*cos(k*x - w*t)
Calls: wave_number.m
       !embedding2.exe
        read_output
        stream_kinematics
```